University of Southampton

Faculty of Environmental and Life Sciences

Graduate School of the National Oceanography Centre Southampton

From Oil Spills to Invasive Species: Lagrangian Modelling of Connectivity in the Arctic Ocean

by

Stephen John Kelly

ORCID ID 0000-0002-8966-5986

Thesis for the degree of Doctor of Philosophy in Ocean and Earth Science

December 2019

University of Southampton

Abstract

Faculty of Environmental and Life Sciences

Graduate School of the National Oceanography Centre Southampton

Thesis for the degree of Doctor of Philosophy in Ocean and Earth Science

From Oil Spills to Invasive Species: Lagrangian Modelling of Connectivity in the Arctic Ocean

by

Stephen John Kelly

Marine connectivity describes the spatial and temporal linkages between separated parts of the global ocean. How different regions are connected, on what timescales, and by which oceanic pathways are important questions for a wide variety of applications. Answering these questions is an inherently interdisciplinary problem, with techniques including in-situ observations, remote sensing, and modelling used in synergy to answer key scientific questions. Here, a modelling approach is employed to contribute to our understanding of the wider field.

This thesis focuses on understanding the importance of marine connectivity in the Arctic Ocean. The Arctic is a particularly important part of the global ocean, not least because of the impacts of climate change and loss of sea ice. This presents both challenges and opportunities - for instance, the retreat of Arctic sea ice is increasing interest in exploiting the region for resource extraction and commercial shipping, and changing circulation associated with a warming Arctic may permit invasive species to traverse the ocean.

These and other drivers motivate research into how connectivity is shaping the ecological, physical, and socioeconomic features of the Arctic Ocean. Primarily using a Lagrangian particle-tracking technique in conjunction with a state of the art, eddy-permitting ocean model, three case studies – one biological, one physical and one socioeconomic – are used to explore the impact of marine connectivity in the Arctic Ocean. These studies respectively focus on: 1. Exploring the change in connectivity between the Beaufort Gyre and the sources of its freshwater contribution (Kelly et al., 2019); and 2. Investigating the spread of pollutants in the event of a shipping accident from the Northern Sea Route (Kelly et al.,

2018); 3. Assessing the role of changing advective pathways linking the Pacific and Atlantic Oceans on potential invasive species to the North Atlantic (Kelly et al., 2020). Individually, each paper addresses one specific aspect of Arctic connectivity. As chapters of a thesis, they are designed to illustrate the importance of marine connectivity in linking physical, biological and socioeconomic factors in a rapidly changing Arctic Ocean.

Table of Contents

Table of Tables

Pathways 8* and 24* were further processed to exclude particles entrained into the Beaufort Gyre by removing trajectories which passed north of 75N in the Beaufort Gyre region. (In both cases, the trajectories removed accounted for < 0.1% of all trajectories which reached the Atlantic). Path-way 16 was non-negligible (0.3% of trajectories) but does not fit well into our classification system and is instead grouped with ‘others.’

Table of Figures

which reach 60N in the Atlantic Ocean, showing the fraction of 'successful' trajectories which take each path way. As in (b), a running 12-month average is used to remove the seasonal cycle, with the exception of the dark green line, to demonstrate that although typically either unavailable or negligible, the green pathway can represent a significant number of trajectories when available.

Figure 5.4: a) Comparison of how connectivity timescale, defined to be the time taken by the first trajectory to reach 60N in the Atlantic Ocean, varies with time of release for each of the routes identified in Figure 5.1d. No clear trend is evident, and variability between releases is considerable in all routes. b) Comparison of connectivity timescales, this time smoothed with 12-montly rolling averages. Years on which no trajectories followed a route are ignored. Due to the green route only being occasionally available, the timescale for each release is plotted as a dot rather than the running average. c) Monthly averages of connectivity timescales for each route. No trend is apparent for the pink, blue or green routes, however the orange and yellow routes have shorter connectivity timescales in summer than in winter.

Figure 5.5: a) Comparison of the 12-monthly rolling mean Arctic Oscillation (AO, blue) index taken from the NOAA, and the annual Arctic Ocean Oscillation (AOO, orange) index over the period 1970-2015. Vertical green lines show the two release times that were associated with the largest fraction of trajectories following the 'green route' (see Figure 5.3c). b) Simplified circulation schematic showing the anti-cyclonic regime in which the green route is blocked and diverted to yellow/orange routes. c) Simplified circulation schematic showing the more cyclonic regime in which the green route is permitted. d) Idealized cross section along red line in Figures 5.5b and 5.5c, under the anti-cyclonic regime. Easterly winds are favored, driving an Ekman transport away from the shore. By continuity, this induces a sea surface slope downwards towards the coast, which supports a barotropic geostrophic flow towards the west (stronger closer to the coast), which blocks the green route as in Figure 5.5b. e) Idealized cross section along the same line, but in the cyclonic case that favors the green route in Figure 5.5c. Cyclonic regime favors westerly winds, which drives Ekman transport to the coast. By continuity, this induces a sea surface gradient up towards the shore, which in turn supports a geostrophic barotropic flow towards the Canadian Archipelago.

Research Thesis: Declaration of Authorship

Print name: Stephen John Kelly

Title of thesis: From Oil Spills to Invasive Species: Lagrangian Modelling of Connectivity in the Arctic Ocean

I declare that this thesis and the work presented in it are my own and has been generated by me as the result of my own original research.

I confirm that:

1. This work was done wholly or mainly while in candidature for a research degree at this University;
2. Where any part of this thesis has previously been submitted for a degree or any other qualification at this University or any other institution, this has been clearly stated;
3. Where I have consulted the published work of others, this is always clearly attributed;
4. Where I have quoted from the work of others, the source is always given. With the exception of such quotations, this thesis is entirely my own work;
5. I have acknowledged all main sources of help;
6. Where the thesis is based on work done by myself jointly with others, I have made clear exactly what was done by others and what I have contributed myself;
7. Parts of this work have been published as: S. Kelly et al. (2018) and Kelly et al. (2019) in *JGR: Oceans*, and Kelly et al. (2020) in *Earth's Future.*

Signature: .....Date: 20/12/2019

In the case of jointly authored papers, comprising Chapters 3-5 of this thesis, Katya Popova (lead supervisor) confirms that I, Stephen Kelly, lead the research and co-authors contributed in a supervisorial capacity. I wrote all three papers, and aside from Figure 4 of Kelly et al. (2019), produced by Andrey Proshutinsky, all figures were created by me.

Acknowledgements

There are many people who have helped and supported me throughout my PhD candidature, and I cannot overstate how much I value each and every one of them. Friends, colleagues, supervisors, family – this thesis would not have been possible without you. There are a few people who I would like to thank specifically:

Firstly, Dr Katya Popova, my lead supervisor. I first met Katya in 2013, when I completed a NERC summer placement under her supervision. At the time, I was an undergraduate physics student looking forward to an interesting summer project, but not expecting to stay in oceanography beyond that. Clearly something went right: I came back to NOC for this PhD, and now I am staying to work on the SOLSTICE project. Katya's constant belief, encouragement and support has been an integral part of why I have been able to complete this thesis, and I am truly grateful for it. Katya: Thank you!

I would also like to take this opportunity to thank my other supervisors: Dr Andrew Yool, Dr Yevgeny Aksenov, and Professor Robert Marsh. I have worked with Andrew since that 2013 summer project, and his ability to improve any text is second to none – this acknowledgements section would probably read a lot better if I'd let him comment on it before submitting! Yevgeny's expertise in the Arctic Ocean has been invaluable to my development as a scientist, and I am grateful for having the opportunity to learn from him. Bob was asked to join my supervisorial team at very short notice, and has since been a fantastic addition who has offered fresh perspectives and helped me develop ideas throughout. Additionally, I would like to thank my panel chair, Professor Adrian New, for taking a genuine interest in my research and strengthening the work throughout this thesis as a result.

For hosting me during my 3-month placement at Woods Hole Oceanographic Institution, making me feel instantly at home, and providing guidance on the second paper of this thesis, I am grateful to Andrey Proshutinsky. My time at WHOI was a highlight of this PhD, and I would like to thank everyone who made it such an enjoyable experience.

In addition to my supervisors, I would like to thank the entire Marine Systems Modelling group at NOC. Colleagues and fellow students have made – and continue to make – this a fantastic place to work. I consider myself very lucky to be part of this group. One member in particular, Jeff Blundell, deserves special thanks for the hours spent going above and beyond to help set up Ariane, investigate various bugs in code, and almost anything else on the computational side. Andrew Coward for his assistance with the NEMO model, Joël Hirschi for his encouragement (and for ensuring that I wasn't the only night owl working late into the evenings!), Josie Robinson-Parker for helping me to settle in at the beginning, and the entire SOLSTICE office and 256/16 officemates past and

present for creating the most positive and supportive working environment that anyone could ask for. Thank you all.

I would like to thank my fellow PhD students at GSNOCS, especially the 2015 intake, for the support, laughs and mad discussions that have kept me going throughout. I'd also like to thank some of their cats – particularly Monty and Althea – who warmed my lap while writing various sections of this thesis.

Now would be a good time to thank friends outside of NOC – friends from undergraduate, friends from outside of university, friends from korfball – thank you all! To my korfball teammates, I'd also like to add that I hope that my science is much more accurate than my shooting.

Another person who deserves special thanks is Kevin Daws, my physics teacher at GCSE and A-level. He was a huge inspiration at the start of my academic journey, and I'd like to take the opportunity to thank him here.

To my brothers Christopher and Simon: you have both been sources of inspiration throughout this thesis. Chris, you've followed a similar academic path to me with our shared physics background. At every step, from school through to university and beyond, I had the motivation of setting a bar high enough that it would be a sufficient challenge for you. You consistently exceeded the standards that I set, and I have no doubt that you will continue this trend with your own thesis in a few months. To Simon, our academic interests are more distinct, but I will never cease to be inspired by your work ethic: I certainly didn't manage as many evenings in Hartley Library during my first year of undergrad! I have really appreciated having you in Southampton with me for the past couple of years, and I look forward to celebrating your achievements in the near future as well.

Finally, but most importantly, my parents. Mum, dad, thank you for everything. I literally would not have been able to do any of this without you. You have always encouraged me to be the best that I could be, and for that I will forever be grateful. I have always been able to rely on your support, you've believed in me even when I haven't believed in myself, and I can't put into words just how important that has been throughout all of my life, especially during my PhD. Again, thank you for everything.

Chapter 1: Introduction

1.1. Aims and Objectives

The aim of this thesis is to contribute to the understanding of marine circulation connectivity in the Arctic Ocean, with a variety of different applications. We begin with an overview of what is known about the oceanography of the Arctic Ocean, before moving onto the topic of marine connectivity and the different approaches to studying it.

Marine circulation connectivity describes the advective pathways linking spatially separated regions of the global ocean (see Chapter 1.3 for a more complete description of the concept of connectivity). The objective of the research presented here is to use three case studies, each with a distinct framing, to further our understanding of circulation connectivity - and issues impacted by circulation connectivity - in the Arctic Ocean. These studies comprise the results chapters (Chapters 3-5) of this thesis. We begin with a purely oceanographic focus in Chapter 3, before moving onto two more applied questions in Chapters 4 and 5. The objectives of each results chapter are:

- To answer the question of how circulation pathways bringing fresh water to the Beaufort Gyre have changed in recent decades, and what has caused this to happen.
- To understand how circulation connectivity determines the areas potentially at risk in the event of an oil spill from Arctic shipping
- To answer whether changing circulation connectivity in the Arctic Ocean could permit invasive species from the North Pacific to reach the Atlantic Ocean.

In a more general sense, the theme tying each of these questions together is the aim of understanding the marine circulation connectivity pathways and timescales in the Arctic Ocean, with each chapter contributing towards that overarching goal.

1.1.1. Thesis Structure

This thesis has been submitted as a thesis by publications. All three results chapters have been published: Chapters 3 and 4 can be found in *JGR: Oceans* as Kelly et al. (2019) and Kelly et al. (2018) respectively, while Chapter 5 appears in *Earth's Future* as Kelly et al. (2020).

The structure of the thesis is as follows:

Chapter 1 introduces the topics studied throughout this work. The purpose of this is to give a general overview of the two core themes connecting each of the later chapters, namely the oceanography of the Arctic Ocean (Chapter 1.2) and the concept of marine circulation connectivity (Chapter 1.3).

Chapter 1.4 discusses the various different approaches that can be applied to studying marine circulation connectivity. Additionally, each of the results chapters include their own discussion subsections with relevant details pertaining to their specific topics.

Chapter 2: The computational tools used throughout this thesis – specifically, the NEMO model and Ariane particle tracking software – are discussed in the main methodology chapter of the thesis. The individual experiment designs are fully described in the methodology subsections of their respective results chapters.

Chapters 3, 4 and 5 are the results chapters: the publications that comprise this thesis-by-publications. By way of an introduction, the plain language summaries of each are included below:

Chapter 3: The Beaufort Gyre, a clockwise ice and water circulation in the Arctic Ocean, is an important feature of the Arctic because it stores a large volume of fresh—relative to the rest of the ocean—water. Depending on the atmospheric circulation driving it, the Beaufort Gyre can either accumulate or release this freshwater. The sources of relatively fresh water to the Beaufort Gyre are Arctic rivers, the Bering Strait, and melting sea ice. By tracking virtual particles in a high-resolution ocean model, we investigate how these sources have changed in recent decades, and identify a change in the pathways bringing them to the Beaufort Gyre. This change in ocean circulation was found to correlate with a change in the mixed layer depth in the model.

Chapter 4: The Earth's climate is changing and the Arctic Ocean is projected to experience ice free summers within decades. This would enable more commercial shipping, which in turn makes an Arctic shipping accident more likely. This could lead to oil (or other pollutants) being spilled into the ocean. Because of the harsh Arctic environment, an oil spill may not be successfully recovered, so we need to consider where it will go in the following months and years. We released virtual "particles" into a computer model of the ocean and tracked their progress for 2 years. In this time, particles travelled, on average, 1,223 km. This demonstrates that pan-Arctic modelling is needed in the event of an unrecovered pollutant spill. Unrecovered oil from one season may be accessible the next spring. By analyzing the spread of our particles, we found that on average 676,917 km2 would need to be searched to find it, but that this is highly dependent on where the spill occurs. Finally, we noted that in some places, particularly the Barents Sea, there was a risk that spilled pollutants could become entrained into deep water, rendering them irrecoverable.

Chapter 5: With a warming Arctic Ocean, it has been suggested that the ocean currents that connect the Pacific to the Atlantic may change. This could have potential biological consequences, including bringing Pacific species of plankton to the Atlantic. We investigate how the pathways bringing Pacific water to the Atlantic have changed, identify a pathway that takes less time that other routes to bring waters from Pacific to the Atlantic (but that is only occasionally available), and note that even the shortest timescales are over 2 years.

Finally, **Chapter 6** synthesises the lessons learned from the preceding results chapters, and discusses them in the context of Arctic circulation connectivity in general. Moreover, additional research conducted during my time as a PhD student but not a formal part of the results chapters is discussed in this chapter, including how the methodology analogous to that used in Chapter 4 was applied to a real-life oil spill near China. The thesis concludes by suggesting areas where it could be built upon, including ideas for a future paper revisiting trans-Arctic Pacific to Atlantic ecological connectivity, but tailored to a specific species to motivate a focus on understanding along-trajectory environmental conditions.

1.2. The Arctic Ocean

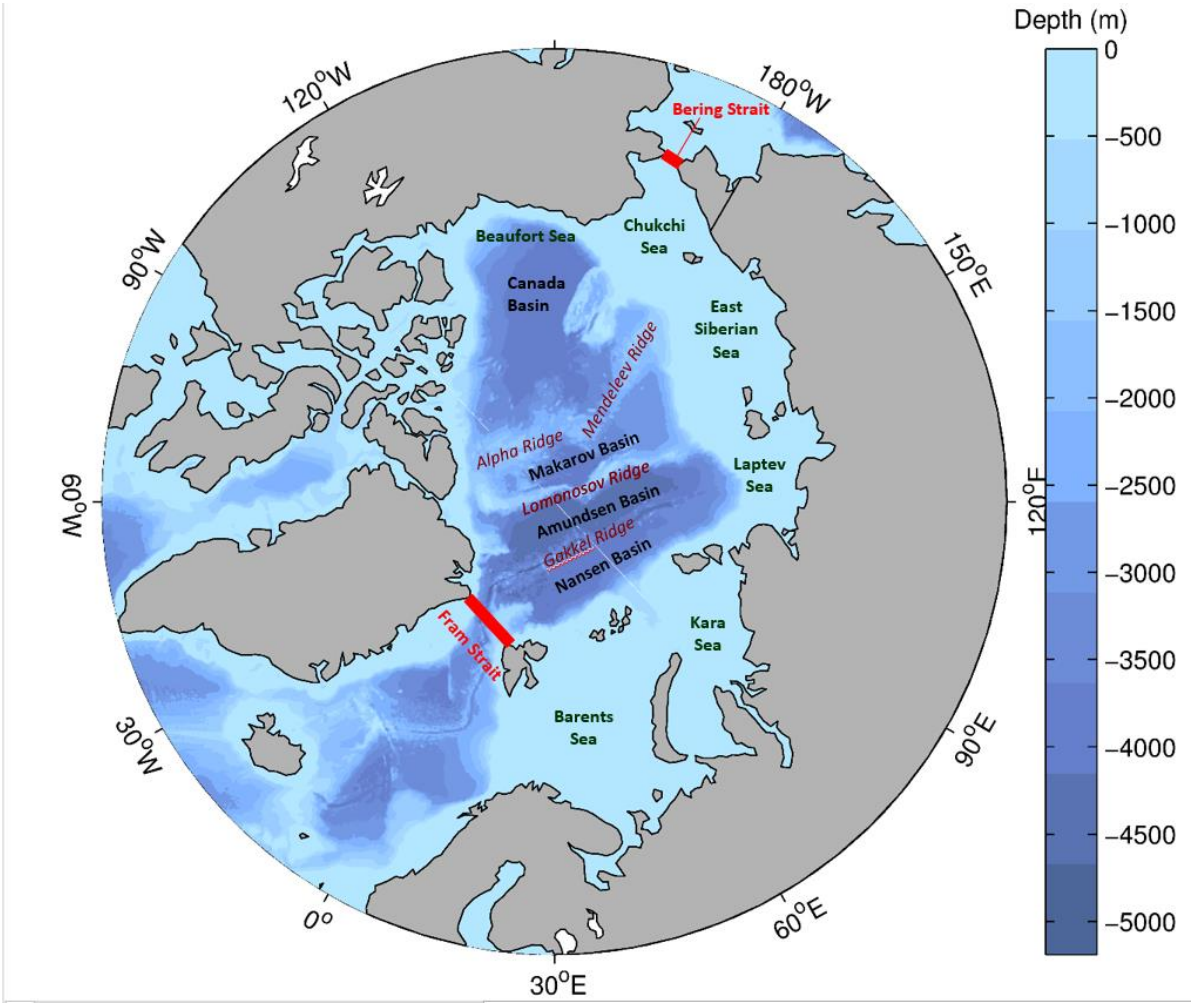

Figure 1.1 – Bathymetry of the Arctic Ocean, with important geographic features highlighted.

At the northernmost extreme of the planet lies the Arctic Ocean, surrounded by land on almost all sides, split roughly evenly between continental shelf and deep ocean, and divided by several oceanic ridges. A map of the Arctic, with key features labelled is presented in Figure 1.1.

The Arctic Ocean and its marginal seas are defined by the International Hydrological Organization (IHO) as follows: The Pacific border is delimited by the Bering Strait (between 66°11'N, 166°14'W and 66°22'N, 170°35'W). On the Atlantic side, borders exist at 60°N in the Davis Strait (between 44°50'W and 64°10'W), as well as borders in the Iceland Sea and Norwegian Sea. The southern borders of the Iceland Sea are (65°30'N,24°32'W to 67°51'N, 32°11'W) between Iceland and Greenland, and (62°21'N, 6°15'W to 64°14'N, 14°58'W) between the Faeroe Islands and Iceland. The southern borders of the Norwegian Sea are (62°21'N, 6°15'W to 61°00'N, 0°53'W) between the Faeroe Islands and Shetland Islands, and continuing along 61°N from the Shetland Islands to the Norwegian coast. (International Hydrographic Organization, 2002). The Nordic Seas (Iceland, Greenland and Norwegian Seas) are often treated separately from the high Arctic. Excluding the Nordic Seas, the southern boundaries of the Arctic on the Atlantic side are the Fram Strait (83°23'N, 25°25'W to 80°04'N, 16°16'E) and the Barents Sea Opening (70°50'N, 9°00'W to 71°10'N – 7°58'W) (International Hydrographic Organization, 2002).

In contrast to the rest of the world, where shallow shelf seas make up only a small portion of the ocean, approximately half of the Arctic is continental shelf. The main topographical feature in the deep ocean is the Lomonosov Ridge, which divides the Arctic into the Eurasian and Amerasian basins. These basins are themselves split into two, with the Eurasian Basin divided into the Nansen and Amundsen basins by the Gakkel Ridge, and the Amerasian partitioned into the Canada Basin and Makarov Basin, with the Mendeleev and Alpha ridges separating the two. The vast majority of the continental shelf is on the Eastern side of the Arctic, comprising of (from west to east) the Barents, Kara, Laptev, East-Siberian and Chukchi seas. On the western side, north of Canada and Alaska, lies the Beaufort Sea, with a thin continental shelf.

Politically, the Arctic Ocean falls mostly under the jurisdiction of five countries, with a small area beyond national jurisdiction (ABNJ, see Popova et al. (2019)) in the central Arctic. Russia, USA (Alaska), Canada, Denmark (Greenland), and Norway (including Svalbard) each claiming exclusive economic zones in the 200 nautical mile strip from their respective coastlines. Additionally, Arctic nations have submitted claims – overlapping in places – for extended continental shelf rights (Riddell-Dixon, 2008). Major shipping routes in the Arctic Ocean include the Northern Sea Route through Russian waters and the North West Passage through Canadian / US waters, both of which provide economic links between the Atlantic and Pacific Oceans (Østreng et al., 2013).

The Arctic Ocean is connected to the rest of the world ocean in four places: to the Pacific only via the Bering Strait, and to the Atlantic via the Barents Sea Opening, the Fram Strait, and the Canadian Archipelago. Pacific Water enters the Arctic via Bering Strait (with negligible flow in the opposite direction), and Atlantic Water enters via the Barents Sea Opening and the Eastern Fram Strait. Additionally, a significant input of fresh water enters from major rivers: the Ob, Yenisey, Lena, Kolyma and Mackenzie rivers all flow directly into the Arctic Ocean. The exit points from the Arctic Ocean

are the western portion of the Fram Strait, and various pathways through the Canadian Archipelago and the Davis Strait – in both cases, outflow is to the Atlantic Ocean.

Before going into more detail about existing literature on the circulation of the Arctic Ocean, we begin by describing the vertical structure of the Arctic Ocean, and how this varies seasonally – including the formation and loss of sea ice.

1.2.1. Arctic Sea Ice

The Arctic Ocean is a highly stratified Mediterranean ocean. It is a unique part of the global ocean in that, unlike all but the Southern Ocean, it is characterised by the year-round presence of sea ice. In contrast to the Southern Ocean, it is an ocean surrounded by land as opposed to land surrounded by an ocean. The Arctic has, historically, been approximately half covered in sea ice even in summer (Stroeve et al., 2007), but in recent years this has declined rapidly due to anthropogenic carbon dioxide emissions (Mueller et al., 2018; Notz and Stroeve, 2016). It is now predicted that the Arctic Ocean will be seasonally ice free as early as the 2030s, and no later than the 2050s, assuming that CO_2 emissions persist at their current rate (Jahn et al., 2016; Overland and Wang, 2013; Wang and Overland, 2012). It is important to note here that 'ice free' is commonly defined as the Arctic having a total sea ice extent of less than 1 million km^2, with a small (relative to the rest of the Arctic Ocean) region in the vicinity of the Canadian Archipelago projected to retain ice cover long after the rest of summer Arctic sea ice is gone (Wang and Overland, 2012).

An example of this sharp decline in Arctic ice cover is illustrated below in Figure 1.2. Using data from the National Snow and Ice Data Centre (as also used for validation in Chapter 4, Kelly et al. (2018)), we show the difference in horizontal extent of Arctic sea ice between 2001 and 2012. 2012 currently (at the time of writing) holds the record for minimum horizontal extent of sea ice (Kwok, 2018), and the loss of ice cover in the marginal seas is pronounced:

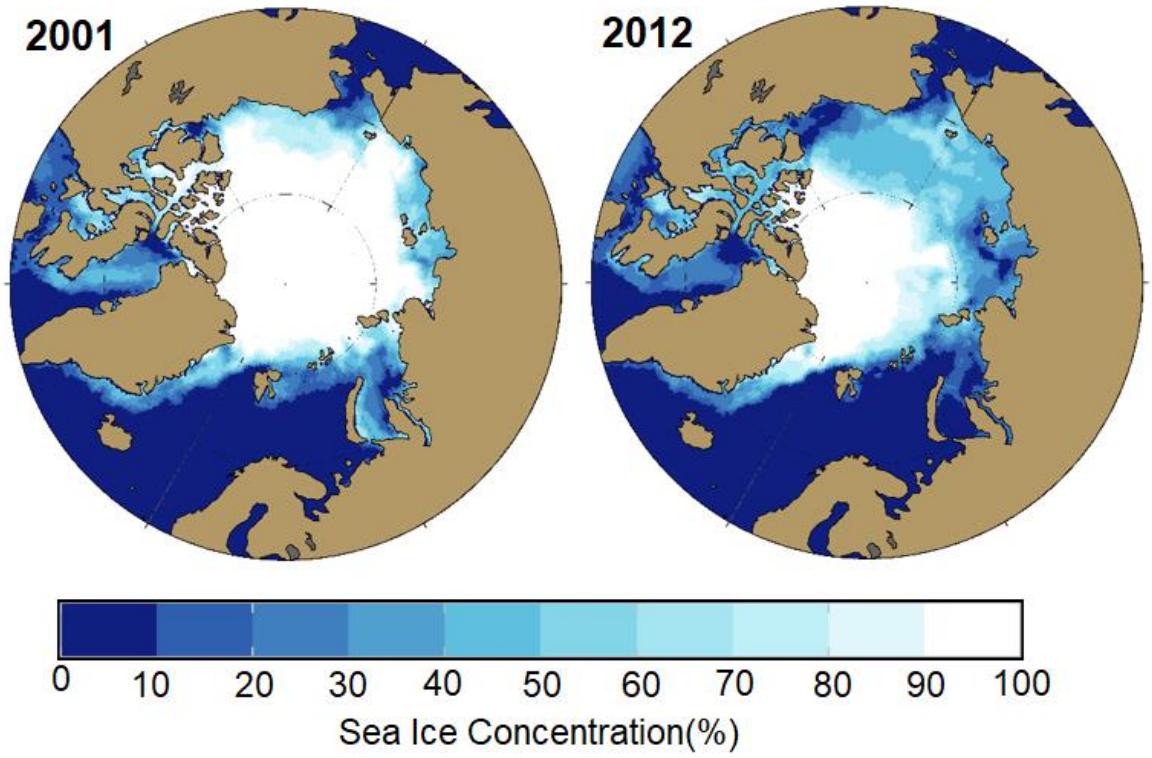

Figure 1.2: Comparison of satellite observed (National Snow and Ice Data Centre, NSIDC) September mean sea ice concentrations for 2001 (left) and 2012 (right). 2012 holds (at the time of writing) the record for minimum Arctic sea ice extent.

As well as sea ice receding in terms of horizontal extent, Arctic sea ice has also thinned considerably over recent decades (Kwok, 2018), with loss of sea ice volume most pronounced during the autumn (Laxon et al., 2013). Based on satellite analysis, comparing Cryosat2 (2010-2012) data to with that from ICESat (2003-2008), 4,291 km^3 of ice was lost in autumn between the two satellite periods (Laxon et al., 2013). The same authors found a reduction in winter sea ice thickness of 1,479 km^3 over between the two periods. Over a longer timescale, Kwok (2018) found that Arctic sea ice thickness has decreased by 2m (66%) by the period 2011-2018 (again based on Cryosat2 data) compared to submarine measurements from 1958-1976.

The loss of Arctic sea ice has been accompanied by a change in the character of the ice which remains: notably, the Arctic is becoming increasingly characterised by less multiyear ice, and a greater proportion of the ice is younger or first year sea ice (Bi et al., 2020; Kwok, 2018). This matters from an ecological point of view, because brine rejection means that multiyear ice is fresher than younger ice. Brine in younger ice harbours ice-dwelling organisms (Krembs et al., 2011), and thus more mobile (due to reduced sea ice concentration) and more saline (due to loss of multi-year ice) could play an increasingly important role in the biogeochemistry of the Arctic.

Reduced Arctic sea ice is also important for a variety of other reasons. Socio-economic consequences of an ice free Arctic include a potential increase in Arctic shipping (Lee and Kim, 2015; Østreng et

al., 2013), which motivates Chapter 4 of this thesis where we consider the advection of pollutants in the Arctic. While that chapter focuses on oil spills at specific point source locations, reduced sea ice cover in the Arctic could be directly important for other pollutants such as atmospheric mercury (Moore et al., 2016). Sea ice acts as a barrier to the ocean/atmosphere interface, and loss of sea ice could allow for more pollutants of atmospheric origin to enter the Arctic Ocean.

Physically, removing sea ice means that the effect of the wind is felt more directly by the upper ocean, and increased stirring of the ocean surface leads to a deepening of the upper mixed layer (Graham et al., 2019; Lincoln et al., 2016), which can in turn be important for the biological productivity of the Arctic (Carmack et al., 2016). Ice-albedo feedback is another important physical consequence of sea ice retreat, with increased areas of dark open water replacing more reflective sea ice, enabling the ocean to absorb more heat from solar radiation (Perovich et al., 2007).

In addition to the long term secular trend of sea ice decline in the Arctic Ocean, there is also a strong seasonal cycle in sea ice cover. Aside from the Barents Sea, which is predominantly ice-free even in winter due to warmer Atlantic waters entering the Arctic here (discussed more thoroughly in Section 1.1.3), the Arctic remains entirely ice covered during winter, with a tail extending down the east coast of Greenland due to sea ice exported from the Fram Strait (Smedsrud et al., 2017). Arctic Sea ice reaches its maximum extent during March, with September seeing minima and the record minimum occurring in September 2012 (Parkinson and Comiso, 2013). Much of the Beaufort, Kara and Laptev Seas are now ice-free in summer, though summer sea ice persists more in the East Siberian Sea (Parkinson and Comiso, 2013). This new normal, with large areas of open water that were previously ice covered even in summer has been invoked a possible explanation for changing ecological connectivity between the Pacific and Atlantic Oceans (Reid et al., 2007).

1.2.2. Vertical Structure and Variability

Beneath the sea ice, the Arctic is highly stratified near the surface, with distinct layers that have limited interactions between them (McLaughlin et al., 1996). Like all of the ocean, the Arctic is stratified by density. However, unlike most of the rest of the global ocean, the Arctic is unique in that the highest temperatures are found at depth. The influence of relatively warm but saline Atlantic Water, fresher Pacific water, a large volume of fresh riverine input and seasonal meltwater leads to a strongly layered ocean (Timmermans et al., 2017), with a cold, fresh polar mixed layer (Section 1.2.2.1) at the surface, and denser layers beneath, with the Atlantic and Pacific side of the Arctic exhibiting different characteristics (Section 1.2.2.2).

1.2.2.1. The Arctic Mixed Layer

The uppermost layer of the Arctic Ocean is the polar mixed layer, which exhibits strong seasonal variability driven predominantly by the seasonal cycle of sea ice formation and melting (Peralta-Ferriz and Woodgate, 2015). The mixed layer is important for a variety of physical and ecological

reasons, from mediating heat exchange between the ocean and sea ice – or atmosphere, in the case of open water areas – (Sirevaag et al., 2011) to bringing nutrients to the surface and hence influencing biological activity (Popova et al., 2010), and typically has a depth of 5-30 m in summer and 25-50 m in winter, and significantly deeper (>100 m) in the Eastern Arctic (Peralta-Ferriz and Woodgate, 2015).

Unlike most of the global ocean, where the wind and surface waves control the depth of the upper mixed layer, the presence of sea ice limits the influence of the wind and damps surface waves in the Arctic. Instead, it is the formation and loss of sea ice which dominates the seasonal deepening and shoaling of the Arctic mixed layer (Peralta-Ferriz and Woodgate, 2015). In the summertime, the Arctic heats and sea ice melts. This releases liquid fresh water into the ocean, which is less dense than the water beneath, creating a relatively shallow mixed layer comprised of this meltwater. This contrasts with winter when, during sea ice formation, brine rejection induces convection and hence deepens the upper mixed layer (Polyakov et al., 2013). This explains the seasonal cycle of a deep mixed layer in winter and shallow summer mixed layer described by Peralta Ferriz and Woodgate (2015).

However, there are other mechanisms which have the opposite effect. Absence of sea ice during the summer provides allows for more direct wind-driven stirring of the upper ocean, however the influence of this was found to be small (explaining <20% of the mixed layer depth variance) compared to ice melt and brine rejection, even in seasonally ice-free regions (Peralta-Ferriz and Woodgate, 2015). Other dynamical processes affecting the Arctic mixed layer depth include advection of fresh water (Kelly et al., 2019), with Peralta-Ferriz and Woodgate (2015) noting particular importance of advection of relatively fresh Pacific water on the Arctic mixed layer. A more detailed, region-by-region analysis of the Arctic mixed layer, comparing the model used throughout this thesis to observations is presented in Section 3.5.

1.2.2.2. Atlantic Layer, Pacific Layer and the Beaufort Gyre

Beneath the upper mixed layer, lies a strongly stratified (near the surface) ocean, with a halocline sitting atop dense Arctic bottom water. With input from and outflow to the Atlantic on one side, and inflow from the Pacific on the other, this creates a vertical structure as depicted in the simplified schematic shown in Figure 1.3:

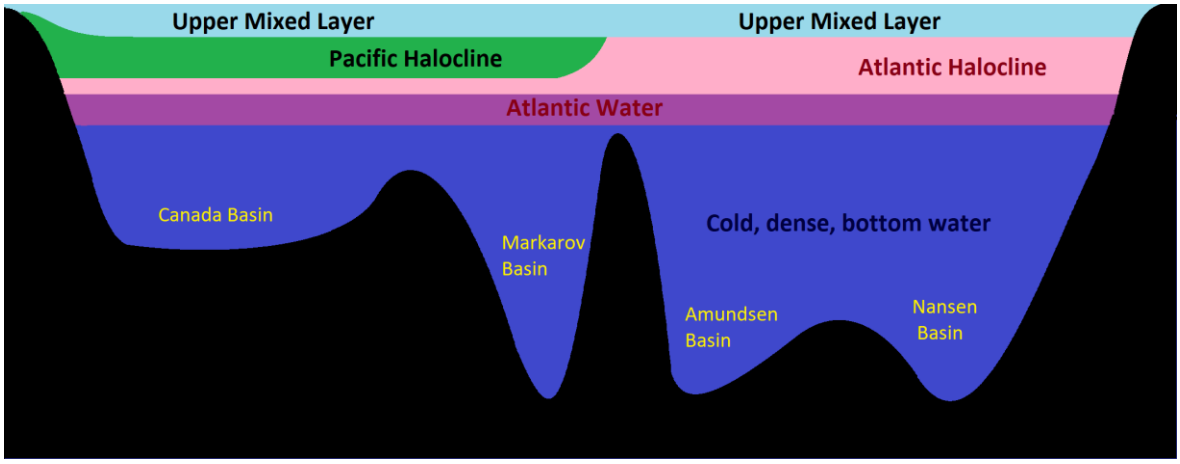

Figure 1.3 – Cartoon schematic of Artic stratification (not to scale).

On the Atlantic side of the Arctic, a fresh upper mixed layer sits above a cold halocline, with increasing salinity at depth due to brine rejection during the formation of sea ice (Aagaard et al., 1981; Rudels et al., 1996). Beneath this lies the warmer Atlantic layer, with cold dense salty bottom water beneath. The Pacific side of the Arctic Ocean is more complicated, with a fresher Pacific halocline positioned above the Atlantic waters. The Pacific layer consists of Pacific Summer Water between 50 – 100m depth, with Pacific Winter Water below this in the 100 – 150m range (Steele et al., 2004).

The dominant circulation feature in the Western Arctic is the Beaufort Gyre, which acts as a reservoir for Arctic freshwater and plays an important role in the dynamics of the Arctic in general (Proshutinsky et al., 2002). The importance of the Beaufort Gyre for the Arctic more generally, and an investigation into its freshwater sources and their changing advective pathways is presented in Chapter 3 of this thesis, (Kelly et al., 2019). Unlike the cyclonic boundary currents and deeper gyres, the Beaufort Gyre is an anti-cyclonic (clockwise) feature. This is because, while the main boundary currents in the Arctic Ocean are topographically steered and driven by geostrophic balance, the Beaufort Gyre is a wind driven circulation feature, and as such is highly sensitive to atmospheric forcing (Giles et al., 2012; Polyakov et al., 1999).

The atmospheric drivers of the Beaufort Gyre are the Beaufort High and the Aleution Low, semi-permanent high- and low-pressure atmospheric systems respectively. Anomalies in these pressure systems can have a profound effect on the Arctic Ocean, with a strengthened Beaufort High leading to a stronger Beaufort Gyre and more anti-cyclonic dominance in the surface layers of the Arctic Ocean, and vice versa (Overland, 2009).

Various metrics exist to quantify these large-scale atmospheric changes and their effect on the circulation of the Arctic Ocean. The Arctic Oscillation (AO) (Thompson and Wallace, 1998) is once such metric, with positive AO indices corresponding to low pressure over the Arctic and hence an anomalously cyclonic Artic Ocean, with negative indices associated with a more anti-cyclonic Arctic which favours a stronger Beaufort Gyre. Proshutinsky and Johnson (1997) sought to define a more

specific metric to describe the Arctic Ocean's response to changes in atmospheric forcing. Using a two-level barotropic model, anomalies in sea surface height were used to define the Arctic Ocean Oscillation index, which characterises the cylonicity or anti-cyclonicity of the Arctic Ocean with oppositely signed metrics – positive values corresponding to a stronger Beaufort Gyre. These large-scale metrics alone cannot capture the full detail of the Arctic Ocean circulation, as evidenced by the fact that they are not always oppositely signed, but have been found to be been found to be useful predictors of freshwater accumulation / release in the Arctic (Proshutinsky et al., 2002; Proshutinsky et al., 1999). Both the AO and AOO metrics are used in Chapter 5 of this thesis to put into context changes in Pacific to Atlantic connectivity pathways.

1.2.3. Pacific Water Pathways

Marine connectivity is driven by ocean currents, and in the following two subsections the circulation pathways of the waters which flow into the Arctic Ocean are described, beginning here with the Pacific pathways and moving onto Atlantic water circulation in the next section. Pacific Water enters the Arctic via the Bering Strait, where it plays an important role in the dynamics of the Western Arctic Ocean. The flow through the Bering Strait is highly variable between years and has a strong seasonal cycle, with mooring observations (over the period 2001-2011) recording a mean annual transport between 0.7 and 1.1 Sv (Woodgate et al., 2012). Recent years have seen this figure increase, up to a maximum of 1.2 Sv in 2014 (Woodgate, 2018).

An important feature of the Pacific inflow to the Arctic is that it brings 'fresh' water to the basin. Clearly, this is not fresh water in the literal sense, but compared to the much larger and saltier Atlantic contribution to the Arctic Ocean, Pacific water has a significantly lower salinity. A standard seawater reference salinity of 34.8 PSU (practical salinity units, a dimensionless quantity) is used to calculate the fresh water contribution to the Arctic. Relative to this reference salinity, the Pacific Ocean contributes 2030–3500 km^3 of freshwater to the Arctic per year (Aksenov et al., 2016; Woodgate et al., 2012). As discussed in section 1.2.2.2., this contribution is important for the stratification of the Western Arctic Ocean, and contributes to the fresh water storage / release cycle in the Beaufort Gyre (Proshutinsky et al., 2009).

The inflow of Pacific Water in the Arctic has been extensively studied in both models and observations (Aksenov et al., 2016; Hu and Myers, 2013; Timmermans et al., 2014; Thomas Weingartner et al., 2005), with three distinct pathways identified: one through Barrow Canyon, another through Herald Canyon, and a third pathway via the Herald and Hana Shoals (Timmermans et al., 2014), as illustrated in Figure 1.4 with yellow, red and magenta arrows respectively. Pacific inflow is comprised of three main water masses: summer Bering Sea Water (sBSW), winter Bering Sea Water (wBSW), and Alaskan Coastal Water (ACW), each of which have different characteristics.

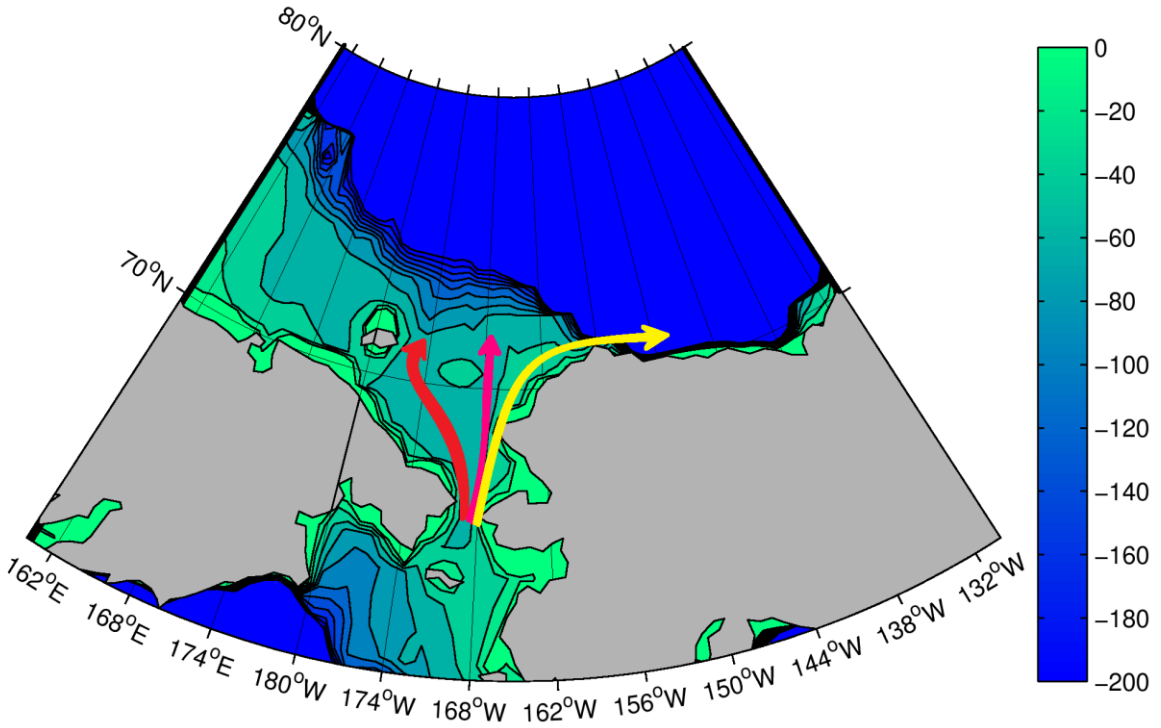

Figure 1.4 – Pacific water inflow pathways to the Arctic Ocean, after Timmermans et al. (2014). Red: inflow through Herald Canyon. Magenta: Inflow through the Central Channel via Herald and Hana Shoals. Yellow: Inflow through Barrow Canyon.

The lightest and freshest water mass is the ACW. The properties of the ACW are set by river runoff in the Gulf of Alaska and Bering Sea (Thomas J. Weingartner et al., 2005), including the Yukon River. ACW enters the Arctic Ocean via Alaskan Coastal Current (Appen and Pickart, 2012), before flowing through Barrow Canyon, following the eastward Beaufort shelf-break jet (Appen and Pickart, 2012; Nikolopoulos et al., 2009). The Beaufort shelf-break jet is a topographically steered geostrophic current that can be strengthened or weakened depending on the wind, and typically peaks during June to October (Lin et al., 2016). Depending on large-scale atmospheric forcing, the ACW can then reverse back to the west (Nikolopoulos et al., 2009; Steele et al., 2004) and continue into the Chukchi Slope Current (Spall et al., 2018), carry on towards the Canadian Archipelago, or become entrained into the Beaufort Gyre (Aksenov et al., 2016). There remains some uncertainty in the ultimate fate of ACW beyond this, including where/if it exits the Arctic Ocean via the Canadian Archipelago (Aksenov et al., 2016).

The other main water mass entering through the Bering Strait is Bering Sea Water, the properties of which vary seasonally, and hence is subset into summer Bering Sea Water (sBSW) and winter Bering Sea Water (wSBW) (Steele et al., 2004). Bering Sea Water (both summer and winter) is denser than Alaskan Coastal Water (Aksenov et al., 2016), and enters the Arctic Ocean via three main pathways; the Barrow Canyon along with the ACW, and through the Herald Canyon, and the Central Channel leading to the Hana Shoal (Aksenov et al., 2016; Steele et al., 2004). Some of this water then follows the Transpolar Drift towards the Atlantic (Aksenov et al., 2016), while another portion remains in the Canada Basin. The summer mode of the Bering Sea Water contributes to Beaufort Gyre and

circulates anti-cyclonically (clockwise) (McLaughlin et al., 2002; Steele et al., 2004). However, less is known about the behaviour of the winter mode, with different studies suggesting different schematics. Primarily anti-cyclonic (clockwise) circulation is proposed by Steele et al. (2004), while McLaughlin et al. (2002) proposed a dominant cyclonic pathway bringing wBSW to the Canadian Archipelago. It is well established that Pacific Water pathways vary interannually (Proshutinsky et al., 2002; Timmermans et al., 2014), but the exact pathways followed by different Pacific water masses is not fully known and remains an open research question (Aksenov et al., 2016).

1.2.4. Atlantic Water Pathways and the Arctic Circumpolar Boundary Current

The largest source of inflow to the Arctic is via the Atlantic Ocean, with Atlantic Water entering the Arctic via two pathways: the Eastern portion of the Fram Strait, and the Barents Sea Opening (Aksenov et al., 2010; Aksenov et al., 2011; Pnyushkov et al., 2015; Spall, 2013). A schematic of the Arctic inflow and circulation pathways is illustrated in Figure 1.5.

In contrast to the (comparatively) fresh inflow from the Pacific Ocean, the Atlantic contribution to the Arctic Ocean is saltier and denser (Aksenov et al., 2010). Once in the Arctic, the dominant circulation feature of Atlantic Water is the Arctic Circumpolar Boundary Current, hereafter ACBC (Aksenov et al., 2011). This can be split into two main branches, the Fram Strait and Barents Sea branches, which eventually join and flow cyclonically (anti-clockwise) around the Arctic shelf break, and in deep cyclonic gyres in the Eurasian, Makarov and Canada basins (Pnyushkov et al., 2015; Polyakov et al., 2011).

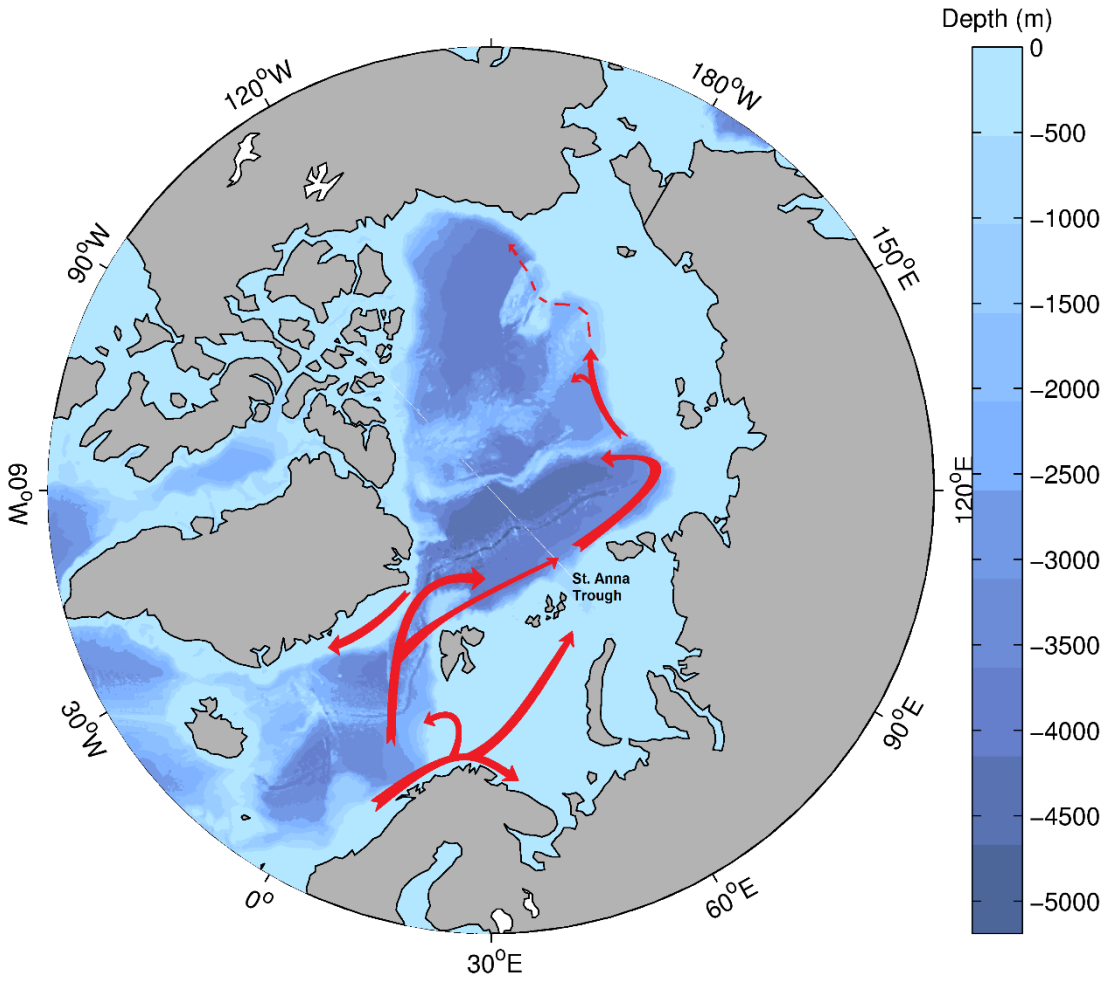

Figure 1.5 – Advective pathways of Atlantic inflow to the Arctic, based on Aksenov et al. (2011). Fram Strait and Barents Sea branches of ACBC shown, with presumed continuation of ACBC shown in dashed lines.

The Fram Strait inflow is complicated, with two pathways flowing either side of the Yermak Plateau to the north of Svalbard, before recombining east of the archipelago and continuing as a boundary current along the Eurasian shelf break (Rudels et al., 2015). As well as this, some water is recirculated in the strait, with outflow from the Arctic to the Atlantic taking place in the west of the Fram Strait (Beszczynska-Möller et al., 2012; Rudels et al., 2015). The total transport into the Arctic Ocean through the Fram Strait has been estimated as 6.6 Sv (Beszczynska-Möller et al., 2012), and is the dominant contributor to the Nansen Basin halocline (Rudels et al., 2015), where it circulates cyclonically (anti-clockwise) (Aksenov et al., 2011; Rudels, 2015; Rudels et al., 2015). Fram Strait branch inflow is advected eastward by the ACBC to the Amundsen and Makarov basins, where it also supplies the cyclonically circulating halocline water (Rudels et al., 2004).

As well as the deep inflow through the Fram Strait, Atlantic water enters the Arctic on the Eurasian shelf via the Barents Sea opening. The inflow varies between season and years, with a mean transport of 1.5 Sv (Skagseth et al., 2008), which is warm (4-6 °C) and salty (>35 PSU) (Rudels et al., 2015). This is complicated by a return flow just south of Svalbard, which exports cooled, denser water back towards the Atlantic at depth (Skagseth et al., 2008). Another contribution to the Barents Sea comes

from the Norwegian Coastal Current, which brings 1.8 Sv of fresher (34.3 PSU) water into the Barents Sea (Skagseth et al., 2011). Barents Sea water is then advected north-east towards the St Anna Trough, where it joins the Fram Strait inflow as part of the Arctic Circumpolar Boundary Current (Aksenov et al., 2011; Dmitrenko et al., 2015). The Barents Sea branch is cooler and fresher than the Fram Strait inflow by the time the Barents Sea branch joins the ACBC due to the influence of net precipitation (Rudels et al., 2004; Rudels et al., 2015). Furthermore, because of brine rejection during sea ice formation, cold dense water is produced in the Barents Sea (Aksenov et al., 2010). The Barents Sea branch is confined to the Eurasian shelf slope before becoming the main source of water to the Atlantic layer of the Canada Basin halocline, below the Pacific halocline (Rudels et al., 2004). Open research questions concerning the Atlantic inflow to the Arctic Ocean include the ultimate fate of Atlantic waters beyond the Chukchi Cup (Aksenov et al., 2011).

1.3. Marine Connectivity

The aim of this thesis is to contribute to the understanding of marine circulation connectivity in the Arctic Ocean. Marine connectivity describes how ocean currents link different regions of the global ocean, and specifically how material dissolved or suspended in the water column are dispersed over time (Condie et al., 2005). This includes ecological connectivity, which describes the exchange of species between spatially separated subpopulations (Cowen et al., 2006; Cowen and Sponaugle, 2009), as well as the dispersal salt, nutrients, and pollutants advected by currents (Condie et al., 2005).

Properties of the ocean are governed not only by local forcing (for example: wind, radiative fluxes, precipitation, river runoff), but also by influences further afield due to advection. The interconnectivity of the ocean, mediated by ocean currents, means that changes in one part of the ocean can have significant impacts in other regions downstream – this is the concept of circulation connectivity. A large-scale example of this is the Atlantic Meridional Overturning Circulation (AMOC), which transports heat towards the polar regions in the upper ocean and brings cooler, denser water back south at depth. Understanding the timescales and pathways associated with advective transport is essential for a full understanding of the ocean system. In the Arctic Ocean, connectivity between the large continental shelf and the deep ocean are important for nutrient cycles (Kipp et al., 2019; Whitmore et al., 2019). Regions downstream of the Arctic Ocean are affected by the dynamics of the Arctic itself: for instance, it has been demonstrated that the salinity anomalies found in the North Atlantic are directly linked to the connectivity between the Beaufort Gyre and Atlantic Ocean, owing to the Beaufort Gyre's role as an important fresh water reservoir in the Arctic Ocean (Proshutinsky et al., 2002). In Chapter 3 of this thesis (Kelly et al., 2019), the upstream connectivity of the Beaufort Gyre is investigated. In addition to the purely physical motivation for studying Arctic connectivity, two key applications of connectivity are discussed here: its role in the advection of marine pollutants (S. Kelly et al., 2018) and the importance of ecological connectivity in a changing Arctic Ocean (Kelly et al, 2020).

1.3.1. Marine Pollutants

With the Arctic environment rapidly changing (Overland and Wang, 2013; Wang and Overland, 2012), understanding the pollution issues which could potentially affect it is a growing concern. As a result of the rapid recession of Arctic sea-ice, interest in using the Artic for commercial shipping has increased (Aksenov et al., 2017; Liu and Kronbak, 2010; Schøyen and Bråthen, 2011). A heightened risk of accidental oil spills (or other pollutants being discharged as a result of shipping activity) has been identified as one potential consequence of this. Should an oil spill occur, its behaviour and ultimate fate is a function of the physical and chemical properties of the type of oil spilled, and where the spill occurs (Afenyo et al., 2015; Mariano et al., 2011). Interactions between oil and ocean dominate its spread in the immediate aftermath of a leak (Mariano et al., 2011), before oceanic advection

becomes the dominant driver on longer timescales (Afenyo et al., 2015). The importance of advection motivates understanding this problem from a connectivity point of view when considering the long term fate of an oil spill.

A recent real-world example of a tanker spill occurred in the East China Sea: in January 2018, the Sanchi oil tanker was involved in a collision, resulting in its cargo of natural gas condensate being released into the ocean (Chen et al., 2019). Based on the work presented in Chapter 4 of this thesis (S. Kelly et al., 2018), Lagrangian experiments were performed to assess the strength of connectivity between the spill site and regions downstream, in part as a demonstration of the validity of the approach used in (S. Kelly et al., 2018). This is further discussed in Chapter 6.

But, other than oil spills, what other pollution risks are (or are predicted to be) present in the Arctic? The Arctic Monitoring and Assessment Programme (AMAP) has identified four main categories of pollutant which pose a threat to the Arctic; persistent organic pollutants (POPs), chemicals of emerging concern, heavy metals, and radioactive pollution (AMAP, 2015).

POPs are long lasting chemicals primarily brought to the Arctic via long range atmospheric transport (Halsall, 2004; Newton et al., 2014). The use of the use of POPs has been controlled in many cases, and as a result, much of the contamination caused is as a result of historic rather than ongoing use (AMAP, 2015). This is in contrast with pollutants in the 'chemicals of emerging concern' category, the uses of which are widely unregulated. This category includes halogenated flame retardants and some currently used pesticides (AMAP, 2015; Ma et al., 2015). High concentrations of brominated flame retardants have been discovered in organisms in East Greenland and Svalbard, suggesting that western Europe and eastern North America are major sources of Arctic BFRs (de Wit et al., 2010).

Heavy metals including mercury are a major concern in the Arctic food web as they can accumulate in predators and pose a risk to human health. Coal burning and gold mining are key sources of mercury in the Arctic atmosphere, and emissions due to both of these have recently increased (AMAP, 2015). Concentrations of atmospheric mercury have been measured, and a strong seasonal dependence has been observed. The highest concentrations are found in the spring, suggesting that freshwater inflow from rivers is the dominant source of mercury in the Arctic (Fisher et al., 2012). Additionally, with sea ice cover reducing and more open water in the Arctic, mercury is increasingly able to enter the Arctic Ocean directly from the atmosphere (Moore et al., 2016).

The final source of pollution identified by the AMAP is radioactivity. Atmospheric weapons tests were performed over the Arctic during the Cold War, nuclear waste has historically been dumped into the Arctic (particularly around Novaya Zemlya in the Barents/Kara Seas), and accidents such as the 2011 incident at Fukushima could also lead to radioactive material being transported to the Arctic (AMAP, 2015). Measurements of radioisotope concentrations in Arctic organisms suggests that the environmental impact of this dumping has been small (Fisher et al., 1999) and it is unlikely to be of serious concern to human health.

Efforts to monitor and assess pollutants in the Arctic are ongoing, including the EU ArcRisk project (Carlsson et al., 2018; Pacyna et al., 2015). The role of ocean circulation on pollutant transport has been noted as playing an important role in the distribution of pollutants across the Arctic, and as such pollutant dispersal is sensitive to the effect of climate change on Arctic currents (Kallenborn et al., 2012; Pacyna et al., 2015). However, it has also been recognised that indirect consequences of climate change, such as shifts in land and resource use, are likely to be the main driver of shifts in Arctic pollutant distributions in the immediate future (Kallenborn et al., 2012). An example of this would be the increased risk of oil spills from increased shipping along the Northern Sea Route that motivated S. Kelly et al. (2018).

1.3.2. Ecological Connectivity

Another element of marine connectivity is ecological connectivity. When considering the full ecological connectivity of the ocean, the picture becomes yet more complicated: ecological connectivity, describing the transport of the biota in the oceans, includes both passive circulation connectivity and active migratory connectivity (Popova et al., 2019). Passive circulation connectivity accounts for the transport of species due to ocean currents (Popova et al., 2019; van Gennip et al., 2017), and active migratory connectivity describes the species swimming from one region to another, e.g. for feeding and breeding (Cowen et al., 2006; Webster et al., 2002). Indeed, passive circulation connectivity and active migratory connectivity are not fully independent of each other, as even larger species which actively migrate typically have a planktonic stage (Selkoe and Toonen, 2011). For smaller, planktonic species, or those which are static in their adult lives but rely on oceanic advection to disperse their larvae (e.g. corals), passive connectivity is the dominant mechanism in distributing organisms away from their parents (Raitsos et al., 2017).

A common theme linking all these forms of marine connectivity is the importance of understanding the timescales on which different regions are connected to each other, and the specific pathways that link them. Every part of the global ocean is connected to every other part, if one waits long enough, but for ecologically important processes, the timescales involved can be short. Understanding whether or not different regions are ecologically connected depends on the timescales on which they are connected (Jönsson and Watson, 2016), and the timescale required depends on several factors, including the species in question. For species with a planktonic stage early in their lifecycles, its pelagic larval duration (PLD) describes the main limit for how long passive circulation connectivity describes their migratory behaviour (Selkoe and Toonen, 2011; Shanks, 2009). This limiting timescale varies considerably between species, from weeks to years, (Bradford et al., 2015; van Herwerden et al., 2006). Other influences, including the survivability of different advective pathways - which in turn can depend on various factors like light, temperature and availability of nutrients (Arteaga et al., 2014; Cowen and Sponaugle, 2009) – can also impact the limiting timescale for ecological connectivity of marine organisms.

In the case of marine connectivity for oceanic pollutants, the timescale required for the pollutant to be degraded or dispersed such that it becomes sufficiently diluted that it has sufficiently limited environmental impact. For example, in the case of oil spills, the timespan required for biodegradation or evaporation to the atmosphere provides the limiting timescale for assessing connectivity between a spill site and downstream locations (Afenyo et al., 2015). Just as the limiting timescale for ecological connectivity depends on the species in question, the limiting timescale for pollutants is affected by the pollutant in question, as well as external factors including the environment in which the pollutants are released, and whether an attempt has been made to clean up the contamination – again using oil as an example, the application of dispersants can affect the spreading of the pollution (Afenyo et al., 2015; Mariano et al., 2011).

Marine connectivity can be an inherently interdisciplinary problem, and many different approaches working in synergy are required to fully understand the entire picture. Observational techniques including remote sensing (Raitsos et al., 2017) and genetic profiling (Bach et al., 2019) contribute to our understanding of ecological connectivity, but are limited by the availability of observations – a particular problem in the Arctic, where the harsh conditions lead to sparse in-situ observations compared to other parts of the ocean, and the high latitude limits the availability of satellite observations. This thesis focuses on the modelling aspect of connectivity: using high resolution ocean models that are capable of resolving physical processes important for transport, such as eddies, help contribute to our understanding of marine connectivity. There are a multitude of ways that ocean models can be used to answer questions of marine connectivity, and these are discussed in section 1.3. A Lagrangian modelling technique, described in Chapter 2, is employed in three case studies here, all part of the wider question of marine connectivity in the Arctic Ocean:

- Chapter 3, Kelly et al. (2019): *On the origin of Water Masses in the Beaufort Gyre*
- Chapter 4, Kelly et al. (2018): *Lagrangian Modelling of Arctic Ocean Circulation Pathways: Impact of Advection on Spread of Pollutants*
- Chapter 5, Kelly et al. (2020): *They Came From The Pacific: How changing Arctic currents could contribute to an ecological regime shift in the Atlantic Ocean*

In each case, a Lagrangian particle tracking approach is used to investigate a facet of Arctic marine connectivity. Chapter 4 was the first to be written, and focusses on a potentially very important ecological issue, using marine connectivity to investigate the potential impact of oil spills from the Northern Sea Route shipping pathway. Chapter 3 focuses on the physics of the Arctic, and uses a similar technique to investigate connectivity pathways in the Beaufort Gyre region. Finally, in Chapter 5, we return to ecological connectivity, assessing how non-native species may be able to traverse the Arctic Ocean to reach the Atlantic.

In Chapter 6, more general lessons learned in the preceding research chapters are discussed, as well musings on how they could have been improved, and ideas for follow-up research are presented.

Furthermore, in the second section of Chapter 6, further research separate from the three main papers is discussed. Two main projects are featured here, both of which use similar methodology to that developed throughout the other results chapters of this thesis (albeit both non-Arctic examples). This includes detailing of my contribution to Popova et al. (2019), *Ecological connectivity between the areas beyond national jurisdiction and coastal waters: Safeguarding interests of coastal communities in developing countries*, in which I performed the Lagrangian particle tracking experiments and calculated the metrics used to quantify the strength of circulation connectivity between the high seas and various developing countries' coastlines. Additionally, results of experiments to assess the fate of the Sanchi oil spill are presented: in January 2018, a real-world oil spill occurred in the East China Sea. Lagrangian experiments, analogous to those presented in Chapter 4 were performed to assess the potential fate of spilled pollutants. This also serves to demonstrate the validity of the approach used in S. Kelly et al. (2018), and the results of these experiments, which received notable media coverage, are discussed in Chapter 6.2.2.

1.4. Different Approaches to Studying Connectivity: Lagrangian or Eulerian?

Connectivity can be assessed in various different ways: either observationally or with models, and from either a Lagrangian or Eulerian perspective (van Sebille et al., 2018). A modelling approach is used throughout this thesis, but it is perhaps more intuitive to explain the difference between the Lagrangian and Eulerian approaches from an observational point of view.

Consider a fixed mooring recording temperature, salinity, and measuring currents in the ocean. This is an example of Eulerian data: it provides a time-series for each variable measured, at one specific point in space. With a series of different moorings in different locations, it is possible to build up a well sampled picture of the ocean. Examples of this include the four fixed Beaufort Gyre Observing System moorings used by Lique et al. (2014) to investigate heat fluxes in the Canada Basin on the Arctic Ocean, and the Bering Strait mooring array utilised by Woodgate (2018) to quantify the Pacific inflow to the Arctic. In any case, an Eulerian approach investigates how certain variables evolve in time at various fixed points.

The alternative to this outlook is a Lagrangian approach. A real-world example of Lagrangian data would be Argo drifters (de Boisséson et al., 2010; Hadfield et al., 2007). Like mooring arrays, drifters record temperature, salinity and other variables. However, rather than producing a time series of each variable for a fixed spatial point, Lagrangian measurements produce a time series along the trajectory of the drifter. In the Arctic, Lagrangian observations often come from ice tethered profilers (ITPs), which drift with sea ice rather than ocean currents, but still measure the properties of the water masses below. Examples pertinent to Chapter 3 of this thesis, focussing on the Beaufort Gyre region include

the work of Timmermans et al. (2017) who used ITP data to describe the properties of the Arctic Halocline, and Zhao et al. (2016) who quantified the increasing eddy density in the Beaufort Gyre. Peralta-Ferriz and Woodgate (2015) used a combination of Eulerian (fixed moorings) and Lagrangian (ice tethered profilers) techniques to characterise the mixed layer depth across the Arctic Ocean, which was used for validation purposes in Chapter 3 (Kelly et al., 2019).

When using models to investigate ocean circulation and connectivity, we can also take either a Lagrangian or Eulerian approach. Ocean models work by dividing the ocean into a grid, and, based on reanalysis forcing data, solving the primitive equations that govern ocean currents (Madec, 2014). These equations are solved at some fixed time interval, sub-hourly in the case of NEMO, and are highly computationally expensive to run, producing large volumes of data. For this reason, only mean flow fields are typically saved – 5 daily means in the model used throughout this thesis. As these flow fields are not static, the effect of time-varying currents must be addressed to answer questions of connectivity. One method is to re-run the model for each experiment, incorporating passive Eulerian tracers into the model and solving the tracer evolution equation via Eulerian meshes. But first, we discuss the offline Lagrangian approach used here.

Lagrangian modelling is analogous to throwing a large number of rubber ducks into the ocean – as actually happened when thousands of bath toys were accidentally released into the ocean in 1992 (Boxall, 2009). By recording when and where the ducks wash up on beaches, we learn about the connectivity timescales linking those places to the initial spill site. But what if those ducks had GPS trackers, were neutrally buoyant, and weren't directly affected by external factors like the wind? We could track the routes they (and hence the water parcels they're entrained in) took to reach different locations. With a large number of ducks, we can build up a statistically significant picture of the connectivity between the spill site and other regions, what pathways the ducks took to reach those regions, and what the associated timescales are. This is essentially how Lagrangian modelling works – except that the rubber ducks are virtual particles, and rather than releasing them into the real ocean, we release them in the model flow field to quantify how they are connected to other regions downstream. Unlike ducks in the real ocean, we are also able to track our virtual particles backwards in time – i.e. follow currents upstream, to find out where the particles came from. It is also possible to record other variables output by the model (temperature, salinity, pressure etc.) along the trajectory of any given particle.

Many software packages are available for this (van Sebille et al., 2018), which make use of pre-calculated model velocity fields. In the research chapters presented here, Ariane (Blanke and Raynaud, 1997) is used, but alternatives include TRACMASS (Döös et al., 2017; Kjellsson and Döös, 2012) and Parcels (Lange and van Sebille, 2017). The basic principle behind the Ariane particle tracking software is that discrete particle trajectories are calculated via a bilinear interpolation of currents in the model grid cell, and an analytic method is used to translate particles throughout the cells. The time required for each particles to reach the edge of each model cell is calculated, with the

shortest time corresponding to the route the particle actually takes. This is repeated for the next grid cell, using the exit point from the adjacent cell as its start point. The formal derivation of the sub-gridscale translation calculations is presented in the appendix of Blanke and Raynaud (1997). The output of these experiments is then saved as a series of latitude and longitude coordinates at a user specified frequency.

Depending on the context of the scientific question being asked, these results can be interpreted in different ways. For instance, using hindcast model results, it is possible to create probabilistic maps showing how likely waters from one area are to be connected to some other region within a defined timescale. This – with appropriate caveats and limitations – can be interpreted as a proxy for risk of a region being contaminated by a pollutant spill (S. Kelly et al., 2018; Main et al., 2016). For example, it is important to note that, using this approach, the trajectories of water parcels rather than real life particles of contaminant. Interpreting these results necessitates discussion of which pathways are realistic or unrealistic: when considering the effect of upwelling and downwelling in the case of pollutants with a non-neutral buoyancy, how realistic are trajectories with significant depth changes? At what point does the dispersal of pollutants mean that dissolved contaminants become too diluted to be significant?

Other examples, such as ecological connectivity, require an understanding of an individual species' biology (e.g. environmental tolerances or requirements) to be combined with the Lagrangian data to fully answer specific questions (Popova et al., 2019). Pelagic larval duration – the amount of time a species exists as plankton before being able to propel itself – is a species-dependant limiting timescale (Selkoe and Toonen, 2011; Shanks, 2009). Other limiting factors, such as the temperature or availability of nutrients along advective pathways, need to be considered as well, and these also vary depending on the species in question.

The main advantage of offline Lagrangian modelling over an online Eulerian approach is that it is relatively computationally inexpensive. The NEMO model used here, ORCA0083-N006, was run with a timestep of 200 seconds. In order to reduce storage requirements, only five-day means of the output are saved. These five-day means are computationally expensive to produce, but having been pre-calculated, are now readily available. The saved average circulation fields can then be used to drive offline Lagrangian particle tracking experiments.

The disadvantage of this approach is that the purely kinematic method employed by Ariane means that diffusive and processes are lost (van Sebille et al., 2018). In principle, this could be partially accounted for by adding a Brownian random walk element to trajectories in cases where this is important. Furthermore, by using mean velocity fields, short lived variations in currents are averaged out. This removes structure and variability that would otherwise be present in the sub-hourly online velocity fields, reducing the accuracy of experimental results. A potentially important negative consequence of this is that, by averaging out the fastest short lived currents, anomalously rapid advective pathways are lost. In contexts where the absolute most rapid pathways are important, such as in

Chapter 5, this is a limitation that must be acknowledged (Kelly et al., 2019). An alternative approach would be to run Lagrangian particle tracking experiments 'online', in order to use the higher temporal resolution that the model is run with. However this is prohibitively computationally expensive as it would require multiple re-runs of the full ocean model.

The main alternative to Lagrangian modelling is using passive Eulerian tracers – named as such because the ocean model uses Eulerian meshes to numerically solve the tracer evolution equations. A significant advantage of this approach is that by using a continuous tracer, the uncertainty due to discretising water masses into a finite number of individual trajectories is removed. Furthermore, by using an online run of the model, diffusion and convection are accounted for, whereas offline Lagrangian approaches are purely advective. Various methods exist for interpreting these experiments (Mouchet et al., 2016), and passive tracer experiments have been performed in the Arctic Ocean to investigate Pacific Water circulation (Aksenov et al., 2016) and freshwater pathways (Dukhovskoy et al., 2016). The major drawback with this approach is that it requires the ocean model to be re-run for each experiment. In the case of experiments which require multiple releases, and especially those requiring tracking for a longer timescales, this is not always practical.

This motivates a Lagrangian approach for experiments which require such an approach, as is the case for the three case studies described in this thesis. Previous research has made use of a similar Lagrangian particle tracking technique owing to its computationally inexpensive nature (Hu and Myers, 2013; Lique et al., 2010; Main et al., 2016; Robinson et al., 2017; Robinson et al., 2016; Srokosz et al., 2015; van Gennip et al., 2017). Using the trajectories produced by Lagrangian particle tracking experiments, it is possible to extract meaningful information about changes in ocean circulation using appropriately defined metrics. For instance, van Gennip et al. (2017) characterised projected shifts in coastal connectivity by defining metrics to quantify the latitudinal and longitudinal shifts in recruitment areas for coastal waters, as well as on-shelf retention. Robinson et al. (2014) defined metrics based on the duration of time which Lagrangian particles remained below a threshold depth, in order to quantify the likelihood of successful carbon sequestration in the Southern Ocean. Metrics to quantify flow fields based on Lagrangian data are also routinely applied to observational studies, for example the Lyapunov exponent used by Liu et al. (2018) in order to identify divergent in flows in the Gulf Stream.

Specifically in the Arctic Ocean, Lagrangian approaches - using the same particle tracking software as in this research – have been employed to answer a variety of questions. Examples of this include Lique et al. (2010), where a particle tracking approach was used to investigate the sources of water exported from the Arctic to the Atlantic Ocean. The validity of Lagrangian modelling, relative to its more computationally intensive Eulerian cousin, was demonstrated by Hu and Myers (2013), which found Pacific inflow pathways in agreement with those found by Aksenov et al. (2016) using a passive tracer approach. This exemplifies the value of Lagrangian particle tracking to understand questions of marine connectivity in the Arctic Ocean, as presented in the results chapters herein.

Chapter 2: Methods

2.1. The NEMO Model

Various aspects of the Earth system are governed by equations which are, in principle, solvable, so long as the values of certain variables are known. Theses equations give a solution for a specific point in space and time, but if these equations could be solved everywhere, a complete picture of the system would emerge. In practice, it is not possible to solve these equations at all points of space and time. For this reason, models are used to discretise the system onto a fixed grid, and solve the relevant equations at these specific grid points and at a discretised time interval. From quantifying ocean currents (Madec, 2014) to describing the influence of space weather on the chemistry of the upper atmosphere (C. W. Kelly et al., 2018), computer models are a useful tool to understand the behaviour of complex systems.

All models require surface forcing to calculate how the ocean responds to different atmospheric conditions. This typically comes in the form of reanalysis data – i.e. observation based datasets that have been interpolated – also using models - in order to create a global dataset to drive (or "force") the model. Using this forcing data, based on historic atmospheric conditions, it is possible to build up a hindcast representation of ocean circulation at some point in the past. Other forced models use projections of how the atmosphere may look in the future (e.g. based on different CO_2 emission scenarios) to investigate how ocean circulation could change in the future (van Gennip et al., 2017). Alternatively, it is possible to run fully coupled rather than forced models – using output from an atmospheric model to drive an ocean model, allowing the modelled ocean and atmosphere to evolve with each other after initial conditions have been specified.

With regards to modelling the ocean, the objective of an ocean model is to solve the equations which govern ocean circulation and water mass transformations. These equations are referred to as the primitive equations, specifically the Navier-Stokes equations which describe the flow of incompressible fluids and a non-linear equation of state which couple temperature to seawater velocities (Jackett and Mcdougall, 1995).

Throughout this thesis, the Nucleus for European Modelling of the Ocean (NEMO) Model is utilised to investigate changing ocean connectivity. NEMO works by solving the aforementioned primitive equations on a curvilinear tri-polar grid (ORCA), designed to avoid the singularity of the North Pole (Madec and Imbard, 1996). Specifically, the grid employed by NEMO is the three dimensional Arakawa C-grid (Arakawa and Lamb, 1977).

A schematic of a NEMO grid cell is shown below in Figure 2.1. Using this structure, different properties are calculated at different points of each grid cell: temperature and salinity are calculated in the centre of each grid cell, while modelled ocean velocities are calculated at the six faces of each

cell. Using the c-grid on the tri-polar ORCA mesh, a ‘north fold’ stitches the grid together across the Arctic Ocean.

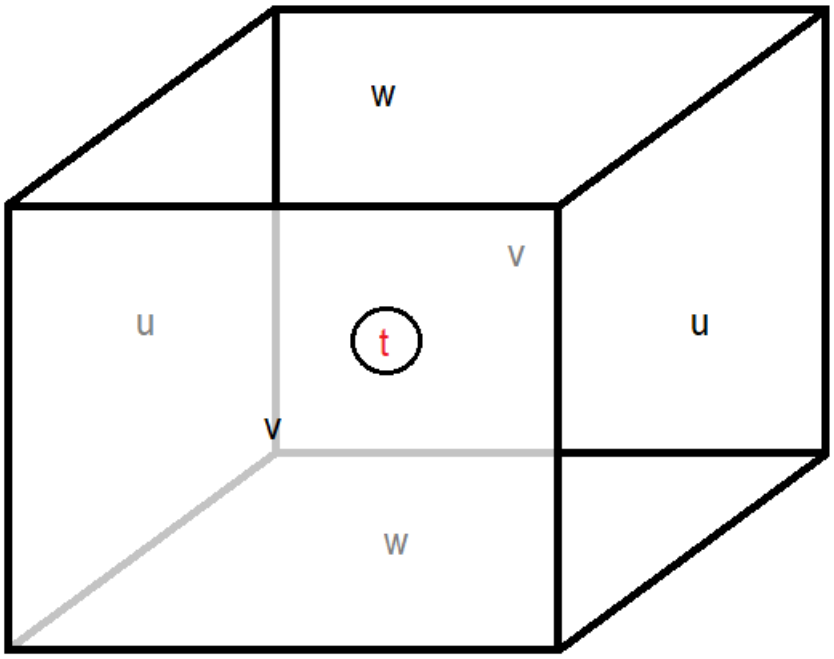

Figure 2.1: Schematic of a model grid cell using the Arakawa C-grid. Modeled velocities are calculated at each grid cell face, in the zonal (u), meridional (v) and vertical (w) directions respectively. Temperature and salinity are calculated in the center of each grid cell (t).

NEMO employs a non-linear free surface to account for the non-static nature of sea surface height, and partially-filled bottom cells to ensure the bathymetry is as realistic as possible, avoiding unnecessarily large step changes. Mixing in NEMO is simulated by the turbulent kinetic energy (TKE) mixing scheme (Blanke and Delecluse, 1993), and the behaviour of active tracers is described by the total variance dissipation (TVD) advection scheme (Madec, 2014).

In order to solve the primitive equations, several simplifying assumptions are made:

- 1) The spherical Earth approximation: The Earth is not a perfect sphere, and it is not of uniform density. However, this correction is small and for sake of simplification, the NEMO model assumes that gravitational geopotential surfaces are spherical and hence gravity is exactly aligned with Earth’s radius.

- 2) The thin shell approximation: We assume that the depth of the ocean is negligible relative to the radius of the Earth. (The radius of the Earth is approximately 600 times larger than even the depth of the Marianas Trench, and over 1,000 times larger than the deepest part of the Arctic Ocean.)

- 3) The turbulent closure hypothesis: Turbulent fluxes, representing the effect of small-scale processes on the largescale, are expressed in terms of large-scale features.

- 4) The Boussinesq approximation: Variations in fluid properties other than density, ρ, can be neglected, and the only non-negligible consequence of density variations is their contribution to the buoyancy force (i.e. terms multiplied by acceleration due to gravity, g).
- 5) The Hydrostatic hypothesis: Convective processes are removed from the Navier-Stokes equation and parameterised rather than being solved explicitly. This means that the vertical momentum equation can be expressed as the balance between vertical pressure gradient and the buoyancy force.
- 6) Incompressibility hypothesis: The ocean is an incompressible fluid, i.e. , where u, v, and w, are the three dimensional components of ocean velocity in the x, y, and z directions respectively.

Given these simplifying assumptions, NEMO solves the Navier-Stokes equations at discretised grid points on the Arakwa C-grid shown in Figure 2.1. for given boundary conditions. This model is then coupled to an ice model (LIM2), as detailed in the next subsection.

2.1.1. LIM2 Ice Model

The oceanic component of NEMO is coupled to an ice model, and in this case the Louvian-la-Neuve Ice Model (LIM2) was used (Fichefet and Maqueda, 1997; Goosse and Fichefet, 1999). LIM2 models sea ice as a compressible 2-dimensional fluid, based on viscous-plastic rheology that describes how external forces cause the ice to deform (Bouillon et al., 2009) and Semtner thermodynamics (i.e. two layers of ice and a single layer of snow). The sea ice model uses two categories of ice cover: consolidated ice and leads, and is driven by both wind forcing and modelled ocean currents. LIM2 is coupled to the liquid ocean part of the model at each ocean timestep, with heat and salt fluxes exchanged between ice and ocean, and lateral momentum is transferred with wind and ocean stresses weighted by sea ice concentration. The modelled sea ice imparts a non-linear quadratic drag onto the ocean surface based on the shear between ice and water. The sea ice component of NEMO has been validated extensively, and found to simulate Arctic sea ice with good skill (Aksenov et al., 2017; Johnson et al., 2012; Wang et al., 2016).

2.1.2. Boundary Conditions

The surface boundary conditions of the NEMO model come in the form of the ocean-atmosphere boundary, the ocean-ice boundary, and the ice-atmosphere boundary. The lower boundary is the ocean floor, based on bathymetry from Amante and Eakins (2009) in the deep ocean and Bourdalle Badie et al (2012) in shallow areas and with a partially filled bottom step of the model to avoid sharp changes in elevation. As a global ocean model is used throughout this this, there are no horizontal

boundary conditions to note, other coastlines and the input of riverine freshwater (added as a salinity anomaly in the upper layer of the model).

The majority of the global ocean is ice free, and the ocean is forced directly at the ocean-atmosphere interface. Based on Drakkar Forcing Set (DFS), this encompasses ocean-atmosphere freshwater fluxes from precipitation / evaporation, heat fluxes from longwave / shortwave radiation, and momentum transfer from wind stress acting on the ocean surface (Brodeau et al., 2010).

In the Arctic, we have the added complication of sea ice. This brings in extra boundary conditions between the coupled ice and ocean model (e.g. freshwater fluxes from the formation and melting of sea ice), and it also means that atmopshere and ocean are not free to directly interact, so and heat fluxes and momentum transfer are mediated by the sea ice. Crucially for the surface advective pathways investigated throughout this this thesis, this means that, in ice covered areas, the boundary conditions for momentum transfer are given by ice-ocean stress, a damped version of the wind stress that directly forces surface currents elsewhere in the ocean.

2.1.3. Choice of Model Run

There were two versions of the 1/12° NEMO model available at the National Oceanography Centre: ORCA0083-N001 and ORCA0083-N006. Both of these were forced with reanalysis data from the Drakkar Forcing Set (DFS). Different versions of the DFS forcing were used in the two runs: DFS4.1 (1978-2006) and DFS5.1.1 (2006-2010) in N001, and DFS5.2 throughout N006. The Drakkar Forcing Set is derived from ERA40 reanalysis, featuring 6 hourly winds, sea level atmospheric temperature and humidity, daily radiative fluxes (both shortwave and longwave), and monthly means for precipitation and evaporation and precipitation taken from CORE2 reanalysis. Riverine freshwater input, added at the surface layer of the model, is taken from a monthly climatology (Brodeau et al., 2010; Timmermann et al., 2005).

During preparation for the first paper of this thesis, a comparison of how the two runs performed in the Arctic was undertaken. Surface circulation was validated against reanalysis data from satellite Dynamical Ocean Topography (DOT) inferred by the CPOM (Centre for Polar Observation and Modelling) Envisat (2003-2011) (Armitage et al., 2016): Using reanalysis sea surface height as a proxy for large scale barotropic circulation, and comparing this to barotropic streamfunction calculated for both iterations of the model and modelled SSH in both cases. In both cases, the model showed good skill at reproducing the large-scale features of Arctic Ocean circulation. (See Figure 2 of S. Kelly et al. (2018)).

When comparing modelled sea-ice, the newer iteration (N006) was found to be superior at reproducing more realistic spatial distributions of sea-ice. This was the main differentiating factor in terms of Arctic skill and, for this reason, N006 was chosen to be used throughout the experiments described in the three papers of this thesis. Output from this model is available as 5-day means. Using this pre-

calculated model output, various Lagrangian particle tracking experiments were designed. The merits and drawbacks of such an approach are discussed in Section 1.3, while the software used (Ariane) is discussed below in section 2.2.

2.2. Ariane Lagrangian Particle Tracking

In section 1.3, the relative merits of Lagrangian and Eulerian approaches to studying marine connectivity are discussed. The main advantage of an offline Lagrangian approach is that, by utilising pre-calculated model output, the computational cost of experiments is significantly reduced. This is especially true of experiments which need to be repeated with releases at various different times, as the computational cost of re-running a high resolution global circulation model multiple times would be prohibitively expensive. However, the main drawback of a Lagrangian approach compared to online Eulerian tracers is that processes such as convection and diffusion are lost, and only the advective signal is retained.

Ariane works by reading in pre-calculated ocean velocity fields from saved output of the NEMO model. As discussed in Section 2.1., the NEMO model uses an Arakawa C-grid (Arakawa and Lamb, 1977), and hence has six velocities associated with it: two vertical, from the top and bottom of the cell, two meridional and two zonal from the remaining faces. Ariane uses a bilinear interpolation to of the velocity field within each cell, and hence calculates the time required to reach the edge of the cell in each of the zonal, meridional and vertical directions. The shortest timescale is the physically important one, and gives the time and place at which a particle exits the cell. This process is then repeated for that particle in the next grid cell, using the exit point from the previous cell as its start location, and so on for all particles as is required. The mathematical formulation of this method is presented in the appendix of Blanke and Raynaud (1997).

Ariane can be used in both a ‘qualitative’ and a ‘quantitative’ mode. Throughout this thesis, the qualitative mode is used, whereby discrete trajectories for infinitesimally small particles are calculated based on model streamlines. An alternative approach, using the quantitative mode results in a distribution function for each grid cell, describing the mass transfer from a large number of Lagrangian water parcels instead of the discrete trajectories used here.

The output of an Ariane comes as an array of longitudes, latitudes and depths for each particle, at requested frequency (daily was typically used here). Various metrics can be used to extract meaningful information from this data, from simple measures of distance travelled, to the circulation footprints defined in Chapter 4 to the ‘traps’ used in Chapters 3 and 5 to classify distinct connectivity pathways. Each of the results chapters has its own methodology subsection where these metrics are discussed in greater detail.

Chapter 3: On the Origin of Water Masses in the Beaufort Gyre

This chapter was published in *JGR: Oceans* as Kelly et al. (2019). I am the author of this work, with my co-authors contributing supervisory guidance, and Figure 3.4 being produced by Andrey Proshutinsky. Interpretation of these results is my own.

Abstract

The Beaufort Gyre is a key feature of the Arctic Ocean, acting as a reservoir for fresh water in the region. Depending on whether the prevailing atmospheric circulation in the Arctic is anticyclonic or cyclonic, either a net accumulation or release of fresh water occurs. The sources of fresh water to the Arctic Ocean are well established and include contributions from the North American and Eurasian rivers, the Bering Strait Pacific water inflow, sea ice meltwater and precipitation, but their contribution to the Beaufort Gyre fresh water accumulation varies with changes with the atmospheric circulation. Here, we use a Lagrangian backward tracking technique in conjunction with the 1/12° resolution NEMO model to investigate how sources of fresh water to the Beaufort Gyre have changed in recent decades, focusing on increase in the Pacific water content in the gyre between the late 1980s and early 2000s. Using empirical orthogonal functions (EOF) we analyse the change in the Arctic oceanic circulation that occurred between the 1980s and 2000s. We highlight a "waiting room" advective pathway that was present in the 1980s and provide evidence that this pathway was caused by a shift in the center of Ekman transport convergence in the Arctic. We discuss the role of these changes as a contributing factor to changes in the stratification, and hence potentially the biology, of the Beaufort Gyre region.

Plain Language Summary

The Beaufort Gyre, a clockwise ice and water circulation in the Arctic Ocean, is an important feature of the Arctic because it stores a large volume of fresh – relative to the rest of the ocean - water. Depending on the atmospheric circulation driving it, the Beaufort Gyre can either accumulate or release this fresh water. The sources of relatively fresh water to the Beaufort Gyre are Arctic rivers, the Bering Strait, and melting sea ice. By tracking virtual particles in a high-resolution ocean model, we investigate how these sources have changed in recent decades, and identify a change in the pathways bringing them to the Beaufort Gyre. This change in ocean circulation was found to correlate with a change in the mixed layer depth in the model.

3.1. Introduction

The Beaufort Gyre is an anticyclonic oceanic gyre in the Canada Basin that stores a large volume of fresh water in the Arctic Ocean, and as such has a significant role in fresh water accumulation in the Arctic, changing upper ocean stratification and, potentially, affecting sea ice retreat and the dynamics of the Arctic Ocean as a whole (Aksenov et al., 2016; McPhee et al., 2009). In order to understand how the Arctic Ocean has changed in recent decades, as well as how it may change in the future, it is vital to understand the mechanisms of the fresh water accumulation, specifically advective pathways of the fresh water in the Beaufort Gyre. Changes in circulation pathways are important for bringing different, potentially warmer and less dense water masses to the Beaufort Gyre (Aksenov et al., 2017; Karcher et al., 2012), which in turn can change stratification and mixed layer depth, modifying the nutrient content of the region (Popova et al., 2013). Stronger stratification inhibits mixing (Rippeth et al., 2015) and reduces the amount of nutrients that can be brought to the upper ocean where there is sufficient light penetration in summer and phytoplankton can grow. Weakening of the stratification, on the other hand, promotes mixing and hence increased biogeochemical activity (Carmack et al., 2016). Changes in stratification and mixing affect heat transfer from the intermediate depth Atlantic Water (AW) to the surface (Polyakov et al., 2010; Polyakov et al., 2017): a more strongly stratified ocean allows less heat to be brought to the surface (and vice versa), thus may play an important role in sea ice retreat in all seasons in the next few decades (Aksenov et al., 2017; Polyakov et al., 2010; Stroeve et al., 2018). For these reasons, studying the changes in advective pathways of water masses can provide valuable insight into understanding a contributing factor to changes in the dynamics and biogeochemistry of the Beaufort Gyre and the Arctic Ocean as a whole.

Previous work (Giles et al., 2012; Polyakov et al., 1999; Proshutinsky et al., 1999) has established that the net accumulation or release of fresh water in the Beaufort Gyre is largely driven by quasi-decadal oscillating patterns in the wind forcing. The ocean's response to these variations is a pronounced bi-modal state of the Arctic Ocean with stronger or weaker Beaufort Gyre, i.e. the Arctic Ocean Oscillation (AOO) index (hereafter AOO). Proshutinsky and Johnson (1997) define the AOO from changes in sea surface heights using a coupled ice-ocean shallow-water barotropic model. The AOO describes whether the barotropic component of the circulation is dominated by cyclonic or anti-cyclonic motion, with the former shown (Proshutinsky et al., 2002; Proshutinsky et al., 2009) to correlate with release of fresh water from the Beaufort Gyre and the latter associated with fresh water accumulation.

A net increase in Beaufort Gyre freshwater content has been observed over the two decades between 1992 and 2012, with increased precipitation and melting of sea ice contributing factors to this (Krishfield et al., 2014; Proshutinsky et al., 2009; Rabe et al., 2014). Meteoric water (riverine input, glacial melt, and precipitation minus evaporation) also contributes to the freshwater budget of the Arctic Ocean. The meteoric water imports / exports to the Arctic Ocean are approximately balanced (Alkire et al., 2017), suggesting that the observed fresh water increase in the Canada Basin is due to

a spatial redistribution of fresh water across the Arctic (Alkire et al., 2017; Wang et al., 2019). The mechanism driving the accumulation of fresh water during anticyclonic atmospheric forcing is Ekman pumping (Aksenov et al., 2016; Proshutinsky et al., 2002; Proshutinsky et al., 2009). Anticyclonic wind drives an Ekman transport to convergence which results in the observations of increasingly domed sea surface heights in the Beaufort Gyre (Armitage et al., 2016; Giles et al., 2012).

Since 1948, the AOO has typically varied with a period of approximately 10-15 years up until 1996. However, this relationship has broken down in recent years, with the AOO being in the anticyclonic circulation regime since 1997 until 2015 and beyond (Proshutinsky et al., 2015). In addition to quasi-oscillatory variability in the Arctic, anthropogenic climate change is having secular effect on the region: 'Arctic amplification' of global warming is seeing temperatures in the polar region increase twice as rapidly as the rest of the world ocean (Cao et al., 2017; Cohen et al., 2014; Graversen et al., 2008). Historically, the Beaufort Gyre has played a 'flywheel' role in influencing the dynamics of the Arctic Ocean as a whole (Proshutinsky et al., 2002), maintaining the negative salinity anomaly in the region and facilitating the dominant anticyclonic geostrophic circulation in the Canada Basin throughout the year, even when the wind forcing becomes cyclonic.

While accumulation of fresh water, and in particular a freshening of the upper mixed layer in the Beaufort Gyre region can act to make the ocean more strongly stratified, there is a competing influence in the form of sea ice cover. Sea ice mediates the reaction between the atmosphere and ocean which limits how much wind driven mixing is possible in the Arctic. With Arctic sea ice rapidly declining, and ice-free summers predicted by mid-century (Boe et al., 2009; Overland and Wang, 2013; Wang and Overland, 2012), more open water allows for increased wind driven mixing and hence would counter the effect of fresh water accumulation and decrease the stratification in the Beaufort Gyre region. These dynamical processes compete with thermodynamic mechanisms which increase the thickness of the mixed layer in winter (during intense new ice formation in the regions free of ice during summer) and increase water stratification in summer due to ice melt and direct heating of the upper ocean layers by solar radiation.

Here, we aim to investigate how the advective pathways bringing fresh water to the Beaufort Gyre region have changed during this period of rapid change for the Arctic Ocean. We then discuss the role of these dynamic changes in potentially contributing (alongside other, thermodynamic processes) to changes in stratification and mixing in the Beaufort Gyre region, and the potential impact for the biology of the region.

We aim to address three main questions. Firstly, how have the sources of water to the Beaufort Gyre changed since 1980? Secondly, how have the advective pathways bringing Pacific water to the gyre changed? And thirdly, what is causing this change? Additionally, we investigate variability in the modelled mixed layer depth across the Arctic over the same period. We discuss the link between this and the change in circulation pathways as a potential contributing factor to variations in the mixed layer depth.

3.2. Methodology

3.2.1. NEMO model and Ariane particle-tracking

The model used in experiments here is the Nucleus for European Modelling of the Ocean (NEMO), coupled to the Louvain-la-Neuve Ice Model (LIM2) sea-ice model (Fichefet and Maqueda, 1997; Goosse and Fichefet, 1999; Madec, 2014). This version of NEMO has 75 depth levels (31 of which are in the top 200m, with resolution as fine as 1m in the uppermost layer), and has a horizontal resolution of approximately 1/12-degree, giving it a grid length-scale of 3-5 km in the Arctic, making it eddy permitting throughout the Arctic, though not fully eddy resolving on the shelves (Nurser and Bacon, 2014). NEMO is forced at the air-sea interface using the version 5.2 DRAKKAR forcing set (DFS) (Brodeau et al., 2010). This includes 6 hourly winds, temperature and humidity from ERA40 reanalysis, daily longwave and shortwave radiative fluxes, and monthly means for precipitation and river runoff from CORE2 reanalysis. The DRAKKAR forcing set utilizes a monthly climatology for riverine input (Brodeau et al., 2010; Timmermann et al., 2005), with fresh water added at the surface level in this configuration of NEMO. The model was run with this DFS forcing between 1958 and 2015.

For our experiments, we use the Ariane software (Blanke and Raynaud, 1997) using model output from NEMO. Ariane works offline, reading in the 3-D velocity fields saved in the NEMO output, interpolating to solve for particle translation through model grid cells, and saving particle positions daily. The output from the global NEMO model used here (run ORCA0083-N006) is saved as 5-day means. Ariane can be run both forwards and backwards in time, and it is the backwards tracking that we employ here.

Ariane, or other Lagrangian packages, are an especially useful tool for investigating the results of high resolution ocean models where running the full model with online tracers would be prohibitively computationally expensive. However, this approach does have limitations. Small scale processes such as diffusion and mixing, which are parameterized in the model, cannot straightforwardly be factored into Lagrangian analysis when investigating advective pathways (Wagner et al., 2019).

The NEMO-LIM2 model and Ariane software are more completely described in (S. Kelly et al., 2018), where validation of the surface circulation in this model configuration was performed. Comparing modelled sea surface heights (SSH), observed SSH (Armitage et al., 2016), and the barotropic streamfunction of modelled circulation showed good agreement between the data sets. Additionally, EOF (see Section 3.2.3) analysis of modelled and observed SSH over the period 2003-2012 shows the same dominant non-seasonal mode of variability in the region observed by satellite. (See supporting information, and Armitage et al. (2016).)

NEMO has previously been validated extensively in the Arctic Ocean. For instance, modelled stratification and water mass types show good agreement with observed Arctic stratification for other NEMO configurations (Aksenov et al., 2016; Janout et al., 2015; Luneva et al., 2015). Additional validation of the modelled mixed layer in the 1/12 degree configuration of NEMO used here is provided in the supporting information to this paper. There we compare the modeled mixed layer depth to that found in observations (Peralta-Ferriz and Woodgate, 2015), and find good model skill. The largest discrepancy was found to be an overestimate of the summer mixed layer depth in the Barents Sea, away from the focus of this research.

Previous work has used Ariane in conjunction with various different configurations of the NEMO model in the Arctic Ocean. Lique et al. (2010) used a global ¼ degree ORCA025 configuration together with a backtracking approach to assess the sources of water exitnig the Arctic Ocean via the Fram and Davis Straits. Hu and Myers (2013) used a regional Arctic configuration of NEMO alongside Ariane to investigate Pacific water inflow pathways during a model spin-up, producing inflow pathways consistent with more recent online passive tracer experiments (Aksenov et al., 2016). Finally, S. Kelly et al. (2018) investigated advective pathways in the context of pollutant spills from the Northern Sea route using Ariane in conjunction with the same 1/12 gloabl NEMO model used here.

3.2.2. Lagrangian Experiment Design

The sources of fresh water for the Arctic Ocean are well established: Siberian and Alaskan Rivers, Pacific Ocean inflow, sea-ice meltwater, and precipitation (e.g. (Aagaard and Carmack, 1989). Less is known about the advective pathways associated with these sources and, in particular, the freshwater components by sources in the Beaufort Gyre region. Thus, the goal of this work is to use a Lagrangian particle tracking technique, in conjunction with a high-resolution ocean model, to investigate water mass (particles representing them) pathways and their temporal variability.

We conducted a set of numerical experiments focusing on the origin of the water in the Beaufort Gyre. To investigate this, we release ‘particles’ throughout the Beaufort Gyre region, and, using the Ariane software, track them backwards for 10 years to their sources. 10 years was chosen to ensure that the majority of particles would have left the gyre within the experiment – this, rather than the timescale to reach each source is the limiting factor in the experiment. This approach allows us to attribute fractions of the fresh water to the Mackenzie River, Pacific Ocean, and Eurasian shelf, but it does not permit investigation of pathways associated with meltwater or precipitation.

Our Lagrangian particles were initially uniformly distributed over a region bounded by 169°W, 129°W, 81°N, and a southern boundary taken to be the 300m depth contour. (See Figure 3.1a for each horizontal release location.) We define this to be our ‘Beaufort Gyre region.’ Particles were released at 5 depth levels: 1m, 21m, 44m, 82m and 140m (chosen to correspond to integer depth

levels in NEMO that sample different layers of the Beaufort Gyre). One particle was released at each horizontal location (total of 156 per depth level) and each depth to give a total of 780 particles per release. Releases were performed monthly between 1980 and 2013 (giving a grand total of 9360 particles per year), and each particle's location was recorded daily for ten years. Since particle trajectories were followed backwards in time, NEMO output was required for the period 1970 to 2013.

Because of the large number of trajectories in our experimental design, we employ 'traps' in our analysis to establish specific pathways taken by trajectories. This enables us to log their timing and quantity through particular regions. Essentially, for each simulated time point, we automatically determine whether trajectories are located within a series of small domains; the traps. We have positioned these in the locations of known circulation pathways, and where they permit clearly distinct routes to be distinguished. Three traps were used in this experiment, to identify particles which were tracked back to three different sources: Pacific, Eurasia, and the Mackenzie River. See Figure 3.1 for a visual representation of these traps.

Particles of Pacific origin are straightforward to define – any particle with a recorded position south of 65°N and with longitude between 150°E and 150°W was classified as Pacific. Secondly, any particles which were tracked back to a trap south of 75°N and between 120°E and 170°E or south of 80°N and between 30°E and 120°E were marked as originating from the Eurasian shelf. Thirdly, a trap based on the plume of the Mackenzie River was defined – particles (which had not already been attributed to either the Pacific or Eurasia) were considered of Mackenzie origin if they spent at least one timestep between 68°N and 70.5°N and between 132°W and 138°W (see Figure 3.1b).

In addition to our three traps, we counted the number of particles which still remain in our Beaufort Gyre region (as defined previously) after 10 years of backtracking, as well as the number of particles which did leave the Gyre but were not attributed to any of the 3 sources using the methodology described above. These are assumed to either have not left the Gyre (due to our rather strict definition of the Beaufort Gyre region), or to be en route to one of the other traps at the time the experiment ended.

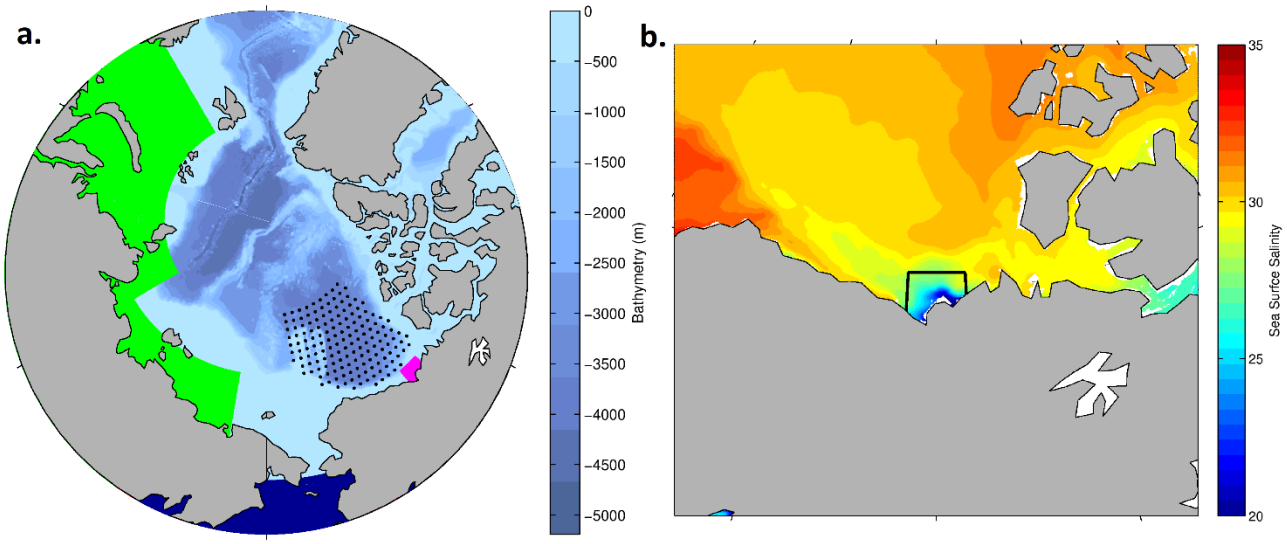

***Figure 3.1**: **1a.** Experiment design. Black dots show the Beaufort Gyre (BG) region where particles were initialized at 5 different depth levels. The colored regions represent the traps used to define sources of BG water, as used for classifying Lagrangian trajectories: Pacific (dark blue), Eurasia (green), Mackenzie River (magenta). Background color scale shows bathymetry. **1b.** shows modelled sea surface salinity (1997 annual mean – illustrative choice of a year with approximately neutral AOO conditions) in the Mackenzie River region, used to define the Mackenzie River 'trap.' The black box in Figure 3.1b is the same as the magenta box from Figure 3.1a.*

3.2.3. Analysis Techniques

Firstly, we compare the number of particles tracked back to each source for each year of particle releases. Secondly, we investigate the subset of particles which originate from the Pacific Ocean separately to highlight a change in advective pathways. For the Pacific, we calculate the year in which particles cross the Bering Strait (regardless of when they were initially seeded in the Beaufort Gyre.) Then, looking at each of the 5 release depths individually, we calculate the concentration of particles throughout the Arctic for particles that cross the Bering Strait in each year. Empirical orthogonal function (EOF) analysis is then performed to compare how these concentrations vary between years.

EOF analysis is a widely employed technique that can be used with spatial and temporal data to highlight different modes of variability which are independent (orthogonal) of each other. It has been used in various Arctic studies, for example in the context of observed SSH patterns across the Arctic (Armitage et al., 2016), and we use the EOF technique to investigate modelled changes in SSH here. This method is particularly useful for identifying temporal trends and determining whether spatial areas vary in or out of phase with one another.

This is achieved by taking a three dimensional variable (latitude, longitude and time), and, by an orthogonal transformation, converting it into eigenvalues and eigenvectors that describe the variance in the data. The first mode of the resulting EOF is the eigenvector that describes the largest amount of the variance. The second mode is the function which describes as much of the remaining variance as possible, and so on for n-1 modes, where n is the number of time slices analyzed.

The result of the EOF analysis is three variables for each mode: a 2-dimensional field describing the spatial pattern of variability, a dimensionless EOF index for each time slice, and the fraction of the variability for that mode. In general, each time slice is described by taking the mean spatial pattern of a given field (e.g. concentration of trajectories), and adding the spatial pattern for each EOF mode multiplied by the respective EOF index for that time slice.

For instance, for some spatial variable X, which is recorded at t points in time, we can calculate t-1 EOF modes. Then, we can write:

$$X(t) = \langle X \rangle + \Sigma\, EOF_n \times index_n(t)$$

Where $\langle X \rangle$ is the mean value of X over all t, and EOF_n and $index_n$ are the spatial fields and EOF indices for each EOF mode. As the EOF procedure is designed to capture as much of the variance as possible in the first few modes, the EOF modes for higher n can be neglected: in all the cases where EOF analysis was deployed here, the 1st mode was sufficient to describe the majority of the variability.

As well as applying this technique to the concentrations derived from our Lagrangian experiments to highlight how the advective pathways have changed, EOF analysis is applied to SSH and mixed layer depth (MLD) fields output from the annual model means. This is done to explain the reasons for the shift in advective pathways, and to explore potential consequences linked to that change in advection.

3.3. Results and Discussion

3.3.1 Variability of sources of Beaufort Gyre water

We begin by analyzing the sources of Beaufort Gyre fresh water, and their variability, both temporally and by depth. We start by considering all particles launched in a given year at each depth level. Figure 3.2 shows a stacked bar chart for each of the release depths, displaying how many particles we attributed to each source (or none at all) for each year:

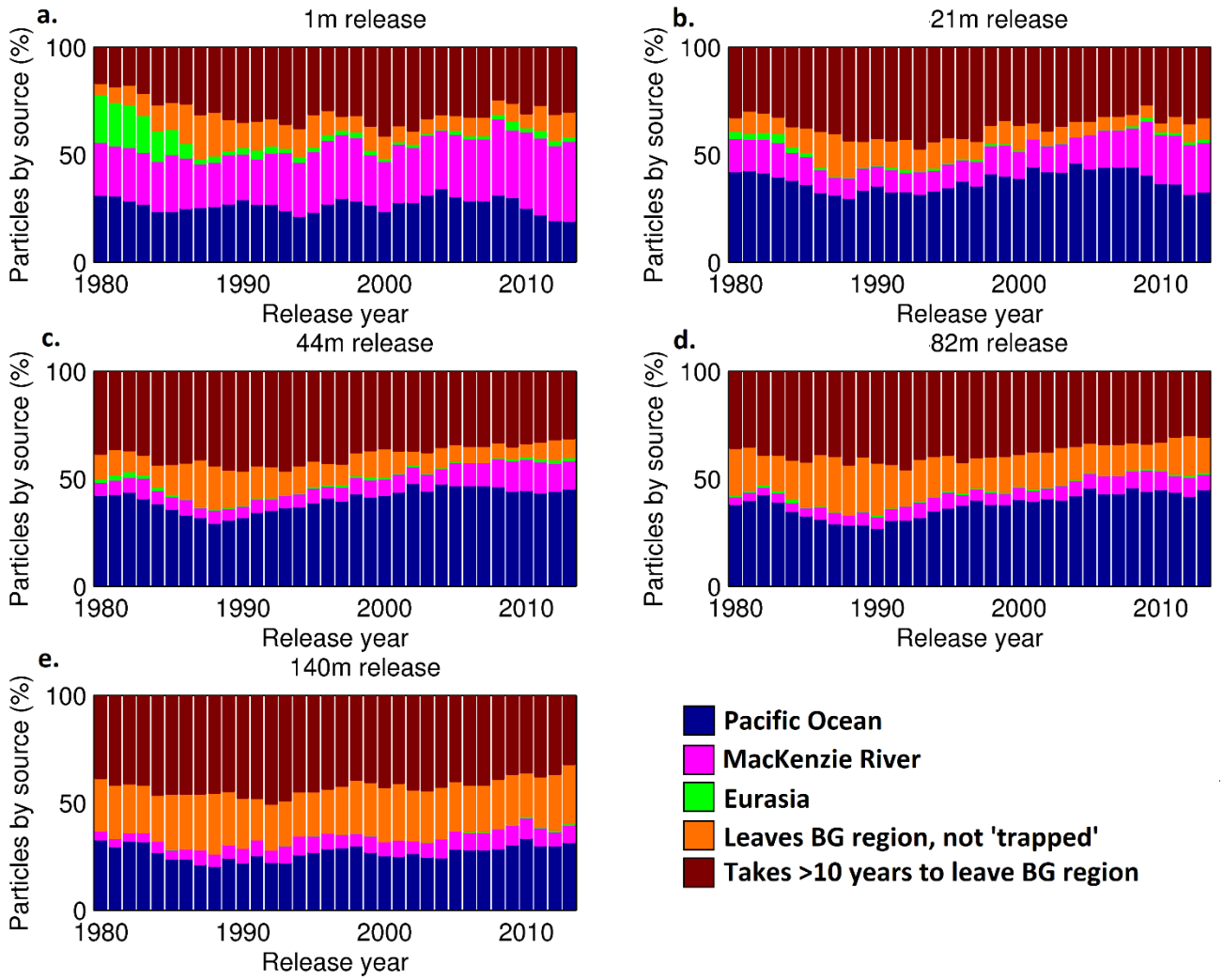

Figure 3.2: *Relative importance of each source to the Beaufort Gyre region after 10 years of backtracking, for the period 1980 – 2013. Dark blue = Pacific, magenta = Mackenzie River, green = Eurasian shelf, red = did not leave BG region, orange = left BG region, but uncategorized. This is shown for each of the 5 depth levels studied: 2**a.** Surface releases; 2**b.** 21m releases; 2**c.** 44m releases; 2**d.** 82m releases; 2**e.** 140m releases*

In Figure 3.2, the years along the x-axis correspond to the years in which particles were initially released. Due both to the advective timescales required to go back from the gyre to one of our three sources, and the fact that particles can persist in the gyre for many years (in many cases, for the full ten years they are tracked for – see the red bars) the year that each particle was released does not directly equate to the year in which it entered the Beaufort Gyre.

From Figure 3.2, it is clear that Pacific Ocean (dark blue) is the dominant source of particles in all years. 34% of all trajectories are tracked back to the Pacific Ocean, and the Pacific dominates most strongly (41% of all trajectories) for releases at 44m depth, which is in the Pacific layer of the Beaufort Gyre. We note the trend of the Pacific contribution increasing from the late 1980s and throughout the 1990s, which is especially prominent in the 44m and 82m releases. However, it is important to note that this does not necessarily imply that it is the dominant source of fresh water to the Beaufort

Gyre – each particle backtracked to the Pacific Ocean represents a much smaller freshwater contribution than a particle backtracked to the Mackenzie River. From observations (Woodgate, 2018), it is known that the freshwater discharge from the Bering Strait (2000 – 3000 km^3 $year^{-1}$) is an order of magnitude larger than the discharge from the Mackenzie River (300 km^3 $year^{-1}$), which is in agreement with our experiment results showing that the majority of trajectories can be traced back to the Bering Strait.

Given that particles traced back to Pacific Ocean must have passed over the Chukchi Plateau, which is only approximately 50m deep, and that particles initially seeded at the 82m and 140m depth levels were found to come from the Pacific, the question of how they reached those depths are inevitably raised. As they circulate backwards around the Beaufort Gyre, they were found to spiral up to shallower layers as they were backtracked to the Pacific. This corresponds to Pacific Water being pumped to these greater depths via the helical circulation pathways, as described in an idealized case by Timmermans et al. (2014).

The contribution of the Mackenzie River is more important at the surface of the Beaufort Gyre region relative to the Mackenzie contribution at greater depths. 27% of trajectories from the 1m release are tracked to the Mackenzie River, however this diminishes in importance in the deeper layers (14%, 8%, 6% and 7% for 21m, 44m, 82m and 140m releases respectively). In contrast, the contribution of Eurasian shelf waters - including inputs from Eurasian rivers - is negligible in all layers in almost all years investigated (1.6% of all trajectories), aside from a contribution to the surface layer in the early 1980s. Due to the small, typically negligible number of particles reaching the Siberian shelf, we do not attempt to consider the relative contribution of the Siberian rivers but acknowledge this as a potential avenue for future research.

The red and orange bars in Figure 3.2 correspond to those particles which either never leave the gyre (red) or leave but have not yet reached another box (orange).

To summarize, the two main results that we can glean from this analysis of sources of Lagrangian particles:

1) The Beaufort Gyre is strongly layered by advective source. The vertical structure of the Beaufort Gyre region is well described (Davis et al., 2016; Lique et al., 2014; Steele et al., 2004) with a fresh upper layer above the Pacific halocline and finally the Atlantic layer at the bottom. This structure is apparent in Figure 3.2, with the majority of Mackenzie and Eurasian particles in the surface release, Pacific particles dominating the 44m and 82m releases (41% and 40% respectively), and a marked decline in Pacific particles from the 140m release (27%), which corresponds approximately to the base of the Pacific layer in the Canada Basin (Steele et al., 2004).

2) The contribution of Pacific water to the Beaufort Gyre has increased since the late 1980s. This trend is most obvious in the 44m and 82m layers, where the Pacific contribution increased by 43% in these layers between 1988 and 2000. This trend is in agreement with observations which have

noted an increase in Pacific inflow to the Arctic via the Bering Strait over the same period (Woodgate, 2018).

3.3.2. Changing Pathways: The "Waiting Room"

To investigate how the circulation pathways have changed between the 1980s and present day, we focused on the contribution from the Pacific Ocean using only the subset of trajectories that crossed the Bering Strait. To get around the problem of particles remaining in the Beaufort Gyre for several years before eventually leaving, we re-categorized them based on the year in which they crossed the Bering Strait rather than the time of their initial release. Particles tracked to other sources (or none) are disregarded in this analysis. As particles were released every year between 1980 and 2013 before being backtracked for 10 years, Bering Strait crossings occur every year from 1970-2013. To avoid biasing the results with under sampled years (e.g. crossing in 1971 are only possible from the 1980 or 1981 releases, and in 2012 only from the 2012 or 2013 experiments), only particles which crossed the Bering Strait between 1980 and 2003 are considered.

Considering only these particles, we divided the Arctic into a 1° (lon) x 0.5° (lat) grid (to make approximately square 3000 km^2 grid cells in the Beaufort Gyre region) and calculated the density of trajectories passing through each cell, weighted by area of each grid cell. These densities were calculated for each year (by Bering Strait crossing) 1980 – 2003, and an empirical orthogonal function (full description in Section 3.2.3) analysis was performed to characterize the variability of the particles' trajectories.

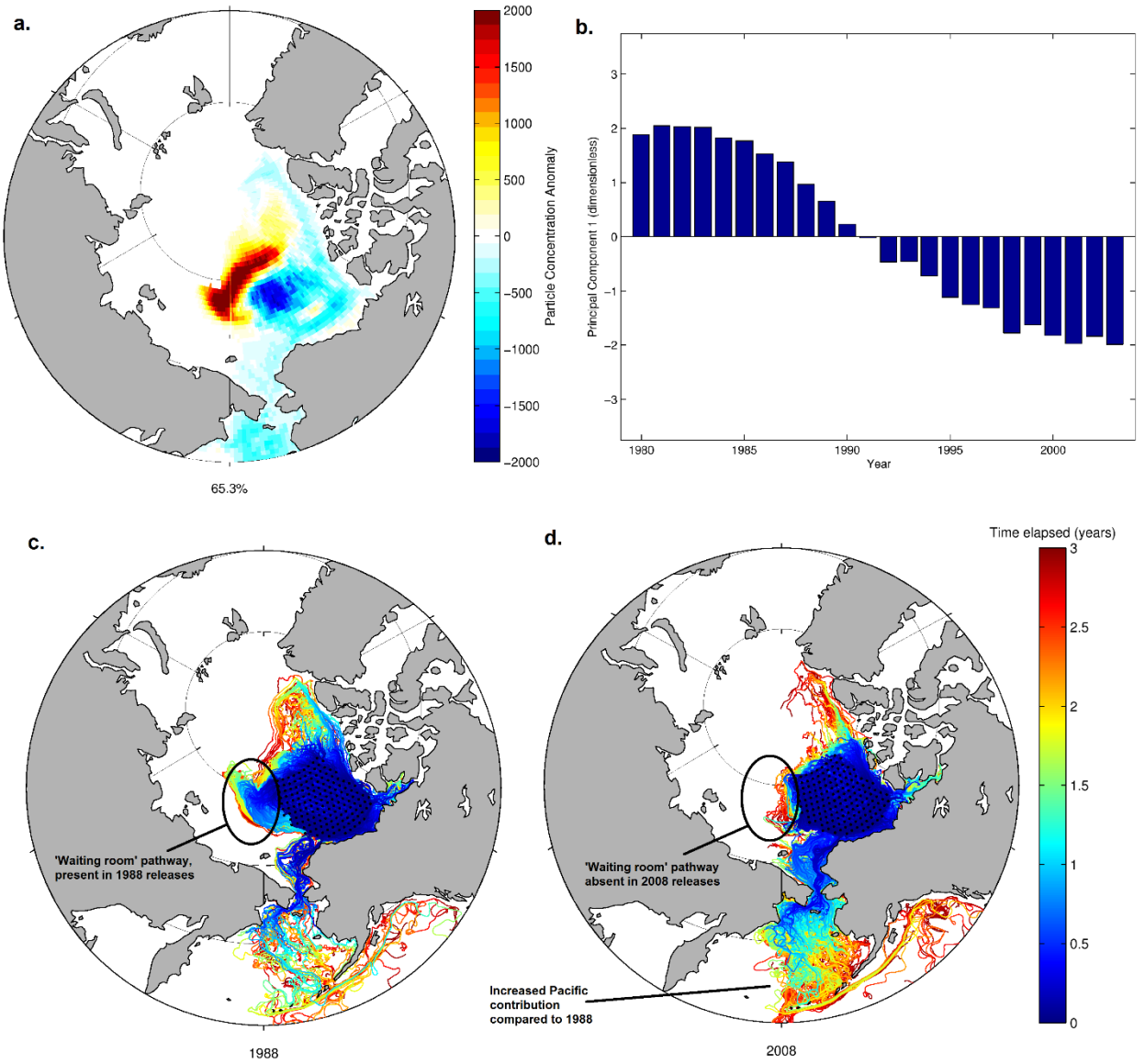

Figure 4.3: 3a: *Spatial pattern of 1st mode of EOF analysis of trajectory densities for particles tracked back to the Pacific Ocean.* ***3b.*** *EOF indices for the first EOF mode. Note that here we classify particles based on the year they crossed the Bering Strait, regardless of when they were initialized. This mode describes 65.3% of the variability of Pacific inflow to the Beaufort Gyre. Years with positive indices correspond to more trajectories flowing through the red regions in 3a, and fewer through the blue. Vice-versa is true for years with negative indices.* ***3c.*** *Comparison of the first three years of Lagrangian trajectories backtracked from 1988 (waiting room) and* ***3d.*** *2008 (no waiting room) respectively. Color of trajectories denotes the time that each particle has been backtracked for.*

Figure 3.3a shows the first mode characterizing 65.3% of variability of the trajectory densities; blues (in both the Beaufort Gyre region and the Pacific Ocean) being negative and reds positive. The interpretation of this map and the indices shown in Figure 3.3b, is that in years with positive indices, more trajectories pass through the red regions and fewer through the blue. Years with negative indices correspond to an above average number of trajectories in the blue regions of Figure 3.3a, but a decrease in the red regions.

The indices for this mode (Figure 3.3b) go from positive in the 1980s to “increasingly” negative throughout the 1990s. As both the Pacific Ocean and Beaufort Gyre region are shown blue in Figure 3.3a, this implies that the Pacific contribution to the Beaufort Gyre in our experiments was reduced in years with positive indices, and increased in years with negative indices. As the indices in Figure 3b go from positive to negative from the 1980s to the 1990s, this suggests that Pacific contribution to the Gyre did indeed increase throughout the 1980s and 1990s, in agreement with the trajectory analysis presented in Figure 3.2.

More interestingly, we see that the increase in Pacific contribution to the Beaufort Gyre also correlated with a change in circulation in the Arctic Ocean: this can be identified from the red region in Figure 3.3a. An increase in particles flowing through this area is out of phase with both particles in the Pacific Ocean and in the Beaufort Gyre.

The interpretation of this is as follows: when the dominant Arctic circulation is less favorable for water to accumulate into the Beaufort Gyre, the water that does come through the Bering Strait is directed into this red region. This contrasts with the years with a favorable circulation, in which Pacific Water is permitted to flow directly into the Beaufort Gyre itself. We term this red area the ‘waiting room’, as it represents a prolonged pathway by which Pacific Water flows to the Beaufort Gyre in years when Pacific Water is less readily able to make it to the Gyre. This waiting room is the dominant feature, accounting for the majority (65.3%) of the differences between the years studied. As Figure 3.3b shows, this feature has diminished in importance throughout our experiments, and suggests a secular trend whereby this pathway is no longer available in a changed Arctic Ocean.

This is further illustrated in Figures 3.3c and 3.3d, where an example of a favorable year for Pacific Water entering the Gyre (2008 release) is compared to an unfavorable year (1988 release). In this case, only the first three years of backtracking are shown, with colors of trajectories denoting how much backtracking time has elapsed since each particle was released. Blues are plotted on top of reds. The waiting room, present in the 1988 release but not in 2008, is clearly visible.

3.3.3. Cause of the Waiting Room

To investigate the dynamics of favourable / unfavourable years for Pacific Water entering the Beaufort Gyre, and to validate the model results, Ekman transport was calculated based on observed wind, ice concentration, ice motion and geostrophic currents. This was done for the years with the most positive (1983-85) and most negative (2003-05) EOF indices, corresponding to least and most favourable for Pacific Water accumulation in our Lagrangian experiments. This is presented in Figure 3.4. External forcing factors accounted for calculations of Ekman transport include geostrophic wind velocities, sea ice concentration and drift, oceanic geostrophic velocities, all calculated using established methods. Ekman transports are determined following the methods of Meneghello et al. (2017) and Meneghello et al. (2018) and are identical to the approach published by Regan et al. (2019) in

this special issue. The geostrophic wind was calculated from NCAR/NCEP (reanalysis 1, (Cavalieri, 1996)) 6-hourly sea level pressure (SLP) fields. Sea ice motion is taken from the Polar Pathfinder Daily 25 km EASE-Grid Sea Ice Motion Vectors, Version 4 (Tschudi, 2019). Daily sea ice concentration for 2003-2018 is from Nimbus-7 SMMR and DMSP SSM/I-SSMIS Passive Microwave Data Version 1 (Cavalieri, 1996). The ocean geostrophic velocity fields are from Armitage et al. (2017).

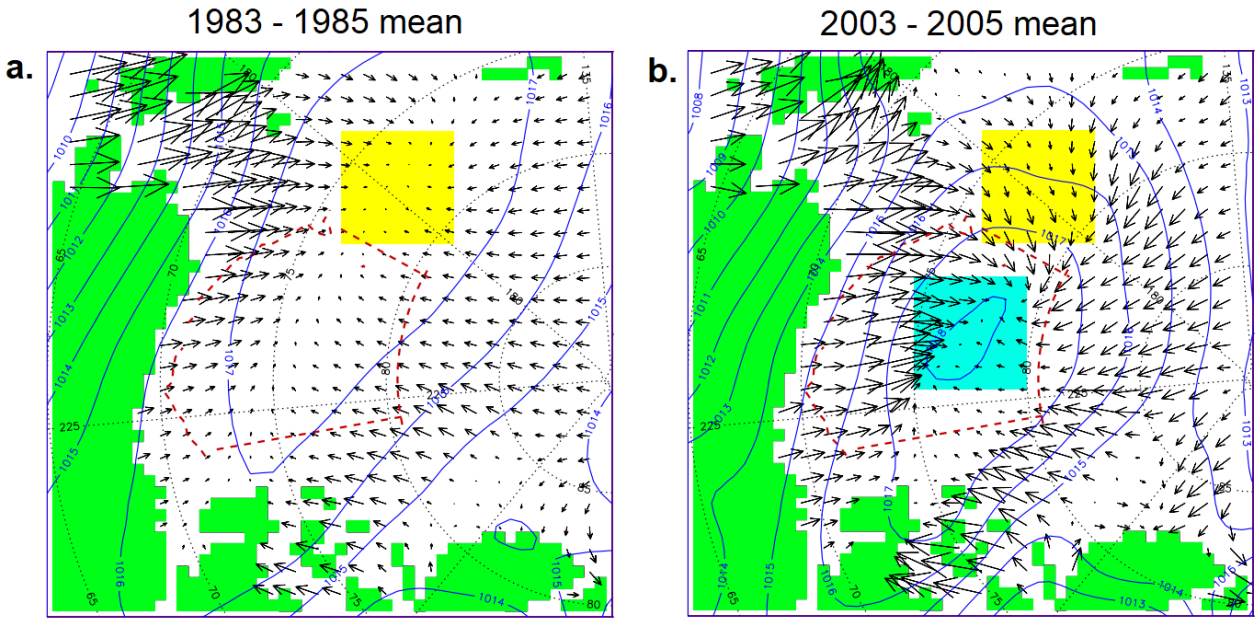

***Figure 3.4**: Ekman transport for the periods **a.** 1983-1985 and **b.** 2003-2005. Blue lines indicate sea level pressure, red dashed line represents the Beaufort Gyre region, and land is shown in green. The waiting room region is highlighted in yellow. Note that this is where the Ekman transport converges in 1983-1985. The cyan region shows the center of Ekman convergence for 2003-2005. Unlike in 1983-85, this is within the Beaufort Gyre region for the 2003-2005 period.*

In 1983-1985 (Figure 3.4a), the Ekman transport converged in the waiting room region (yellow box) and hence particles accumulated there. This observational evidence provides supports for the suggestion from Figure 3.3 that 1983-85 wind forcing (inferred from sea level pressure, hereafter referred to as SLP) was favourable for accumulation of particles in the waiting room but unfavourable for fresh water accumulation in the Beaufort Gyre region.

In 2003-2005 (Figure 3.4b), the wind pattern was different. The center of high SLP shifted toward the center of the Beaufort Gyre, and Ekman transport convergence was also in the Beaufort Gyre's center (cyan box). This SLP and wind pattern was favourable for accumulation of fresh water (particles) into the Beaufort Gyre region. In Figure 3.4b, it is also apparent that Ekman transport was responsible for bringing particles from the "waiting room" to the Beaufort Gyre center.

The size and shape of the Beaufort Gyre depends on the strength and location of the SLP maximum (Beaufort High). Analysis of the observed spatial extent and shape of the Beaufort Gyre (Regan et al., 2019) showed a north-westward shift of the Beaufort Gyre center and hence an expansion of the Beaufort Gyre between 2003 and 2014. Regan et al. (2019) noted that SLP maxima to the west of the gyre (as in Figure 3.4b here) lead to an enlargement of the western extent of the Beaufort Gyre,

into the “waiting room” region identified here. We suggest that the advective pathways identified in Figure 3.3 are a consequence of Pacific Water becoming entrained in the Beaufort Gyre in this “waiting room” region outside of the Gyre’s usual extent, due to a wind-forced expansion of the Beaufort Gyre. Pacific Water first passes through this region (hence the term “waiting room”) before entering the main Beaufort Gyre region.

As has already been established previously (e.g. (Giles et al., 2012; Polyakov et al., 1999; Proshutinsky et al., 1999) wind forcing is the primary driver of the Beaufort Gyre, and the Arctic Ocean Oscillation – which describes the Ocean’s response to the atmospheric forcing – explains the net accumulation or release of fresh water. This response manifests itself as a barotropic change in sea surface height (see Proshutinsky and Johnson (1997) and Proshutinsky et al. (2015) for full details of the Arctic Ocean Oscillation index).

Balancing this wind-driven accumulation of fresh water, eddies play a key role in bringing waters away from the shelf break currents (Spall et al., 2008) and the Beaufort Gyre, constraining the maximum freshwater content in the region (Manucharyan and Spall, 2016). Observations have demonstrated that this is indeed happening, with ice-tethered profilers recording an increase in eddy density over the period 2005-2015, in response to more baroclinic instabilities which balance the input of wind energy in the Beaufort Gyre region (Zhao et al., 2016). This is in agreement with idealized model studies, which demonstrate that the intensity of the Arctic surface circulation is set by the balance between Ekman pumping and eddy-driven transport towards the boundary over a decadal timescale (Lique et al., 2015).

With NEMO, we are able to consider both barotropic and baroclinic effects. Changes in sea surface height in the Arctic are a function of wind forcing, as reflected by the AOO (Proshutinsky and Johnson, 1997). We compared the modelled annual mean SSH fields on a pan-Arctic scale as a proxy for the ocean’s response to wind forcing and, as with the trajectory densities, we performed empirical orthogonal function analysis to extract the trend in SSH over the years studied. The EOF analysis was performed over the domain north of 66N, excluding 80W to 70E to avoid considering Atlantic waters away from the vicinity of Gyre. (The same domain is also used in Figure 3.6, for the same reasons.) The result of this analysis is presented in Figure 3.5:

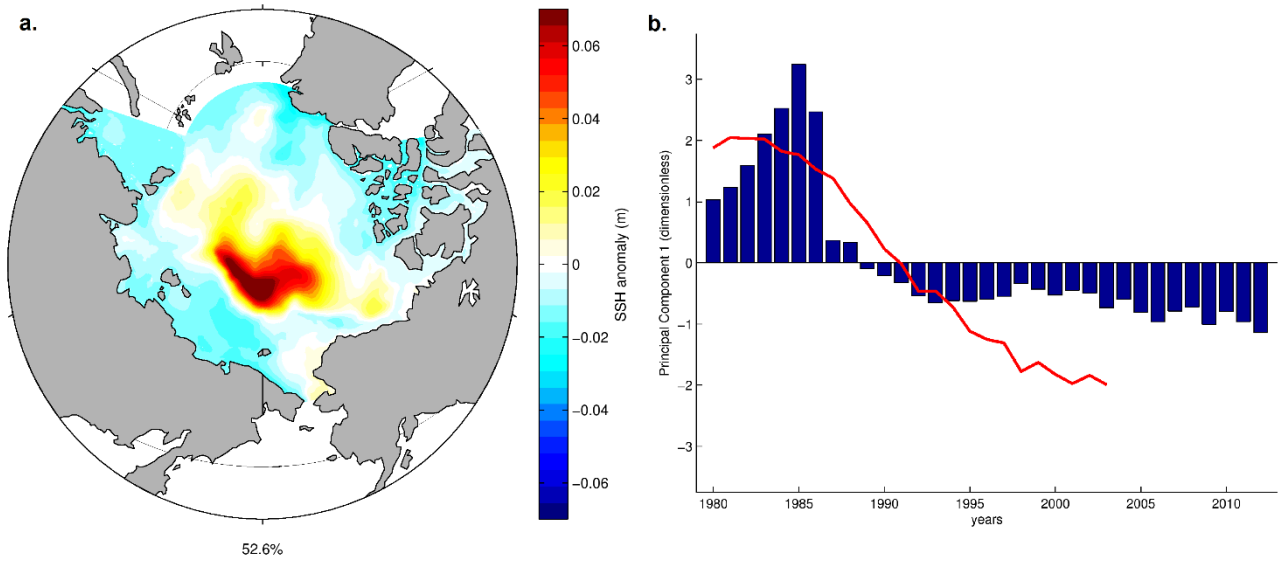

Figure 3.5: *1st mode of EOF analysis of sea surface height across the Arctic Ocean. This mode describes 52.6% of the variability. A raised area that approximately corresponds to the "waiting room" region identified in Section 3.3.2 is apparent and varies on a timescale that correlates (r = 0.83) with the EOF indices calculated in Figure 3.3. The indices from Figure 3.3b (from 1980-2003) are replotted as a red line on Figure 3.5b.*

From the first mode of EOF map in Figure 3.5, it is apparent the majority (52.6%) of the variability in sea surface height is explained by a feature centered towards the Eurasian side of the Beaufort Gyre which largely coincides with the "waiting room" region identified from Lagrangian trajectories. The EOF indices (blue bars) show that this region was raised relative to the 1980-2013 mean throughout the 1980s, and shallower from the 1990s onwards.

The timing of this correlates (r=0.83) with the appearance / disappearance of the waiting room pathway identified in Section 3.3.2. The first mode of EOF indices calculated in Figure 3.3 are replotted as the red line on Figure 3.5 to highlight this.

The fact that the change in circulation evidenced by the Lagrangian trajectories can be explained by changes in sea surface height suggests that the "waiting room pathway" is primarily a consequence of a change in the surface circulation rather than a shift in deeper currents. Given that the Arctic has changed rapidly in recent decades - warming, and with reduced sea ice to mediate the effect of the wind on the ocean surface – we suggest that this change in circulation is a secular trend rather than a consequence of known variability (e.g. the Arctic Ocean Oscillation.) However, it is worth noting that the AOO remained positive for 20 years after 1997, rather than its previous 5-7 years in either mode.

Previous work (S. Kelly et al., 2018) has shown that this configuration of NEMO does a good job of representing observed (Armitage et al., 2016) sea surface height, and additional validation (see supporting information) shows that for the Envisat observational period, the main non-seasonal mode of variability is comparable in both model and observations.

3.3.4. Implications of the Waiting Room

Having presented evidence that changes in the surface circulation switched off the modelled "waiting room" advective pathway between the 1980s and early 2010s, we now discuss why this is important for the Arctic in general.

Using the same EOF technique as previously, we investigated how the modeled mixed layer depth (MLD) throughout the Arctic Ocean changed between 1980 and 2013. The mixed layer depth used here was calculated based on a density criterion (de Boyer Montégut et al., 2004), where the potential density differs by 0.01 kg m^{-3} relative to a reference density at 10m depth.

There is an observational evidence that in recent decades, the mixed layer depth throughout the Arctic has shoaled as the Artic has freshened (Peralta-Ferriz and Woodgate, 2015). This result is reflected in the model simulation underlying this work, and we also find that this is not uniform over the Arctic. Rather, the shoaling has been especially pronounced in the Beaufort Gyre region and the Canada Basin (Figure 3.6). However, it is worth noting that the observations note one exception: a deepening of the mixed layer in the Southern Beaufort Sea between 1979 and 2012 (Peralta-Ferriz and Woodgate, 2015), which does not feature in our model result – though the modelled shoaling in the Southern Barents Sea is markedly lower than in the Canada Basin itself.

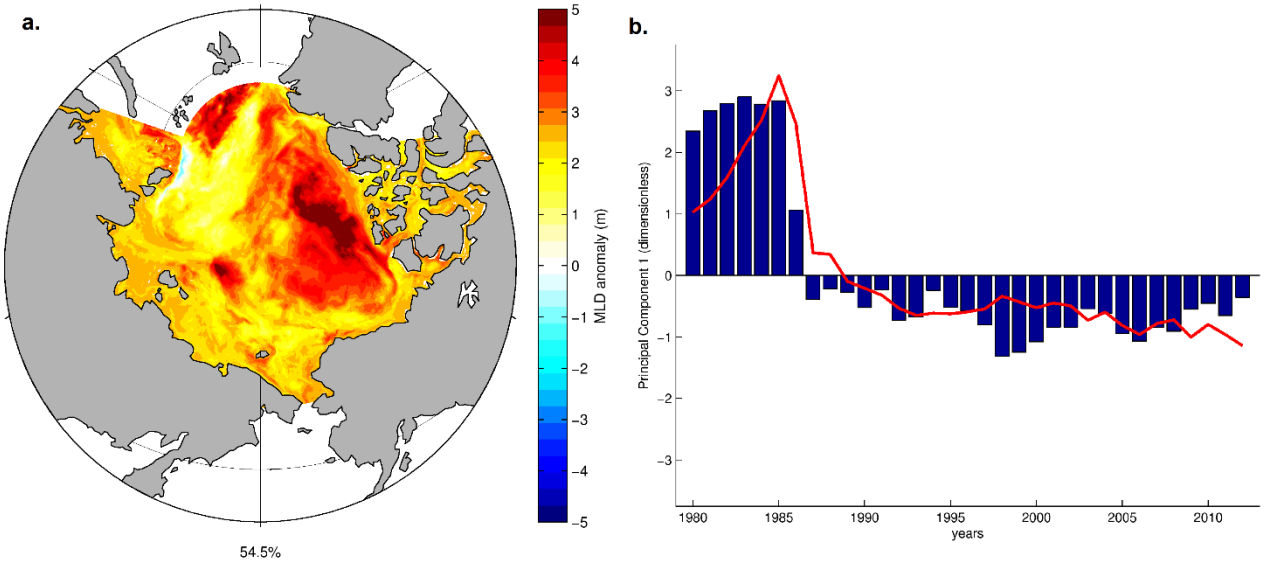

Figure 3.6: *1st mode of EOF mixed layer depth in the Arctic Ocean. Blue bars show EOF indices for this mode, red line replots the indices from Fig 3.5 for sake of comparison. This mode describes 54.5% of the variability in the region shown and shows a shoaling of the Arctic mixed layer depth since the mid-1980s, with this effect most pronounced in the Canada Basin. The timescale of this variability correlates (r = 0.89) with the indices in Figure 3.5b and replotted as the red line here.*

Interestingly, the change in mixed layer depth correlates very strongly (r = 0.89) with the change in sea surface height from Figure 3.5. We propose that the change in circulation, which led to an increase in Pacific contribution to the Beaufort Gyre, may have played a role in this amplified shoaling of the mixed layer depth in the Beaufort Gyre region.

The Beaufort Gyre region is strongly stratified, with a fresh upper mixed layer above the Pacific halocline, in turn on top of the Atlantic halocline and Arctic bottom water. We argue that the disappearance of the "waiting room" pathway since the 1980s, as evidenced by Lagrangian trajectories and Ekman transports derived from observations, allowed more Pacific water to directly enter the Beaufort Gyre. Furthermore, we note that this increased Pacific contribution coincided with a shoaling of the mixed layer in the Beaufort Gyre region. Given the strong correlation between the shift in circulation and shoaling of Beaufort Gyre mixed layer depth, we hypothesize that the change in advective pathways may have contributed to explaining why the MLD in the Beaufort Gyre changed more than the rest of the Arctic. Further analysis is required to investigate the link between the Pacific layer of the Beaufort Gyre and the MLD in the region.

It is important to note that this is not the only factor at play: sea ice has declined rapidly over recent decades, and this has feedbacks which directly affect Arctic mixing. For instance, this causes freshening of the surface of the ocean, which in turn strengthens the stratification and therefore works to shoal the mixed layer. Nevertheless, melting of sea ice means more open water for longer, and therefore an increase in wind-driven mixing across the Arctic Ocean. We note that these effects, along with the changed circulation, are all involved in governing the mixed layer in the Arctic Ocean. Additional experiments are required to ascertain the relative importance of different contributing factors.

The shoaling of Beaufort Gyre mixed layer depth suggested by NEMO is potentially important not just for the mixing in the Beaufort Gyre region, but also for the biology of the Arctic. The biogeochemistry is governed in part by the stratification (e.g. Popova et al., 2010) – weaker stratification and increased mixing enables more nutrients to be brought to the surface which improves growing conditions for phytoplankton and can potentially increase marine productivity. Meanwhile, a more strongly stratified ocean inhibits mixing and can place a limit on the availability of nutrients and hence on the biological activity in the Arctic.

The link between changed advective pathways and shoaled MLD is of particular interest, as an increased Pacific contribution to the gyre naturally means an increase in Pacific biomass entering the region (Wassmann et al., 2015). With climate change induced shifts in Arctic circulation hypothesized as a potential explanation for "invasions" of non-native species (Reid et al., 2007), the potential link between changed circulation pathways and the hospitability of the ocean is important for assessing the viability of these "invasion" hypotheses.

3.4. Summary and Conclusions

Based on our analysis and experiments described above, we note and hypothesize the following:

- Between 1980 and 2000, our analysis finds that the Pacific contribution of fresh water to the Beaufort Gyre increased;
- This increase coincided with a change in atmospheric and sea ice and ocean circulation that more directly supplies Pacific fresh water to the Beaufort Gyre instead of using a longer advective pathway, the "waiting room";
- Analysis attributes the change in circulation to a shift in prevailing wind patterns, as evidenced by a change in sea surface height that correlates with the changed circulation pathways. Further analysis demonstrated that this change was caused by a shift in the center of Ekman convergence from the “waiting room” region in the 1980s to the Beaufort Gyre region from the 1990s onwards;
- In turn, shoaling mixed layer depths in the Beaufort Gyre correlate with this changing circulation, and this change is much stronger than the increasing stratification across the wider Arctic;
- Our analysis supports the conjecture that the changes in circulation are responsible for the increased Beaufort Gyre stratification, mediated by the enhanced freshwater supply;
- Because of the critical role of stratification for marine productivity, as well as the role of Pacific inflow waters in supplying nutrients, we speculate that these changes potentially have wider impacts for Arctic ecology.
- Further modelling experiments and analysis of observational data are needed to test these hypotheses.
- We note that this research is limited in that while it can help to describe changes in the Pacific contribution to the Beaufort Gyre, it cannot address the freshwater contribution to the Beaufort Gyre from meltwater or precipitation, and that the contribution from the Mackenzie River is only approximated by tracking particles back to the vicinity of the its plume.

- Additionally, we are constrained by only using the NEMO model and Ariane particle tracking package. Intercomparison work, using different models and different particle tracking software would be useful to validate the results presented in this paper.

- Further work could focus on the Siberian contribution to the Beaufort Gyre. Due to the small number of particles tracked back to the Siberian shelf, a thorough analysis of the contribution (or lack thereof) of Siberian river water to the Beaufort Gyre would be an interesting avenue for future research. A Lagrangian forward-tracking approach, following particles seeded at the mouths of these rivers could contribute to this work.

3.5. Supplementary Information

Validation of the 1/12° NEMO model, based up on satellite altimetry (Armitage et al., 2016) has already been performed in the Arctic Ocean (Kelly et al., 2018). Modelled sea surface height (SSH), observed SSH and the model's barotropic streamfunction were compared to demonstrate that the modelled circulation is generally in agreement with observations. Here, we expand on that work by investigating the spatiotemporal variability of modelled SSH compared to the same observational dataset. We perform Empirical Orthogonal Function (EOF) analysis over the period 2003-2012 to compare to the EOF analysis presented in Figure 8 of Armitage et al (2016) and hence further validate the performance of NEMO in the Arctic Ocean. Additionally, we present the NEMO modelled mixed layer depth (1979-2012) for comparison with Peralta-Ferriz and Woodgate (2015) as extra validation to support the analysis undertaken in the main part of this paper.

3.5.1: Validation of Arctic SSH Spatiotemporal variability

Validation of the 1/12° NEMO model, based up on satellite altimetry (Armitage et al., 2016) has already been performed in the Arctic Ocean (Kelly et al., 2018). Modelled sea surface height (SSH), observed SSH and the model's barotropic streamfunction were compared to demonstrate that the modelled circulation is generally in agreement with observations.
Here, we expand on that work by investigating the spatiotemporal variability of modelled SSH compared to the same observational dataset. We perform Empirical Orthogonal Function (EOF) analysis over the period 2003-2012 to compare to the EOF analysis presented in Figure 8 of Armitage et al (2016) and hence further validate the performance of NEMO in the Arctic Ocean.

Figure 8 of Armitage et al (2016) shows that the dominant non-seasonal mode of variability is characterized by an out of phase relationship between the Beaufort Gyre region and the East Siberian and Laptev Seas especially close to the coast. Little to no variability in the Kara and Barents seas is

accounted for in this mode.

To validate the interannual variability in SSH, we performed EOF analysis of the modelled annual mean SSH fields (annual means to remove the seasonality) between 2003 and 2012. Only data from the region south of 81N (so as not to consider regions not observed by satellite) and excluding data between 20E and 90W (to remove the North Atlantic) were considered.

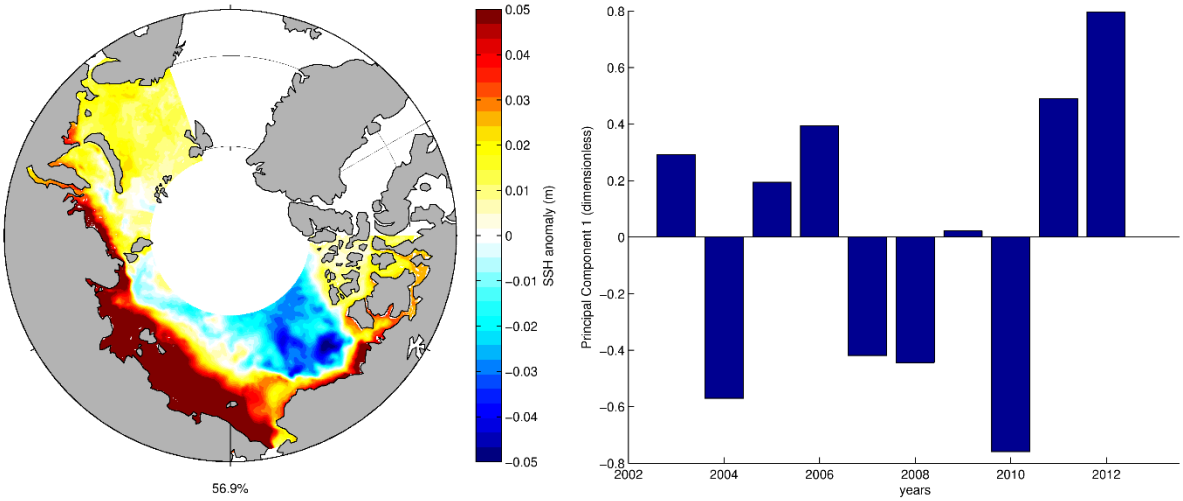

Figure 3.7: 1st mode of EOF analysis of modelled SSH, 2003-2012. This mode describes 56.9% of the modelled variability.

From Figure 3.7, we see that NEMO produces a similar pattern in spatiotemporal variability. We note that, as in the Armitage dataset, the main mode of variability shows an out of phase relationship between the Eastern Eurasian shelf seas and the Beaufort Gyre region. As with the Armitage analysis, we see little variability in the Barents Sea. The immediate vicinity of the coastlines in both the Kara and Beaufort Seas are in phase with the East Siberian and Laptev in our analysis, whereas they appear neutral in this data set. Aside from this discrepancy, NEMO shows agreement with Armitage et al (2016).

3.5.2: Validation of Mixed Layer Depth

Peralta-Ferriz and Woodgate (2015) conducted an extensive study of observed mixed layer depth (MLD) throughout the Arctic Ocean between 1979 and 2012. For validation purposes pertinent to the results presented in this paper, we compare our modelled mixed layer with the those observations.

To do this, we took the September and March mean mixed layer depths between 1979 and 2012, and averaged them to produce Figure 3.8. below:

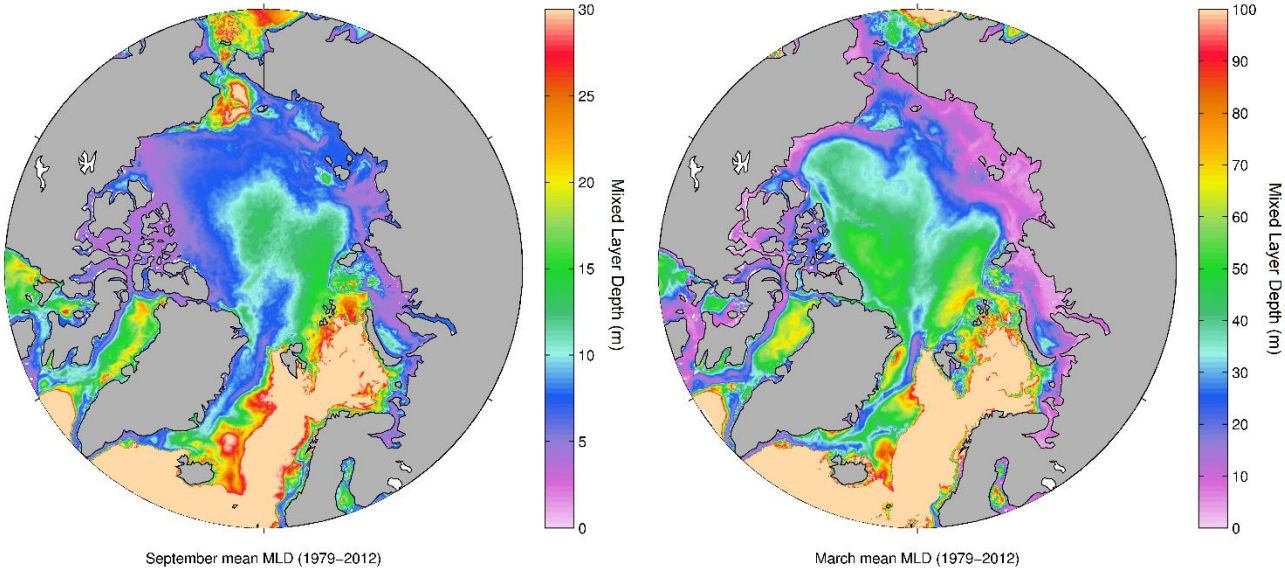

Figure 3.8: NEMO modelled monthly mean mixed layer depth (m) for September (left) and March (right), averaged over the period 1979-2012, as in Peralta-Ferriz and Woodgate (2015). Note the different color scales in each case.

This can be directly compared to Figure 14 of Peralta-Ferriz and Woodgate (2015). They divided the Arctic into six regions: Chukchi Sea, Southern Barents Sea, Canada Basin, Makarov Basin, Eurasian Basin, and Barents Sea. In each region, a typical summer and winter MLD is quoted. We compare these values with those shown in Figure 3.8.

Chukchi Sea

Peralta-Ferriz and Woodgate (2015) quote the Chukchi Sea MLD as 12m (summer) and 35m (winter). The modeled winter mixed layer depth is in reasonable agreement, with the cyan region corresponding approximately to the 35m derived from observations. However, parts of the Chukchi Sea show an MLD shallower than 20m (purple regions). The modeled summer MLD varies between approximately 15m (greens) to 30m (reds). In small patches in the south of the Chukchi Sea, the summer MLD is deeper than the winter MLD, however the overall pattern agrees with the observations of a deeper winter mixed layer. This region was unobserved in Peralta-Ferriz and Woodgate (2015).

Southern Beaufort Sea

The observed MLD is quoted as 8.5m (summer) and 29m (winter). The modeled summer MLD varies between approximately 3m (purple) and 10m cyan, whereas the winter MLD varies from <10m at the coast to 30m at the shelf slope.

Canada Basin

Here, the MLD was observed at 9m (summer) and 33m (winter). From Figure 3.8, the NEMO modeled summer MLD is 5-10m in the Canada Basin, and the winter MLD is 30-45m.

Makarov Basin

Peralta-Ferriz and Woodgate recorded MLDs of 16m (summer) and 52m (winter). In NEMO, we found a small underestimate (10-15m) during the summer, and good agreement (40-60m) during the winter.

Eurasian Basin

In the Eurasian Basin, the observed mixed layer depths were 22m (summer) and 73m (winter). As with the Makarov Basin, this is slightly underestimated by NEMO during the summer (typically 10-20m). During the winter, the modeled MLD in the Makarov Basin varies between 40m towards the Lomonosov Ridge and 80m towards the Barents Sea.

Barents Sea

Finally, Peralta-Ferriz and Woodgate quote MLD values of 18m (summer) and 170m (winter) in the Barents Sea. Figure 3.8 shows the Barents Sea as saturated (>30m in summer, >100m in winter) in order to allow for easier comparison of the other regions. NEMO overestimates the summer MLD compared to Peralta-Ferriz and Woodgate at 30-50m, although the winter MLD of 150-250m is in better agreement with the observations.

In summary, aside from over-estimates of the summer MLD in the Chukchi and Barents Seas, the modeled mixed layer depth in NEMO is in good agreement with the observations presented in Peralta-Ferriz and Woodgate (2015).

Chapter 4: Lagrangian Modeling of Arctic Ocean Circulation Pathways: Impact of Advection on Spread of Pollutants

This chapter was published in *JGR: Oceans* as Kelly et al. (2018). I am the author of this work, with my co-authors contributing supervisory guidance.

Abstract

Sea-ice-free summers are projected to become a prominent feature of the Arctic environment in the coming decades. From a shipping perspective, this means larger areas of open water in the summer, thinner and less compact ice all year round, and longer operating seasons. Therefore, the possibility for easier navigation along trans-Arctic shipping routes arises. The Northern Sea Route (NSR) is one trans-Arctic route, and it offers a potential 10-day shortcut between Western Europe and the Far East. More ships transiting the NSR means an increased risk of an accident, and associated oil spill, occurring. Previous research suggests that current infrastructure is insufficient for increased shipping. Therefore, should an oil spill occur, the window for a successful clean-up will be short. In the event of a failed recovery, the long-term fate of the unrecovered pollutants must be considered, at least until the next melt season when it could become accessible again**.** Here, we investigate the role of oceanic advection in determining the long-term fate of Arctic pollutants using a high-resolution ocean model along with Lagrangian particle-tracking to simulate the spread of pollutants. The resulting "advective footprints" of pollutants are proposed as an informative metric for analysing such experiments. We characterise the circulation along different parts of the NSR, defining three main regions in the Eurasian Arctic, and relate the distinctive circulation pathways of each to the long-term fate of spilled oil. We conclude that a detailed understanding of ocean circulation is critical for determining the long-term fate of Arctic pollutants.

Plain Language Summary

The Earth's climate is changing and the Arctic Ocean is projected to experience ice free summers within decades. This would enable more commercial shipping, which in turn makes an Arctic shipping accident more likely. This could lead to oil (or other pollutants) being spilled into the ocean. Because of the harsh Arctic environment, an oil spill may not be successfully recovered, so we need to consider where it will go in the following months and years.

We released virtual ‘particles’ into a computer model of the ocean and tracked their progress for two years. In this time, particles travelled, on average, 1,223 km. This demonstrates that pan-Arctic modelling is needed in the event of an unrecovered pollutant spill.

Unrecovered oil from one season may be accessible the next spring. By analysing the spread of our particles, we found that on average 676,917 km^2 would need to be searched to find it, but that this is highly dependent on where the spill occurs. Finally, we noted that in some places, particularly the Barents Sea, there was a risk that spilled pollutants could become entrained into deep water, rendering them irrecoverable.

4.1. Introduction

Marine oil spills are a major concern both environmentally and economically. The financial cost of accidental oil spills can run to billions of dollars, and they have the potential to cause significant damage to marine habitats by contaminating the food web and polluting large stretches of coastline (Carson et al., 2003). It is not possible to completely eliminate the risk of an oil spill occurring, and even thorough clean-up operations can leave some unrecovered oil with environmental impacts (Peterson et al., 2003). Therefore, it is important to understand where spilled oil is likely to be transported to, in order to predict the likely environmental, economic and social consequences of an unrecovered spill.

An oil spill in the Arctic Ocean is becoming increasingly likely. Permanent Arctic sea-ice is retreating rapidly, and it is predicted that the ocean will be seasonally ice-free by the middle of this century if greenhouse emissions continue at their current rate (Boe et al., 2009; Overland and Wang, 2013; Wang and Overland, 2012). This "opening up" of the ocean is fuelling increased interest in using the Arctic for commercial shipping (Aksenov et al., 2017; Lee and Kim, 2015). Figure 4.1a illustrates one such shipping route, the Northern Sea Route (hereafter NSR), which connects the Atlantic gateway to the Arctic with the Bering Strait and the Pacific Ocean. A schematic of this route is presented in Figure 4.1.

In turn, this increased shipping activity (Østreng et al., 2013) increases the probability of an accidental oil spill from a commercial tanker or from off-shore operations occurring. Winter sea-ice will persist in the Arctic for the foreseeable future, however it is likely to be reduced in thickness and extent, and it will be more mobile (Aksenov et al., 2017). Nonetheless, sea-ice remains a considerable risk for potential shipping accidents, and thus for potential oil spills. The harsh Arctic environment and remoteness of the ocean make this a particularly risky place for a spill to occur.

Once released into the ocean, many factors can govern the fate of spilled oil. These depend on the type of oil released, whether dispersants have been applied, and the environment in which the spill occurs (Afenyo et al., 2015; Mariano et al., 2011). Mixing or dissolution into the water column, photo-oxidation, emulsification, evaporation, sedimentation, biodegradation and ingestion into the food web are all potential fates for spilled oil (Mariano et al., 2011; Xie et al., 2007).

Oil spills in ice-covered areas behave differently to those in other parts of the world due to their interaction with sea-ice (Afenyo et al., 2015). Ordinarily, oil within the water column, or at the ocean's surface, is transported by ocean currents. However, oil can become trapped and corralled in leads between areas of sea-ice, and may even become fully 'encapsulated'

into growing ice, effectively isolating it from the ocean below. In this manner, oil can be transported by sea-ice and later, upon ice melt, released back to the ocean in a different location, far from the original spill (Afenyo et al., 2015; Izumiyama et al., 2004).

Leaving aside sea-ice interactions, advection due to ocean currents is the dominant process in determining what will happen to oil that has been mixed, dissolved, or otherwise entrained into the water column in the following months and years (Afenyo et al., 2015). Therefore, understanding the advective pathways in the ocean is key for understanding the long-term fate of spilled oil. The other option is that oil could for at least some of its trajectory) be transported by sea-ice, however that is beyond the scope of this work.

Biodegradation is a likely eventual fate of an oil spill, but biological processes are inhibited by the freezing temperatures in the Arctic. This means that biodegradation would take longer in the Arctic compared to the rest of the global ocean, meaning that spilled oil would remain an active pollutant for months to years and so long-term consideration of its fate is required (Fingas and Hollebone, 2003). Additionally, due to the short operational season, large distances to ports and other infrastructure, and the generally challenging Arctic environment, there is a significant chance that if a spill occurs, it will not be fully recovered before the winter freeze up makes it inaccessible. During this time, ocean currents and sea-ice can transport oil hundreds of kilometres away from the initial spill location (Main et al., 2016).

Aside from in the Arctic, recent major oil spills have included the Deepwater Horizons incident in the Gulf of Mexico. Ocean models were used to investigate the spread of pollutants here (Macfadyen et al., 2013; North et al., 2013; Weisberg et al., 2017), including Lagrangian analysis of modelled currents. It was found that ocean currents played a dominant role in determining where oil would go, and this held until oil reached the coast, when Stokes drift became the important factor for determining how the oil would beach (Weisberg et al., 2017).

To date, no major spill has occurred in the Arctic. An oil rig ran aground in the Chukchi Sea in 2012, but this did not lead to actual pollution (Meier et al., 2014). However, there has been one particularly notable oil spill in ice-affected waters: In 1989, a major spill from the Exxon Valdez tanker occurred off the coast of Alaska (Peterson et al., 2003). One contributing factor to this event was the tanker deviating from its normal shipping lane to avoid icebergs. This caused an accident, and 11 million gallons (50,000 m^3) of Prudhoe Bay crude oil was spilled into the ocean. The financial cost of the spill ran to billions of dollars, with Exxon spending over $2 billion on oil spill response and restoration (Carson et al., 2003).

Consequently, preparedness modelling around ocean circulation in the Arctic is vital to understand where oil spilled in the region will be located in the springtime when it becomes accessible again, both to permit estimation of the level of the potential recovery costs, and to understand the likely domain and severity of environmental and ecological impacts should a spill similar to Exxon Valdez occur within the Arctic Ocean.

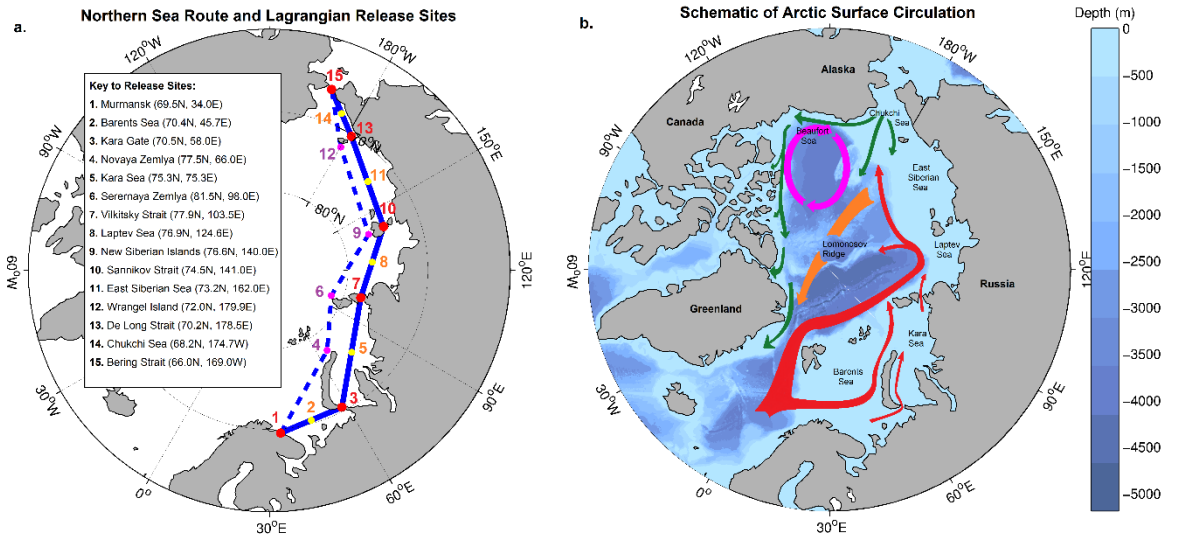

Figure 4.1 a) *The Northern Sea Route (NSR) and release sites for Lagrangian experiments (see Section 4.2.2.). There is no fixed definition of the NSR, so we have defined a 'main' route via straits (solid line) and a more poleward 'alternative' route (dashed.)* ***b)*** *Schematic of Arctic surface circulation. Red: Atlantic inflow following the Arctic Circumpolar Boundary Current (including Barents Sea Branch) and branching at the Lomonosov Ridge. Green: Pacific inflow, following 3 main pathways: the Alaskan Shelf-break Jet, into the Chukchi Sea through the Herald Canyon, and central flow across the shelf. Note that the flow north of the Canadian Archipelago is currently not definitively established, and presumed flow is shown. (Aksenov et al., 2011). Magenta: Beaufort Gyre. Orange: Transpolar Drift Stream, from Siberia to the Fram Strait.*

By way of a summary, large-scale circulation pathways in the deep Arctic Ocean are primarily driven by the wind and by the inflows from the North Atlantic and Pacific oceans (Aksenov et al., 2011; Pnyushkov et al., 2015; Pnyushkov et al., 2013; Proshutinsky et al., 2015; Proshutinsky and Johnson, 1997). Since the ocean stratification below the Arctic halocline is week, the intermediate depth currents strongly influenced by the by the oceanic ridges and steep topography of the continental shelf slope (Aksenov et al., 2011). The exchanges between the shelf and the deep part of the ocean occurs through cascading of the dense shelf waters (Ivanov et al., 2015; Ivanov and Golovin, 2007) and the cross-slope currents, driven by the along-shelf component of the wind stress through the Ekman transport mechanism (Bacon et al., 2014).

The presence of sea-ice serves to decrease wind forcing and makes the ocean circulation relatively slow, however this "inhibition" is anticipated to decline as the ice retreats. In bathymetric terms, the Arctic Ocean is roughly evenly divided between shelf seas (up to 200m

depth) and deep ocean, with the latter split by the Lomonosov Ridge into the Amerasian and Eurasian basins (Björk et al., 2007).

As Figure 4.1b illustrates, the anti-cyclonic Beaufort Gyre (magenta) dominates the circulation in the Amerasian Basin (Bluhm et al., 2015; Proshutinsky and Johnson, 1997). Meanwhile, cyclonic regimes govern circulation in the Eurasian Basin (red), with currents guided by local bathymetry, and following shelf breaks and ridges (Carmack and Wassmann, 2006; Wassmann et al., 2015). Between the cyclonic and anti-cyclonic regimes of the two basins, the Trans-Polar Drift Stream (Orange) carries water from Siberia to the Fram Strait across the deep Arctic (Bluhm et al., 2015).

The NSR shown in Figure 4.1a predominantly crosses the Eurasian Arctic shelf. This region is comprised of five seas: the Barents, Kara, Laptev, East-Siberian and Chukchi. The Barents and Chukchi seas are inflow shelves, and are influenced by incoming Atlantic and Pacific water respectively (Carmack and Wassmann, 2006; Williams and Carmack, 2015). Atlantic water entering the Barents Sea Opening flows east across the shallow shelf. Dense water is formed in the Barents Sea, sinks, and becomes a branch of the Arctic Circumpolar Boundary Current (ACBC) (Aksenov et al., 2011). The ACBC has 3 cores: the main of which is a lower shelf slope current centred at around the temperature maximum in the Atlantic Water (AW) layer at ~300 m depth, originated from the AW inflow through Fram Strait , a deeper Barents Sea Branch at ca 1000 m , and as well as a surface/sub-surface branch (down to 150-m depth in the water column), aka Arctic Shelf Break Branch (ASBB) (Aksenov et al., 2011). We refer to all these as part of the ACBC. We assert that the above boundary current structure has been observed by the NABOS and other observational programmes and has been simulated in high-resolution models.

At the other end of the Eurasian shelf, a smaller amount (~1 Sv) of Pacific Water enters the Chukchi Sea via the Bering Strait (green in Figure 4.1b), where it can follow the Alaskan Shelf-Break Current towards Canada, flow into the East Siberian Sea and potentially join the transpolar drift downstream, or enter the Beaufort Gyre (Aksenov et al., 2011; Carmack and Wassmann, 2006).

Between the Barents and Chukchi seas lie the interior seas of the Arctic (Kara, Laptev and East-Siberian.) These are influenced by freshwater runoff from the Ob and Yenisei near the coast, and from the ACBC along the shelf edge in the north (Carmack and Wassmann, 2006; Williams and Carmack, 2015). Wind forcing, plays an important role here, with cyclonic summer atmospheric circulation favouring an eastward transport in the Laptev Sea. (Bauch et al., 2009). Significantly for communication with the deeper interior of the Arctic Ocean,

Ekman pumping drives upwelling and downwelling at the shelf break and associated cross-shelf exchange (Williams and Carmack, 2015).

While this sketch describes the general pattern of ocean circulation in the Arctic Ocean, the region is unsurprisingly also characterised by strong seasonal and interanual variability (in addition to the secular trend driven by anthropogenic climate change). All of these factors combine to make the Arctic Ocean a complex and variable region for understanding and planning spill responses.

In the following section, we outline the Lagrangian modelling technique used to investigate the impact of advection on a potential Arctic oil spill from various locations along the NSR (marked on Figure 4.1a). We then quantify this with various metrics, and discus the consequences of ocean circulation for the spread of pollutants from in the Arctic Ocean.

4.2. Methodology

4.2.1. NEMO (Nucleus for European Modelling of the Ocean)

In this study, we use the ORCA0083 1/12-degree resolution configuration of the NEMO (Nucleus for European Modelling of the Ocean) general circulation model (GCM) coupled to the Louvian-la-Neuve Ice Model (LIM2) sea-ice model (Fichefet and Maqueda, 1997; Goosse and Fichefet, 1999; Madec, 2014). Here we present model description relevant for this study, for more detail the reader is referred to (Madec, 2014).

NEMO is a global z-level model with a fully non-linear free surface. Horizontal resolution in the Arctic is 3-5km, making it eddy-resolving in the central Arctic Ocean but only eddy-permitting on the shelves due to the small Rossby radius of deformation (Nurser and Bacon, 2014). The model has 75 vertical levels, with spacing varying from 1 m at the surface to 204 m at 6000 m (there are 31 model levels in the upper 200m). The model simulates vertical mixing using the turbulent kinetic energy (TKE) mixing scheme (Blanke and Delecluse, 1993) and uses the total variance dissipation (TVD) advection scheme for active tracers (Madec, 2014).

The LIM2 ice model uses Elastic-Viscous-Plastic rheology (EVP) (Hunke and Dukowicz, 1997), implemented on a C-grid (Bouillon et al., 2009), with thermodynamics based on two layers of ice and one layer of snow (Fichefet and Maqueda, 1997). It is coupled to the ocean model at every ocean time step, with a non-linear quadratic drag of the sheer between the ice and ocean. The model has been found to accurately simulate sea-ice in the Arctic Ocean (Aksenov et al., 2017; Johnson et al., 2012; Wang et al., 2016).

The model is forced at the surface boundary using the DRAKKAR forcing set (DFS) atmospheric reanalysis (Brodeau et al., 2010). This is comprised of 6-hourly data for atmospheric winds (from the ERA40 reanalysis), temperature and humidity, daily radiative fluxes (short- and long-wave) and monthly means for precipitation (rain and snow; from the CORE2 reanalysis) and runoff (Brodeau et al., 2010; Timmermann et al., 2005). In the simulation used here, NEMO was run from rest, with forcing from the beginning of 1978 until the end of 2015, and output saved as 5-day means.

NEMO is widely used by the research community for global studies at a variety of resolutions, including ORCA0083, e.g. (Duchez et al., 2014; Janout et al., 2015; Marzocchi et al., 2015; Srokosz et al., 2015). In the Arctic, it has been used extensively in the coarser 1/4 degree configuration e.g. (Aksenov et al., 2017; Lique et al., 2010; Popova et al., 2013). Evaluation of the circulation in NEMO (ORCA025), by way of calculating the barotropic streamfunction across the Arctic is presented in Lique et al., though the authors note the difficulty in accurately observing surface currents as sea surface height cannot be directly observed (Lique et al., 2010) – although reanalysis products are available and used here.

Although the recent realisation of ORCA0083-N06 used here had undergone extensive validation globally, it has not been comprehensively evaluated in the Arctic. Further evaluation of the 1/12 degree NEMO ORCA0083-N06 run is presented in Section 4.3.1. Here, we compare ice cover against satellite derived reanalysis data. We also compare modelled sea surface height with satellite observations. This is used in conjunction with an analysis of the model's barotropic stream function to evaluate the simulated circulation.

As with all models, NEMO is not without its limitations. For example, the configuration of NEMO used in these experiments lacks tides and wave model. We do not expect these to have a significant effect on our results, but it does place restrictions on the conclusions that we can draw in some coastal areas where tides play a particularly significant role in the ocean dynamics (Luneva et al., 2015; Padman and Erofeeva, 2004). Specifically, tides and waves are both important for mixing oil into the water column and dispersing it. However, given that we are modelling advective pathways – rather than directly modelling the physics of the oil itself, which would vary strongly based on the type of oil spilled – mixing is not directly accounted for anyway. We instead aim to describe the circulation pathways followed by the ocean currents in order to give a more general overview of where spilled oil could go, assuming it has already become mixed into the water column.

4.2.2. Lagrangian Modelling

There are two approaches by which ocean models can address pollutant dispersal: 1) online representation via a passive tracer, whose concentration is determined by the resolved circulation and the parameterized mixing - for more detail, see (Madec, 2014)**f**; and 2) offline, using saved output from a pre-existing run of the model. This approach uses Lagrangian 'particles', whose positions in space and time are updated according to the saved mean velocities and does not require the full model to be re-run (Blanke and Raynaud, 1997). Both have advantages and drawbacks.

The transport of online tracers is consistent with model transport processes of advection and diffusion, and mixed layer processes such as convection. NEMO employs Eulerian meshes to solve the tracer evolution equation numerically, thus this approach is often called "Eulerian". However, this Eulerian approach comes at a significant computational cost because it requires re-running the high resolution global model itself for each simulated spill scenario.

In contrast, by making use of output from an already existing (and computationally expensive) simulation, and by calculating for only a fixed number of trajectories, offline Lagrangian particles require significantly less computational resource. This reduced cost can particularly suit studies where trajectories are repetitively initialised from multiple sites at multiple time points, a situation which would require many separate simulations for online tracers. Using hundreds of thousands of discrete trajectories, it is possible using Lagrangian particles to identify advective pathways and their variations. The downsides of using this offline approach are that individual Lagrangian particles effectively represent large quantities of pollutant, and parameterized mixing processes are unrepresented, so we can only consider the effects of advection but not diffusion. This can be compensated for by using many particles over an ensemble of releases. Furthermore, while the Lagrangian method does allow for subduction due to non-zero vertical velocities, it cannot account for convection – i.e. vertical mixing due to water-column instability. This is most likely to affect the results in the areas of Atlantic inflow where convection is prevalent.

For the purposes of this study, we use the Ariane particle-tracking software package which uses the Lagrangian methods outlined above to calculate the evolution of trajectories (Blanke and Raynaud, 1997). Here, Ariane reads in 3D velocity fields from the 5-day mean NEMO output, and uses this to disperse virtual 'particles' released into the model's flow field. These particles are transported per a bilinear interpolation of the velocity field, using an analytical method to solve for particle translation through model grid cells, and the resulting trajectories are stored for analysis at daily frequency. Although Ariane does not include horizontal mixing (which, in part, represents subgrid processes in the ocean model), the high resolution

of NEMO used here accounts for most of the relevant transport explicitly. Ariane is mass-conserving and powerful for describing the large-scale, long-term impact of advection. However, it does not account for turbulent mixing, and since it works with 5-day mean advection fields, it does not guarantee that particles will exactly follow constant density surfaces.

Individual trajectories from each simulated pollution event can be plotted to highlight the different pathways followed by each particle, with the distribution of particles after some given time indicating dispersal size, distance and shape. Using multiple releases initially close in space and time can provide information on the uncertainty associated with different spill sites and dispersal routes. Here, we use the term 'advective footprints' to describe the ensemble of trajectories from a given release site. Lagrangian analysis, specifically using Ariane and the advective footprint approach advocated here, has previously been employed to model oil spills and other pollutants (Main et al., 2016; Robinson et al., 2017).

4.2.3. Experiment Design

In order to evaluate the impact of advection of a potential Arctic oil spill, we consider the parts of the ocean most at risk of an accident occurring. The Northern Sea Route (NSR) is a major shipping corridor running between the Barents Sea in the west and the Bering Strait in the east (Lee and Kim, 2015). It offers a connection between North West Europe and the Far East which, in the future, could be more economically viable than the normal shipping route via the Suez Canal (Liu and Kronbak, 2010; Schøyen and Bråthen, 2011). It offers a 40% reduction in distance compared to the Suez route (Schøyen and Bråthen, 2011), and this has the potential to cut sailing times by up to 10 days (Aksenov et al., 2017). Both the reduced time at sea, and associated saving in fuel, make this a potentially attractive route for shipping companies.

To model the impact of advection on an oil spill from the NSR, virtual Lagrangian particles were released into the NEMO flow field at 15 sites along the Northern Sea Route (see Figure 4.1a). These locations were selected to sample the length of the NSR, between Murmansk in the west and the Bering Strait in the east, via the Barents, Kara, Laptev, East-Siberian and Chukchi seas. The NSR is not strictly defined as a single corridor, and different definitions have been used in previous literature, e.g. (Aksenov et al., 2017; Lee and Kim, 2015). Here, we take this into account by defining a 'main' route via straits connecting each sea, as well as a more northern 'alternate' route.

Release sites at Murmansk and the Bering Strait were selected as the start and end points of both routes. The straits along the 'main' route are potentially high-risk locations due to variable sea-ice cover, shallow water and restricted room for manoeuvre, which could increase the risk of a shipping accident. A further five sites were taken at the midpoints between these straits to sample each of the Eurasian Arctic seas. Finally, the borders between each sea were sampled from our northward 'alternate' route to complete the set of release locations. The locations of each release site are marked on Figure 4.1a.

At each of the 15 sites, 100 particles were seeded over a regular 10 km x 10 km grid, chosen to represent an area covered by oil after several days of spreading. These releases were repeated every 10 days throughout the navigable season of the NSR (taken to be start of June – end of October), every year from 1990-2009, to take into account seasonal and interannual variability of the circulation. All releases from a given year were conducted as part of the same experiment, resulting in twenty experiments of 22,500 particles.

All trajectories were advected with the full 3-D velocity field for 2 years from their respective launches, with the particles' positions recorded daily. We consider this 2-year period to account for spills which are not recovered before the Arctic freeze up begins, and therefore persist in the Arctic for beyond one winter. Previous research has evaluated dispersal over shorter time periods (1 year) but this has been in regions with warmer waters and no sea-ice (Main et al., 2016).

It is important to note that these particles do not directly represent real particles of oil. With only 100 particles per release, each is potentially representative of a large quantity of pollutant (see Section 4.3.2.6. on the sensitivity of this assumption). Also, the particles are modelled here as being neutrally buoyant, and represent oil that is dissolved (or emulsified) within seawater rather than that which is floating as a sea surface slick or whose density changes with time.

4.2.4. Transport Metrics and Advective Footprints

We begin by simply plotting trajectories from each release site in order to give a qualitative description of the pathways that they follow (see Section 4.3.2.1.). Additionally, we define quantitative metrics to describe the distances travelled by particles, the uncertainty associated with where they go, and the sensitivity to when a spill occurs:

Firstly, we are interested in how far particles go. This is trivial to quantify, and we used two metrics: total distance travelled (the sum of all the distances travelled in each time step) and

A-B distance travelled by particles from each release site. These distances were calculated after a) 9 months, to represent the typical time between a spill occurring in the summer and the melt season beginning next spring, and b) after 2 years, to assess the fate of irrecoverable oil.

In order to better describe the spread of Lagrangian particles, we introduce the concept of 'advective footprints'. Footprints are defined as the area of ocean covered by Lagrangian particles some time T after release. We choose T = 9 months (270 days) to correspond the approximate time between an oil spill occurring and the beginning of the melt season next spring.

To calculate the area covered by particles, we define a grid and count the number of cells occupied during the 270^{th} time step. (i.e. only cells occupied in the 270^{th} time step, and not counting cells passed through on their way.) We use a coarsened version of the ORCA12 grid – 10 cells in the i direction and 11 in the j direction. This was chosen to approximately regularly sized square cells, and of a size that typically produced continuously filled footprints. The 'area of advective footprint' is then defined to be the sum of the areas of each occupied grid cell.

This is calculated for each release (so 15 releases for each of the 20 years studied) individually. This figure is then averaged over the 300 releases for each site to give an estimate of the area that would likely be affected by a spill from a particular location – i.e. a measure of the horizontal spreading of our particles. We then compare how this value varies with respect to both season and year of launch to assess the inter- and intra-annual variability of our experiments.

Additionally, we consider the "envelope" of all of these footprints – i.e. the total area covered by all 30,000 particles from a given launch site. The size of this "envelope" is representative of the uncertainty associated with pathways from a given location. Spilled oil could go anywhere reached by the Lagrangian particles, but it won't necessarily follow every pathway: each trajectory represents one of many possible pathways. This metric gives an overview of the areas potentially at risk.

Finally, we investigate the likelihood of subduction and the pathways followed by subducted particles. Oil that is entrained deep into the water column would probably not be recoverable, therefore it is necessary to understand where there is an enhanced risk of this happening. We take 100m as an approximation for the maximum mixed layer depth in the Arctic Ocean, and compare the fraction of particles below this threshold after 9 months. While this is deeper than the shallow mixed layer depth in the Arctic Ocean, this threshold was chosen to

ensure that particles reaching these depths were definitely below the upper mixed layer regardless of where in the Arctic they sank below 100m.

4.3. Results

4.3.1 Model evaluation

The global NEMO model has previously been validated in 1°, 1/4° and 1/12° resolution configurations (Marzocchi et al., 2015). Here we use the latest (as of 2017) run of 1/12° NEMO, although thorough evaluation of the Arctic at this resolution has only been done in the Kara and Laptev seas (Janout et al., 2015). However, Arctic circulation and exchanges have been extensively validated in the coarser 1/4° version, with the model reproducing observed features (Aksenov et al., 2016; Lique et al., 2010; Popova et al., 2013). Nonetheless, model evaluation is an ongoing endeavour, and here we focus on the performance of key model features that are most pertinent to the present study: ocean circulation and sea-ice cover.

4.3.1.1 Ocean circulation

In order to evaluate the surface currents produced by the NEMO model, two variables are investigated: sea surface height (SSH) and the barotropic stream function (BSF).

Sea surface height is verified against satellite Dynamical Ocean Topography (DOT) inferred by the CPOM (Centre for Polar Observation and Modelling) Envisat (2003-2011) (Armitage et al., 2016). The SSH field is used as a pan-Arctic proxy for observed and modelled surface geostrophic currents. To compensate for the two datasets being measured relative to different reference level – a geoid for satellite data and a spherical reference SSH for the model – the anomalies rather than absolute SSH are compared and presented in Figure 4.2.

In both the satellite-derived and modelled data, the magnitude of the differences in sea surface height (SSH) between the highest and lowest parts of the Arctic is approximately 1m on average between 2003 and 2011. Key features such as the raised Beaufort Gyre are present in the model results and consistent with the satellite data. This suggests that NEMO accurately simulates the large scale geostrophic flow at the surface.

The barotropic stream function was calculated for the average NEMO velocity fields (not shown, though the barotropic stream function for the 1/4 degree version is discussed thoroughly in other work (Lique et al., 2010)). It shows a similar spatial pattern to the SSH for

the same period. Because most of the stratification in the Arctic is confined to the upper 200m, the ocean circulation at intermediate depth is largely barotropic (Aksenov et al., 2011; Pnyushkov et al., 2015), and supports the interpretation that the barotropic flow in the model is also qualitatively in agreement with the satellite-inferred data – see Figure 4.2.

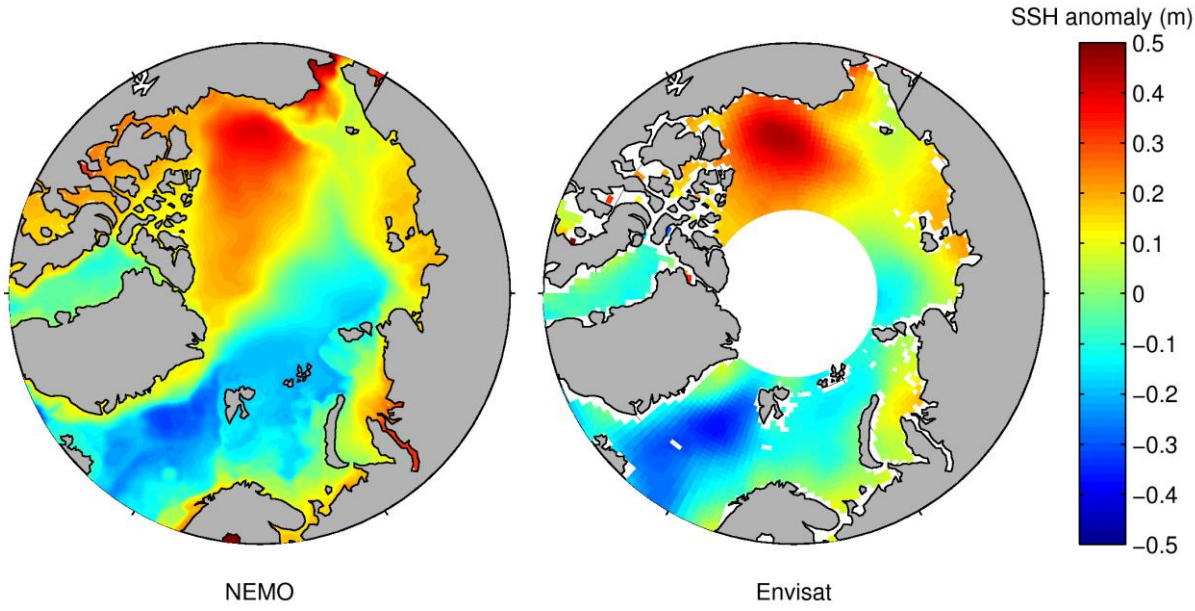

***Figure 4.2**: Comparison of NEMO modelled and satellite observed (from Envisat sea surface height (SSH), as a proxy for ocean circulation. The barotropic stream function calculated for the NEMO model (not shown) shows a similar pattern. Key features visible in both datasets are a higher SSH in the Amerasian basin compared to the Eurasian / North Atlantic. The doming of the Beaufort Gyre is also clear in both. Note that Envisat has missing data over the pole due to lack of satellite coverage.*

4.3.1.2. Sea-ice

Further evaluation is provided by comparing modelled and reanalysis (from the National Snow and Ice Data Center (NSIDC)) sea-ice extent. This is presented in Figure 4.3. Two measures are used to analyse the horizontal extent of sea-ice cover: we compare the mean summer (June – September) ice extent in the NEMO and NSIDC data sets (Figure 4.3a), and we look at how well NEMO reproduces the seasonal cycle of ice growth / decline (Figure 4.3b). Both metrics are compared between 1900 and 2012 to cover the period of our Lagrangian experiments. Sea-ice extent is taken to be the area covered with ice concentration greater than 15%.

Generally, NEMO reproduces real ice conditions well. The current downward trend in summer sea-ice extent is clearly visible (Figure 4.3a) with minima in 2007 and 2012 minima reproduced. Figure 4.3b shows the monthly cycle of ice growth and decline, were NEMO is consistently within one standard deviation of the reanalysis data.

NEMO's seasonal cycle is also in good agreement with the NSIDC reanalysis data (Figure 4.3b). The total extent of the modelled ice cover is typically an overestimate, especially during the winter months, but it is accurate to within two standard deviations of NSIDC reanalysis data. Spatially, the ice cover in NEMO and NSIDC is reasonably similar, with sea-ice present / absent in approximately the same areas.

For a more detailed evaluation of NEMO / LIM2, the reader is referred to (Wang et al., 2016).

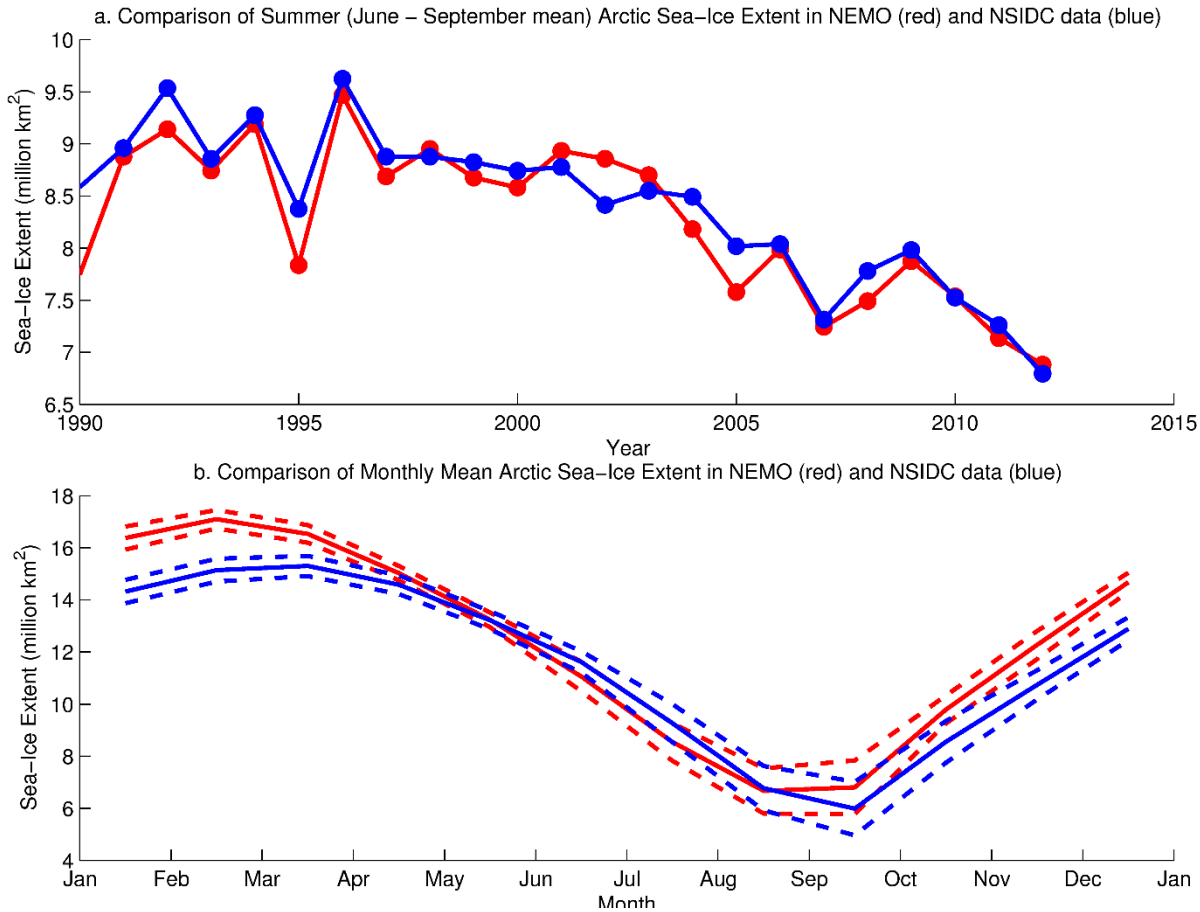

Figure 4.3: *Sea-ice extent in NEMO vs NSIDC reanalysis data.* ***a:*** *Summer (June-September) extent in the 21st Century.* ***b:*** *Seasonal cycle using monthly averages from 1900-2012. Dashed lines indicate 1 standard deviation above and below the means.*

4.3.2. Lagrangian Experiments

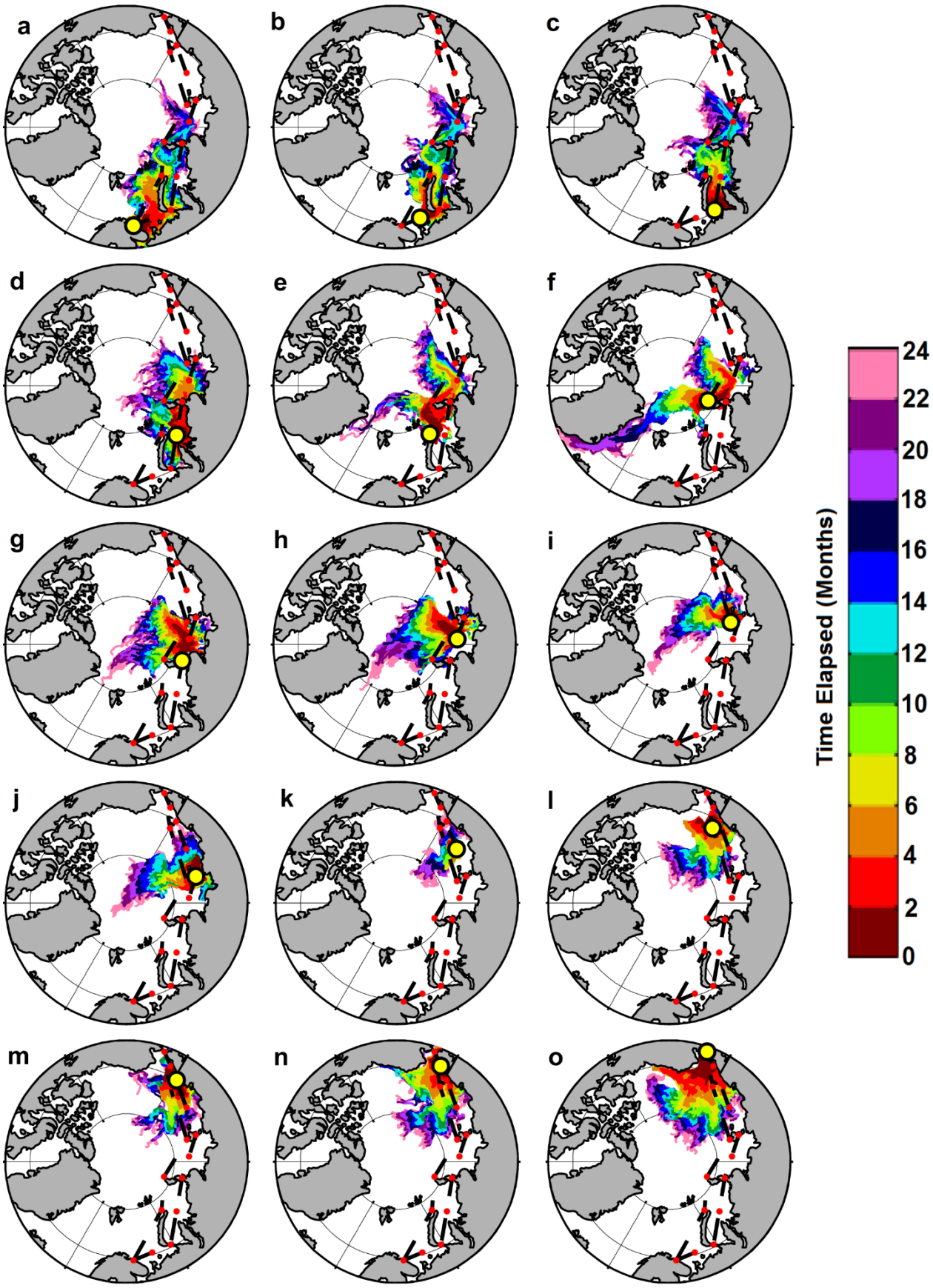

***Figure 4.4**: Advective pathways from each of the 15 release sites, showing all releases from every release in the year 2000 (arbitrary choice as an illustrative example.) Release sites are: a) Murmansk, b) Barents Sea, c) Kara Gate, d) Kara Sea, e) Novaya Zemlya, f) Severnaya Zemlya, g) Vilkitsky Strait, h) Laptev Sea, i) New Siberian Islands, j) Sannikov Strait, k) East Siberian Sea, l) Wrangel Island, m) De Long Strait, n) Chukchi Sea, o) Bering Strait.*

4.3.2.1. Arctic Circulation Pathways and Timescales

In order to assess the advective pathways likely to be important for an Arctic oil spill, Lagrangian particles were released from 15 sites along the Northern Sea Route. Releases were performed every 10 days from May – October, from 1990 – 2009. Examples of trajectories from each site are presented in Figure 4.4, showing all releases from 2000. Note that reds (corresponding to the earlier parts of trajectories) are plotted over yellows/greens/blues from later in the particles' journeys to highlight the fastest advective timescales.

From Figure 4.4, the first result that is immediately apparent is that, depending on where the particles were released 1 year can be sufficient to reach the centre of the Arctic Ocean. Within 2 years it is possible for them to leave the Arctic completely and flow into the North Atlantic. The spatial scale of these advective pathways confirms that a pan-Arctic outlook is necessary to understand the long-term fate of potential oil spills from the NSR.

As is also clear from Figure 4.4, advective pathways in the Arctic are highly variable depending on where (and when) Lagrangian 'particles' are released. Firstly, we address the sensitivity to release site. Below we detail the spread of the particles through different regions of the Arctic Ocean and Arctic seas:

Barents and Kara releases:

The north-eastward flow of the Atlantic Water through the Barents Sea, the Barents Sea Branch (Aksenov et al., 2010; Aksenov et al., 2011), is the main circulation feature, and Lagrangian particles released in the Barents Sea show this pathway (see Figures 4.4a and b). The particles followed two main trajectories; (1) eastward flow within the Murmansk Current, then through the Kara Gate into the Kara Sea, and (2) flow northward of Novaya Zemlya towards the Eurasian shelf break within the West Novaya Zemlya Current, where they flow via the St.Anna Trough and across the northern Barents Sea shelf into the deep Arctic Ocean (Aksenov et al., 2010). Trajectories are relatively fast in this part of the Arctic, with 4-5 month transient times to cross from Murmansk to the Kara Gate. The trajectories also map the cyclonic gyre in the Central Basin of the Barents Sea, with some of the particles entrained in the gyre and following the westward flow towards the Barents Sea Opening (cf. Figure 4.4a and Aksenov et al., 2010).

As in the Barents, northward and eastward currents dominate in the Kara Sea (Figures 4.4c–e). The particles released in the Kara Sea travel via the St. Anna Trough in the Nansen and Amundsen basins of the Arctic Ocean (Dmitrenko et al., 2015), and also via the Vilkitsky Strait Current into the Vilkitsky Strait and the western Laptev Sea (Janout et al., 2015). There is an episodic flow back from the Kara Sea through the Kara Gate into the Barents Sea. This is the Litke Current, observed on some occasions (Pfirman et al., 1997), and found to be correlated with an atmospheric sea level pressure

gradient across Novaya Zemlya between the Barents and Kara Seas, and by seasonal variations in the buoyant eastward current at the southern end of the Kara Gate.

After leaving the St. Anna Trough, particles go on to follow the Eurasian shelf break within the Shelf Break Current (SBC). This is one of the cores of eastward flow, guided by topography Arctic Circumpolar Boundary Current (ACBC; Aksenov et al., 2011), and along the rest of their trajectories subduction down the shelf slope was seen to occur (Figures 4.4c–e). From there, particles recirculate in the Nansen and Amundsen basins (Figures 4.4e,f), eventually heading to exit the Arctic Ocean via the western part of Fram Strait towards the Atlantic. Very few particles released in the Kara Sea reach the Atlantic within the 2 years studied.

Laptev, East Siberian and Chukchi releases:

Lagrangian particles released on the Laptev Sea shelf depict the well-established circulation pattern: they flow towards the shelf slope, where they can follow one of two routes: the ACBC or the Transpolar Drift Current (hereafter Transpolar Drift) from Siberia to the Fram Strait (Aksenov et al., 2011; Dmitrenko et al., 2005; Janout et al., 2015; Newton et al., 2008). (See Figures 4.4f-i) Trajectories following the ACBC are strongly guided by the seabed topography of the Arctic, and branch away from the shelf break at the Lomonosov Ridge (Woodgate et al., 2001). Here, they join the Transpolar Drift and flow towards the Atlantic. Particles released from all sites around the Laptev Sea are able to reach the Atlantic Ocean within 2 years.

Trajectories in the East Siberian Sea are notably slower than those in other shelf seas (See Figure 4.4l in particular.) Currents in the area vary in time and space, and the particles are carried in all directions, owing to oppositely directed inflowing waters from the Laptev Sea on one side (which carries particles east when it dominates) and the Chukchi on the other (which carries particles west.) (Timmermans et al., 2014). Particles from the East Siberian Sea remain on the shelf for a considerable time, typically beyond a year. Once these trajectories enter the central Arctic Basin, the Transpolar Drift is the principal pathway.

Circulation in the Chukchi Sea is driven by inflow from the Pacific and by the wind (Aksenov et al., 2016; Timmermans et al., 2014). The majority of particles in our experiments follow Pacific Water pathways, of which 3 main routes are noted: (1) the western route into the Chukchi Sea through the Herald Canyon, (2) the eastern route via the shelf-break jet through the Barrow Canyon and along the Alaskan Shelf-break (Appen and Pickart, 2012) and (3) the route across the shelf crossing the Herald Shoal and the Hanna Shoal via the Central Channel (Timmermans et al., 2014). Trajectories originating in the Chukchi Sea can become entrained into the Beaufort Gyre within 2 years. This is illustrated in Figures 4.4m-o. Further detail of the variability of these pathways is discussed in section 4.3.2.5.

4.3.2.2. Distance Travelled

As a first-order metric, we are interested in how far particles go. The mean distances (across all experiments) travelled by particles from each launch site is presented below in Table 4.1. The distances travelled after 9 months and after two years are presented, both as direct A-B and the total length of the path travelled for each of the 15 release sites used, listed from west to east. The full path is a proxy for average current speed along a trajectory, whereas the A-B distance represents how far away from the initial spill site a recovery operation would need to consider.

	Distance in 9 Months		**Distance in 2 Years**	
Site	**Full Path [km]** (S.D. [km])	**A to B [km]** (S.D. [km])	**Full Path [km]** (S.D. [km])	**A to B [km]** (S.D. [km])
1. Murmansk	**1641** (374)	**826** (290)	**3333** (552)	**1549** (820)
2. Barents Sea	**1440** (522)	**709** (346)	**2943** (667)	**1662** (882)
3. Kara Gate	**1490** (346)	**537** (354)	**3228** (479)	**1559** (848)
4. Novaya Zemlya	**1273** (388)	**1062** (456)	**2814** (710)	**1551** (543)
5. Kara Sea	**1450** (372)	**713** (527)	**3074** (502)	**1420** (535)
6. Severnaya Zemlya	**1534** (404)	**685** (277)	**3046** (586)	**1081** (984)
7. Vilkitsky Strait	**1701** (394)	**883** (292)	**3409** (536)	**1212** (506)
8. Laptev Sea	**1463** (428)	**754** (229)	**3103** (623)	**1661** (802)
9. New Siberian Islands	**1249** (299)	**491** (248)	**2824** (658)	**1351** (1086)
10. Sannikov Strait	**1631** (369)	**375** (221)	**3364** (515)	**906** (806)
11. East Siberian Sea	**1721** (439)	**327** (179)	**3349** (671)	**484** (293)
12. Wrangel Island	**1312** (418)	**341** (198)	**2850** (658)	**786** (506)
13. De Long Strait	**1754** (425)	**333** (159)	**3429** (421)	**613** (356)
14. Chukchi Sea	**1336** (346)	**425** (215)	**2957** (520)	**874** (418)
15. Bering Strait	**1450** (431)	**960** (201)	**2966** (563)	**1629** (382)

Table 4.1: *Average distances travelled by particles from each release site (and standard deviations). Two metrics are used here: 'Full path: adding up all the distances travelled in all time steps, and 'A to B': the straight-line distance between where the particle started and where it ended up after 9 months / 2 years.*

From Table 4.1, the distance travelled shows only modest sensitivity release site when the full path length is considered. All sites fall within 300 km of the mean distance travelled (1497 km) across all sites for the first nine months of advection: i.e. particles are transported at approximately the same speed regardless where they are seeded from.

However, this is not the case when considering the direct A to B distance (calculated as the shortest distance along the surface of the Fischer Spheroid) for each site. Excluding the Bering Strait, particles starting from release sites at the west of the Northern Sea Route travelled significantly further (typically about twice as far) as those from the eastern end of the NSR (excluding the Bering Strait site, which was more in line with the western sites.)

Here, the cut off between west and east was the boundary between the Laptev and East Siberian seas. Particles originating from the Barents, Kara and Laptev seas travelled on average 771 km in nine months and 1454 km in two years, whereas those from the East Siberian Sea (including New Siberian Islands and Sannikov Strait release sites) and Chukchi sea (excluding Baring Strait site) travelled an average of 382 km in nine months and 834 km in two years.

The marked difference in A-B distance despite the similar total path distance demonstrates that particles launched towards the west of the route (and also in the Bering Strait) follow more direct routes, whereas those in the east are more prone to recirculation.

4.3.2.3. Advective Footprints: Horizontal Spread and Uncertainty

We now characterise the horizontal spread of particles. This is done by dividing the ocean into a grid (full details in Section 4.2.4) and counting the total area of occupied grid cells. Here we consider grid cells that are occupied 9 months after their particles were initially released. Again, 9 months was chosen to represent a typical time between a spill occurring and the next melt season beginning. In the context of an oil spill, this corresponds to the area that should be expected to be reached by potentially contaminated waters.

Each release of 100 particles per release site is considered separately (so a total of 300 releases per site: 20 years of releases with 15 releases per year) and these are averaged to give a typical release footprint size for each release site. Particles were initially distributed over an area of 100 km^2. These footprint sizes are presented below in Table 4.2:

Site	a) Footprint Area After 9 Months [km^2] (S.D. [km^2])	b) Area of 'envelope' of all footprints [km^2]	Ratio (b/a)
1. Murmansk	**67,239** (9,905)	796,824	11.9
2. Barents Sea	**66,083** (10,167)	772,741	11.7
3. Kara Gate	**74,411** (8,217)	767,301	10.3
4. Novaya Zemlya	**52,989** **(**15,403)	895,653	16.9
5. Kara Sea	**78,608** (9,635)	871,982	11.1
6. Severnaya Zemlya	**42,367** (18,373)	884,118	20.9
7. Vilkitsky Strait	**47,606** (14,519)	767,249	16.1
8. Laptev Sea	**25,028** (15,487)	644,895	25.8
9. New Siberian Isl.	**30,650** (15,208)	545,667	21.8
10. Sannikov Strait	**26,122** (15,860)	562,873	21.5
11. East Siberian Sea	**9,154** (8,293)	317,715	34.7
12. Wrangel Island	**30, 474** (15,750)	586,770	19.3
13. De Long Strait	**40,346** (14,567)	472,674	14.5
14. Chukchi Sea	**48,613** (14,555)	593,230	12.2
15. Bering Strait	**46,732** (13,663)	674,067	14.4
Average:	**45,762** (13,307)	**676,917**	**14.8**

Table 4.2: a) *Mean and standard deviation of the total area of 'advective footprints' by release site. These correspond to the total area of grid cells occupied by Lagrangian particles 9 months after they were initially released. 300 distinct releases (20 years, 15 releases per year) were used to calculate these figures.* ***b)*** *The same metric, but considering the 'envelope' around footprints from all 300 experiments.* ***c)*** *Ratio of a/b.*

Table 4.2 shows that the spreading of particles is strongly dependent on where they are initially released from. There is a clear east /west divide, with western release sites (1-5) typically producing larger footprints and central (6-11) and eastern (12-15) ones producing smaller footprints.

The smallest footprints were associated from the middle of the Northern Sea Route, around Siberia in the Laptev and East Siberian seas (including the New Siberian Islands and Sannikov Strait release sites between them.) The East Siberian Sea site produced anomalously small footprints, on average less than 10,000 km^2. The average area for the other three sites in this group was 27,267 km^2 (average standard deviation 15,518 km^2), making them only half the size of the average footprint area for the remaining 11 release sites.

The five westernmost release sites (Murmansk – Kara Sea) produced the five largest footprints. The mean area of footprints from these sites was 67,866 km^2 (average standard deviation 10,665 km^2); 48% bigger than the average for the other release sites, excluding the anomalously small footprint from the East Siberian Sea release site. Including all sites between Murmansk and the Vilkitsky Strait, the average area of footprints from the west of the NSR was 61,361 km^2 (average standard deviation 12,317 km^2).

Considering each of the 300 releases from each of the 15 releases sites, the average area of advective footprints 9 months after particles were releases was 45,762 km^2 (average standard deviation 13,307 km^2). Excluding the five largest and four smallest sites highlighted, the typical area of a footprint was 44,161 km^2 (average standard deviation 15,233 km^2).

Additionally, the area of the 'envelope' surrounding all 300 footprints from each site (again after 9 months) was calculated, i.e. the total area affected by at least one release. While the first metric addresses how waters from a particular release spread, this metric addresses part of the uncertainty in where they will go. As with the individual footprints, western release sites were found to have the largest 'envelopes' while the smallest were in and around the East Siberian Sea. The large footprint 'envelopes' in the west were typically associated with particles being rapidly entrained into a well-organised current (the ACBC), which enabled them to travel further (see Table 4.1) and hence produce a larger envelope than particles which stay closer to their release sites.

Finally, we calculate the ratio of the 'individual footprints' and the 'envelopes.' This demonstrates that the uncertainty in where spilled oil could go (the envelope) is an order of magnitude larger than the area over which contaminated waters would be expected to spread (the individual footprints). This ratio provides a measure of the variability of advective pathways from a given site: larger ratios correspond to footprints with less overlap between experiments, suggesting more variable circulation. The combination of the especially large envelope and ratio from the Severnaya Zemlya site is partly due to the highly variable circulation around this area – discussed further in Section 4.3.2.5. The largest ratio was produced by the East Siberian Sea releases, but it should be noted that this was due to both an abnormally

small envelope and individual footprints, which stay relatively close to their initial release site.

4.3.2.4. Subduction

Having addressed the horizontal spread of our particles, we now look in the vertical direction. It is important to note that we are only considering subduction due to advection, as our Lagrangian technique does not explicitly include convection. All particles were initially released at the ocean surface, but they were not constrained to stay there. Here, we investigate the fraction of particles which sink below 100m depth. This was chosen as a rough approximation for the depth of the upper mixed layer, as any oil entrained deeper into the water column will be especially difficult to recover / unrecoverable.

Two snapshots were investigated: the timestep after 9 months of advection and the timestep after 2 years of advection, as with the distance travelled metrics. At these snapshots, particles were classified as either above or below a 100m threshold. The results are presented below in Table 4.3:

Site	**% of Trajectories Deeper than 100m**	
	After 9 Months	**After 2 Years**
1. Murmansk	8.01	17.67
2. Barents Sea	18.36	28.68
3. Kara Gate	1.19	5.80
4. Novaya Zemlya	22.63	38.97
5. Kara Sea	0.34	2.10
6. Severnaya Zemlya	1.25	5.07
7. Vilkitsky Strait	0.05	0.65
8. Laptev Sea	n/a	0.49
9. New Siberian Islands	n/a	0.16
10. Sannikov Strait	n/a	0.01

11. East Siberian Sea	n/a	0.14
12. Wrangel Island	0.13	1.00
13. De Long Strait	0.25	2.25
14. Chukchi Sea	2.48	7.58
15. Bering Strait	5.61	9.71

Table 4.3: *Percentages of particles from each release site which are below a 100m depth threshold during the 270th time step of the experiment (9 months) and during the 730th (2 years) for each release site. The history of trajectories is not considered here, only whether they are above or below the threshold for the two snapshots studied.*

From Table 4.3, it is clear that subduction is not a major concern for the majority of releases locations, with two notable exceptions: the Barents Sea and Novaya Zemlya sites (and, to a lesser extent, Murmansk and the Bering Strait.) One in five particles seeded from the first two sites ends up below the 100m threshold after 9 months of advection, and is potentially unrecoverable.

No particles from any release in any year were below 100m after 9 months from four central release sites: these were in the Laptev and East Siberian seas, as well as the two release points on the border between these seas. We then investigated where this subduction occurs. An illustrative example, with trajectories coloured to indicate their depth, is presented in Figure 4.5. In this figure, trajectories from 2007 are shown in three different groups, to highlight the regional differences in subduction.

From Figure 4.5, we can see that subduction mainly occurs for the western group of release sites, as noted in Table 4.3. It is apparent that this occurs mostly around the Eurasian shelf break, where particles downwell across the shelf slope. These deep trajectories are guided by the bathymetry of the Arctic Ocean and tend to follow the Arctic Circumpolar Boundary current along the Eurasian shelf-break.

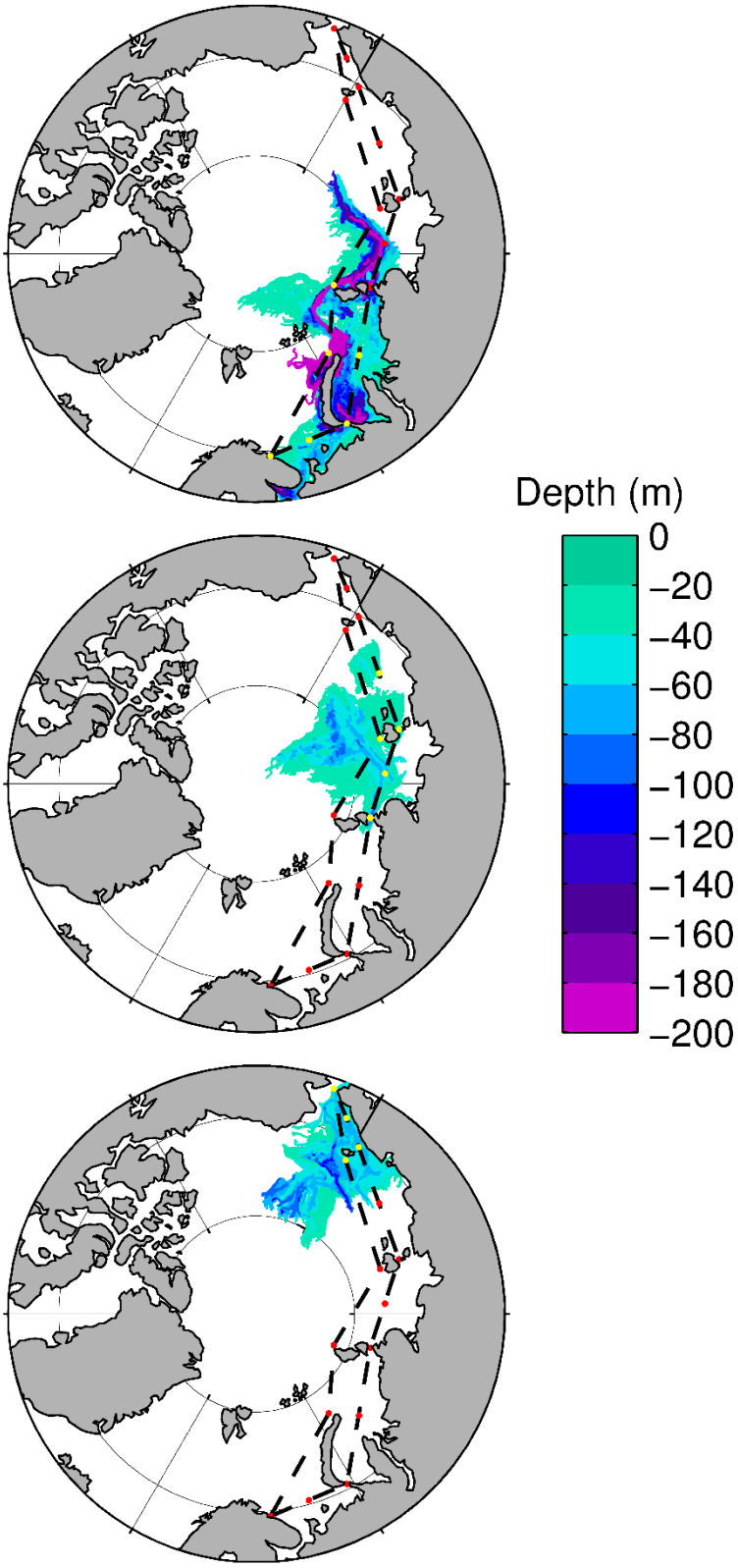

***Figure 4.5**: Trajectories from a typical year (2007) plotted to highlight their depth. Trajectories run for two full years and are broken down into western, central and eastern groups of release sites to make the pathways more obvious. Deeper trajectories (purples) are plotted on top of shallower ones to highlight the pathways followed by subducted particles. The release sites used in each figure are denoted by yellow dots.*

4.3.2.5. Sensitivity to Time of Release

The distance travelled, 'advective footprints' and subduction metrics discussed in the previous sections were compared with respect to launch site. Here, we repeat that analysis, but instead of comparing different release locations, we compare how these metrics vary with respect to time of release. This is presented in Table 4.4: first we compare the sensitivity to year of release (averaging over all release sites and all releases within the given year) and then across each of the 15 releases per year (averaging over all release sites and all years.) For each of the three metrics, we look at a snapshot 9 months after particles were initially released.

Sensitivity to Year of Release			
Year	**Mean Footprint Area [km^2]**	**Mean A-B Distance [km]**	**% of Particles Below 100m depth**
1990	48,322	629	5.43
1991	48,975	706	3.77
1992	46,964	730	6.02
1993	45,892	560	2.97
1994	47,799	808	4.64
1995	42,863	583	3.07
1996	37,397	590	3.46
1997	44,147	573	3.73
1998	41,031	525	3.28
1999	40,816	599	5.32
2000	43,487	596	4.72
2001	46,147	621	3.24
2002	47,045	568	3.99
2003	52,520	646	3.89
2004	43,004	599	3.55

2005	47,168	637	2.99
2006	46,057	605	4.13
2007	46,954	664	2.82
2008	51,107	699	4.94
2009	48,595	576	4.37
Sensitivity to Season of Release			
Season	**Mean Footprint Area (km^2)**	**Mean A-B Distance (km)**	**% of Particles Below 100m depth**
June (early)	49,310	631	2.60
June (mid)	49,021	647	2.99
June (late)	49,842	634	2.62
July (early)	49,349	632	3.30
July (mid)	48,622	633	3.31
July (late)	48,500	635	3.67
August (early)	48,058	636	3.88
August (mid)	47,032	621	3.92
August (late)	45,461	612	4.64
September (early)	44,787	602	4.53
September (mid)	44,326	619	4.59
September (late)	42,632	615	5.22
October (early)	41,145	615	4.82
October (mid)	38,769	618	5.11
October (late)	38,392	623	5.36

Table 4.4: *Sensitivity to year and season of release: The metrics described in the previous 3 section (area of footprint after 9 months, straight-line distance travelled in 9 months, and fraction of particles below 100m deep after 9 months) are re-calculated with respect to year and season of release.*

From Table 4.4, it is clear that none of these metrics show a no significant sensitivity to year of release. Inter-annual variability is present, but with no clear trend in any of the metrics used here.

However, two of the metrics showed significant intra-annual variability. The mean footprint area metric suggests slightly reduced spreading of particles correlating with later releases. The most notable trend came in the subduction metric. Here, the fraction of particles subducted below 100m steadily increases towards the end of the season, and it more than double between the first set of releases in June and the last set of releases in October.

As noted in Section 4.3.2.5., subduction is not a major occurrence for most release sites. However, for those where it does matter, it is more likely to happen for particles launched in the autumn than those starting in the spring.

Investigating the sensitivity to time of release highlighted variability in the pathways that trajectories follow. Multiple major pathways exist for some sites, and three examples (specifically the Bering Strait, Kara Gate and Severnaya Zemlya releases) with clear contrasts are presented in Figure 4.6 below:

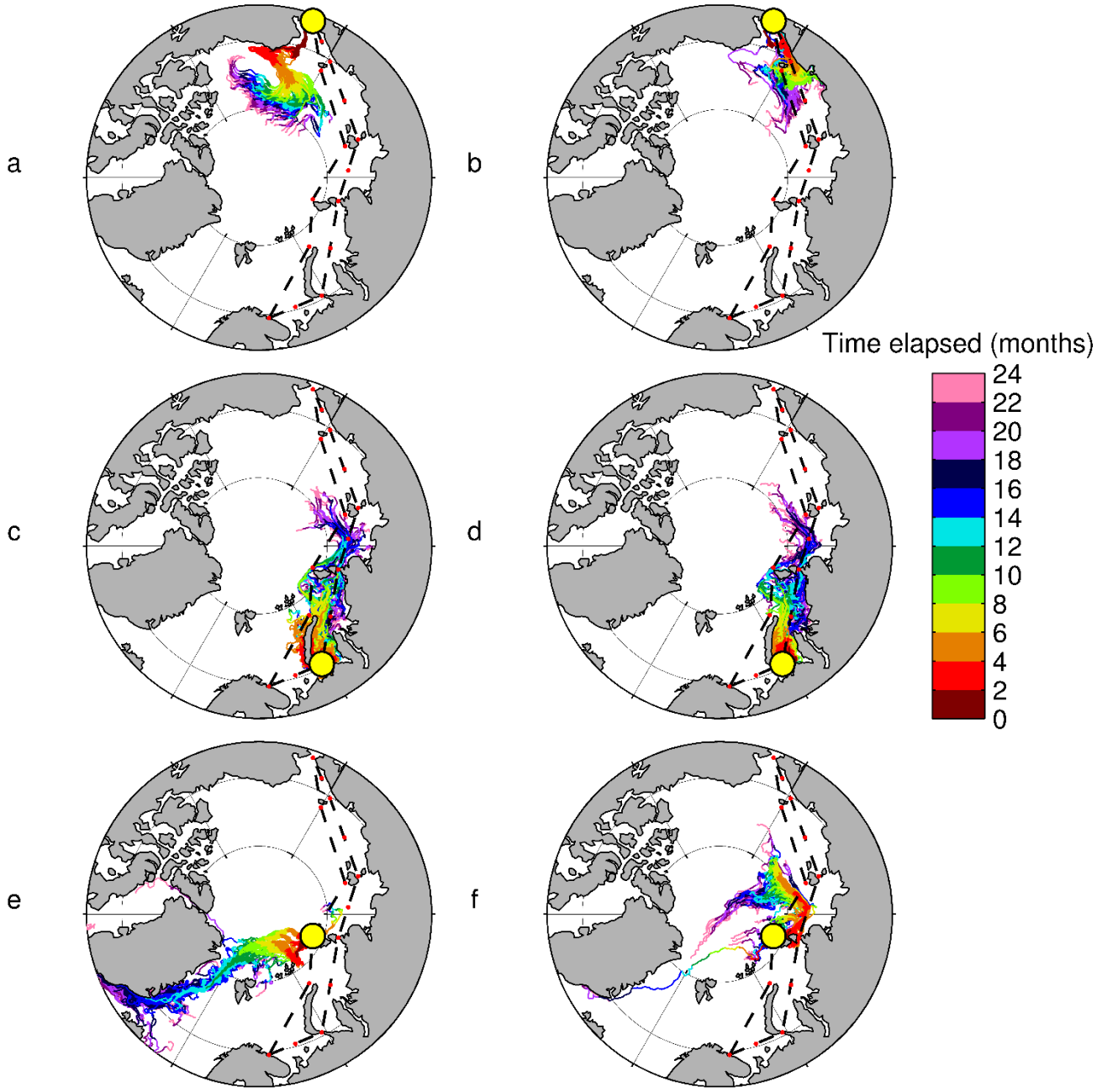

Figure 4.6: *Comparison of changing advective pathways from 3 release sites. Bering Strait: a) 23/07/2000 release, b) 12/08/2000 release. Kara Gate: c) 14/06/1993 release, d) 03/08/1993 release. Severnaya Zemlya: e) 14/07/2007 release, f) 24/07/2007 release.*

Figure 4.6 highlights some of the variability of pathways discussed in Section 4.3.2.1. Figures 4.6a and 4.6b show particles which were only launched 20 days apart from each other, yet flow in markedly different directions. Figure 4.6a highlights the Alaskan Shelf-Break current, which leads to trajectories along the North American coastline, before seeming to join the Beaufort Gyre. 6b shows the other extreme, with particles flowing into the Chukchi Sea and affecting the Russian coastline.

Figures 4.6c and d show a more subtle variation. As previously noted, the dominant flow in the Kara Gate is from the Barents into the Kara Sea, but occasionally this is reversed. An

example (Figure 4.6c) which shows this 'reversed' flow west through the Kara Gate and then north-eastwards along the Novaya Zemlya coast is shown. Figure 4.6d shows the usual eastward-only flow. This could be indicative of a wind-driven blocking event, analogous to similar events in the Vilkitsky Strait (Janout et al., 2015). Further investigation (not shown) suggests that the usually dominant buoyancy driven current (west to east) interplays with a wind-driven current in the opposite direction, which correlates with increased atmospheric pressure to the north-west of Novaya Zemlya.

Figures 4.6e and f compare consecutive releases from the Severnaya Zemlya site. Despite being launched just 10 days apart, they flow in opposite directions: all travel towards the Atlantic Ocean via the Fram Strait in 6e, and all bar one follow the Arctic Circumpolar Boundary Current in 6f. Both pathways are seen frequently, as this marks a region of variable flow: it is the boundary between where the eastward flow dominates in the Barents and Kara seas, and the east where the Transpolar Drift Stream is more common.

4.3.2.6. Sensitivity to initial area of release

So far in this study, we have used 100 km^2 as the initial area covered by our Lagrangian 'particles'. This was chosen as a first order approximation for the size of a typical oil spill. We have investigated the spread of these particles and how this varies depending on when and where particles are released, but it is also important to assess how our choice of initial conditions could affect these results.

In order to do this, we repeat our experiment for a typical year (2000 was chosen as it is in the middle of the period studied), but with particles released over different sized areas: 400 km^2 (20 km x 20 km), and 25 km^2 (5 km x 5 km). We keep the number of trajectories the same in each case. Exactly as before, we then calculate the area covered by particles 9 months after their release. We also compare this to the results from year 2000 in the standard 10 km x 10 km initial release experiments.

Differences in dispersion were apparent but small, with larger release areas leading to slightly larger distributions after nine months, see Table 4.5 below. Results from the 5 km x5 km, 10 km x10 km and 20 km x 20 km experiments are compared:

Mean Area [km^2] covered after 9 months from initial releases of area (Standard Deviation)**:**

Site	a) Initial area 25 km^2	b) Initial area 100 km^2	c) Initial area 400 km^2	Ratio (c / a)
1. Murmansk	**69,308** (10,195)	**71,806** (6,444)	**74,168** (5,802)	1.07
2. Barents Sea	**53,635** (6,597)	**56,641** (5,292)	**58,901** (3,314)	1.10
3. Kara Gate	**72,971** (7,671)	**76,015** (6,990)	**77,668** (4,086)	1.06
4. Novaya Zemlya	**52,946** (15,838)	**58,683** (15,427)	**62,019** (15,757)	1.17
5. Kara Sea	**79,577** (4,075)	**84,184** (3,814)	**85,905** (5,245)	1.08
6. Severnaya Zemlya	**42,874** (18,022)	**47,437** (12,525)	**49,782** (9,079)	1.16
7. Vilkitsky Strait	**46,731** (15,402)	**48,715** (13,303)	**46,941** (8,831)	1.22
8. Laptev Sea	**19,346** (4,017)	**22,490** (7,709)	**32,425** (6,961)	1.68
9. New Siberian Islands	**16,926** (6,771)	**22,283** (8,886)	**30,360** (10,107)	1.79
10. Sannikov Strait	**27,471** (13,064)	**34,226** (12,320)	**42,537** (11,083)	1.55
11. East Siberian Sea	**2,428** (855)	**3,844** (929)	**5,153** (2,075)	2.12
12. Wrangel Island	**23,031** (11,852)	**27,935** (10,009)	**31,694** (7,512)	1.38
13. De Long Strait	**19,832** (14,197)	**22,434** (12,346)	**26,519** (10,307)	1.34
14. Chukchi Sea	**51,334** (9,808)	**47,184** (12,439)	**57,515** (8,332)	1.12
15. Bering Strait	**39,599** (13,160)	**49,856** (16,537)	**60,357** (12,901)	1.52

Table 4.5: *Sensitivity to initial area of release. The footprint sizes (in 1000 km^2) after 9 months from release are compared for 3 different experiments in 2000, with initial releases of 25 km2, 100 km^2 (as in the main experiments) and 400 km^2. The ratios between the largest and smallest initial releases are also presented.*

It is apparent from Table 4.5 that the sensitivity to size of initial release is low. Excluding the East Siberian Sea release site, which had an anomalously low footprint area anyway, the experiments from the largest release boxes spread to an area only 30% larger than those from the smallest release boxes, despite the 800% increase in initial area.

Sensitivity to initial area of release was found to vary throughout the NSR. Particles launched from the west of the route (which had the largest footprints) showed less variability than those in the east. The 7 western release sites (Murmansk – Laptev Sea) had an average increase of 12% between the largest and smallest release sites. This contrasted with a 48% average increase in the easternmost release sites (New Siberian Islands to Bering Strait, excluding the New Siberian Islands site.) In short, the larger the footprint size, the more sensitivity to the size of the initial release box.

4.4. Discussion

Understanding the advective pathways in the Arctic Ocean is an essential prerequisite for understanding the long-term fate of oil (or other pollutants) that could be released into the Arctic Ocean. Although interest in using the Arctic Ocean for commercial shipping is already increasing, particularly along the Northern Sea Route (NSR) (Liu and Kronbak, 2010; Schøyen and Bråthen, 2011), the Arctic remains a unique logistical challenge due to its harsh environment and relative lack of infrastructure and marine services (Ho, 2010). This lack of infrastructure, coupled with the often-considerable distances to ports along the NSR mean that should an oil spill occur, cleaning up an oil spill in the Arctic is more challenging than in other parts of the world. Therefore, it is necessary to consider the risk of significant amounts of oil not being recovered before the winter freeze up begins.

Should this happen, oil is likely to remain an active pollutant for a number of years due to the slowed biodegradation in the cold Arctic waters (Fingas and Hollebone, 2003). This presents a serious risk for the polar ecosystem: the food web in the Arctic is short and therefore contamination of one species can strongly affect the whole ecosystem - trophic interactions in the Arctic are simple compared to in other parts of the world, so population changes in just one key species would have cascading effects throughout the whole ecosystem (Hop and Gjøsæter, 2013; Palumbi et al., 2008). Previous research has worked towards a quantitative risk assessment of Arctic oil spills, and the locations reached by spilled oil have been

identified as key variables for understanding the ecological impacts of a potential spill (Nevalainen et al., 2017). This means that understanding the circulation patterns in the Arctic is of key importance, and it makes the advective footprints technique used here a particularly powerful tool for assessing the long-term impact of potential Arctic oil spills.

When considering the long-term fate of spilled oil, we need first to know how far it is likely to be transported during some specified time-frame. We took 9 months as the likely time between a spill occurring and it becoming accessible after the next melt season, and 2 years to provide a longer-term outlook, and then measured how far particles were from their start points at these intervals. Within 9 months, particles travelled a mean distance of 1497 km from their start point (calculated along the full path.) The straight-line distance showed considerable variation. 628 km was the average for all release sites, but there was a clear east-west divide: particles from the west of the route (Barents, Kara and Laptev) seas travelled almost twice as far as those in the east (East Siberian and Chukchi Seas, excluding the Bering Strait.): 771 km compared to 382 km. This suggests that the location of a spill is key for determining how far oil could be transported. After 2 years, particles were on average 1223 km from their start point. (484-1662 km, depending on release location.) Although the circulation in the Arctic is relatively slow compared to the rest of the world ocean, this demonstrates the first key result of this experiment: pan-Arctic modelling is required to understand the long term (order of years) fate of spilled oil.

Having quantified the distance that spilled oil could travel, we move on to addressing the question of where it will go to and the uncertainty in how it will spread. To do this, we introduced the concept of advective footprints. This technique has recently been used in other parts of the world to study changing circulation patterns and potential impacts for environmentally sensitive areas (Polyakov et al., 2017; van Gennip et al., 2017). The trajectories from our Lagrangian experiments are in agreement with circulation pathways described in previous literature, e.g. (Aksenov et al., 2011; Carmack and Wassmann, 2006; Williams and Carmack, 2015). Known pathways are clearly reproduced, with key features such as the Arctic Circumpolar Boundary Current (ACBC) (Aksenov et al., 2011) clearly visible in trajectories launched from all along the Northern Sea Route. These, along with the Transpolar Drift Stream (Steele et al., 2004) and Pacific inflow (Aksenov et al., 2016) are the main large scale features seen in our experiments. More detailed descriptions of specific pathways are presented in Section 4.3.2.1.

We defined the metric ‘area of advective footprints’ to quantify the uncertainty associated with these pathways. We divided the Arctic into a regular grid and counted the number of grid cells that were occupied by particles a set time after particles were released (Full details

in Section 4.2.4.). The sum of the areas of occupied grid cells was taken to be the area of the advective footprint. In the context of an oil spill, the size of a footprint from an individual experiment represents the spreading of the spill, while the area of the 'envelope' of all footprints corresponds to the uncertainty in where it will go – and hence the area of ocean that would need to be searched to find it. Location of oil has been identified as a key variable for environmental risk assessments (Nevalainen et al., 2017), so it is necessary to quantify the uncertainty associated with where oil is likely to end up. Advective footprints provide a robust mechanism for doing that.

It was found that after 9 months, a typical footprint had an area of 45,762 km^2, with a standard deviation of 13,307 km^2, considering all release sites with an ensemble of particles initially distributed over an area of 100 km^2. In terms of an oil spill, this figure corresponds to the area of ocean that would likely need to be affected in the spring following an unsuccessful clean-up from the previous year. This also highlights the areas likely to be at risk of potentially acute biological impact.

The size of footprints was found to be sensitive to release location, and using the results presented in Section 4.3.2.2., we can define three main areas along the NSR, each with its own characteristic behaviour: a western region (in the Barents and Kara Seas, release sites 1-7), a central region (Laptev Sea and the East Siberian Sea, release sites 8-11), and an eastern region (in the Chukchi Sea and Bering Strait, release sites 12-15.) The west of the NSR was associated with the largest footprints after 9 months – up to 78,608 km^2 (from the Kara Sea) and on average 61,361 km^2. The middle of the route was associated with the smallest footprints, on average 22,739 km^2. The eastern group of release sites had typical footprints of 41,541 km^2 after 9 months.

In addition to considering the spread from individual experiments, the area covered by all 30,000 trajectories from a given site (all years / seasons of release) was calculated. This metric, termed the area of the 'envelope' of footprints represents the uncertainty in where the oil will go – i.e. the area of ocean that would need to be monitored the next spring in order to find the spilled oil. This demonstrates another important conclusion: the uncertainty in where oil could go is highly dependent on where a spill occurs. Particles from the west of the NSR tend to follow the Arctic Circumpolar Boundary Current (ACBC). They travel the farthest and are associated with the largest envelopes of footprints, and therefore a spill here would likely to require a large area (over 800,000km^2) of ocean to be searched. Particles from the Siberian and eastern groups of release sites didn't travel as far, and were associated with smaller envelopes of footprints – especially in the case of the East Siberian Sea, where the envelope was only 317,615 km^2 – less than half the size of that of the largest envelopes.

In short, the impact of advection on an oil spill occurring in the east of the NSR is likely to be more predictable than for a spill occurring in the west.

In addition to horizontal advection, it is important to consider the risk of potential subduction of oil. After the Deepwater Horizons spill in the Gulf of Mexico, unrecovered oil became suspended in deep water layers before eventually settling on the ocean floor (Valentine et al., 2014). We considered potential surface spills from shipping accidents in this research, but if some of this oil becomes entrained into deeper water, it is also likely to be irrecoverable. Therefore, it is important to understand where subduction occurs. We considered the fraction of particles that had sunk below 100m depth after 9 months and also after 2 years. This was found to be of greatest concern for particles launched from the west of the NSR, particularly for release sites in the Barents Sea (see Section 4.3.2.4).

From the three release sites in the Barents Sea (Murmansk, Barents, and Novaya Zemlya), 16% of particles were below 100m depth after 9 months, rising to 28% after 2 years. A negligible (< 1%) fraction of particles from the central group of release sites (in the Laptev and East Siberian Seas) experienced subduction. The eastern group showed only modest subduction, mostly from particles released in the Bering Strait: 6% of particles from this site were below 100m after 9 months and 10% after 2 years. Subduction primarily occurred as downwelling at the Eurasian shelf slope. This is consistent with results from previous investigation into downwelling in the Arctic Ocean. (Shapiro et al., 2003).

4.4.1. Limitations and Future Work

We are limited by dependency on a single simulation with the NEMO model: though this is a leading edge high resolution model, intercomparison work would provide added verification and estimates of model structural uncertainty. Limitations associated with this configuration of NEMO, such as its lack of tidal forcing, means that areas strongly affected by tides may be less well represented than the Arctic in general (Padman and Erofeeva, 2004). Furthermore, despite its 1/12 degree resolution, given the small internal Rossby radius of deformation in the Arctic (Nurser and Bacon, 2014), NEMO is only Eddy-permitting rather than fully Eddy resolving in all of the Arctic. As ever, this means that higher resolution would resolve more physical processes and thus potentially provide better results.

This study is also limited in that we are only considering the portion of the oil which remains mixed into the water column and does not become trapped in sea-ice – as can happen when oil becomes encapsulated into growing ice (Afenyo et al., 2015). This can, in principle, be

addressed with a similar study where the Lagrangian software used here is modified to track ice drift rather than ocean currents. However, realising this would require significant modification of the particle tracking software used here that is beyond the scope of this research. Additionally, oil would only be encapsulated in ice during the winter, and deciding when to follow ice or waters is itself a non-trivial question. This presents an interesting opportunity for further research, in which similar analysis using the concept of advective footprints could be put to use.

As discussed in Section 4.3.2.6., interesting small-scale changes in current direction were seen from certain release sites in these experiments. Some can be attributed to processes described in previous literature (Janout et al., 2015) while others, such as a potential wind-driven blocking in the Kara Gate, provide scope for further investigation.

While this study has focussed upon considering the long-term fate of spilled oil, this is not the only pollutant that is of potential interest. In principle, a similar approach could be used to assess the impact of advection on other Arctic pollutants. As with the encapsulated oil example, this may require modification of the Lagrangian software to realise this. The Arctic Monitoring and Assessment Programme (AMAP) identified four main categories of pollutant which pose a threat to the Arctic: persistent organic pollutants (POPs), 'chemicals of emerging concern' (including flame retardants and pesticides), heavy metals and radioactive waste (AMAP, 2015). Some of these (e.g. riverine pollutants and pollution from nuclear submarines) are well suited to Lagrangian modelling as they spread from an easily defined source. This approach is not applicable in cases where we cannot accurately predict the locations where they interact with the ocean.

4.5. Conclusions

Circulation pathways and associated timescales in the Arctic Ocean have been investigated, and impact of oceanic advection for potential oil spills from the Northern Sea Route (NSR) has been explored. It has been demonstrated that pan-Arctic consideration of an oil spill's fate becomes necessary after a relatively short (1-2 years) timescale. The circulation patterns simulated are in agreement with observations.

Three main regimes have been defined to describe different sections of the NSR: western, central and eastern. These are predominantly controlled by Atlantic Water, interior shelf-sea dynamics, and Pacific Water respectively. Spills occurring at the west of the NSR are likely to travel the furthest (on average, 771 km within 9 months) and have the largest uncertainties

associated with their pathways. Spills from the eastern and central groups travel less far (382 km), though those in the east have more uncertainty associated with their pathways than those in the centre.

'Advective footprints' were introduced to quantify the area of ocean that would likely be affected in spring following an unsuccessfully cleared up oil spill the previous season. On average, this figure is 45,762 km^2, but it is notably higher in the western section (61,361 km^2) and notably lower in the central section (22,739 km^2) of the NSR. The 'envelope' of these footprints was introduced to quantify the uncertainty in where the oil could go – and hence how much of the ocean would need to be searched / considered potentially at risk. For a typical Arctic oil spill, this area was 676,917 km^2.

Subduction of oil, potentially leading to unrecoverable pollution, was identified as a risk for oil spills in the Arctic, especially those occurring in the west of the NSR. It also poses a risk in the east, though to a lesser extent. Subduction is unlikely to be a concern in the Laptev or East Siberian Seas.

This study has provided a broad overview of the circulation features that would be likely to play a significant role in the event of an oil spill from the Northern Sea Route. We have been able to provide a general description of the directions that spilled oil would likely to be carried in, and the uncertainties associated with different regions. This provides the ground-work for more focused case studies in the event of an actual spill occurring.

.

Chapter 5: They Came From The Pacific: How changing Arctic currents could contribute to an ecological regime shift in the Atlantic Ocean

This chapter was published in *Earth's Future* as Kelly et al. (2020). I am the author of this work, with my co-authors contributing supervisory guidance.

Abstract

The Arctic Ocean is rapidly changing. With warming waters, receding sea ice and changing circulation patterns, it has been hypothesized that previously closed ecological pathways between the Pacific and Atlantic Oceans will be opened as we move towards a seasonally ice-free Arctic. The discovery of Pacific diatom *Neodenticula seminae* in the Atlantic suggests that a tipping point may have already been reached, and this 'opening up' of the Arctic could already be underway. Here we investigate how circulation connectivity between the Pacific and Atlantic Oceans has changed in recent decades, using a state-of-the-art high resolution ocean model and a Lagrangian particle-tracking method. We identify four main trans-Arctic pathways, and a fifth route that is sporadically available with a shorter connectivity timescale. We discuss potential explanations for the existence of this 'shortcut' advective pathway, linking it to a shift in atmospheric and oceanic circulation regimes. Advective timescales associated with each route are quantified, and seasonal and interannual trends in the main four pathways are discussed, including an increase in Fram Strait outflow relative to the Canadian Archipelago. In conclusion, we note that while tipping points for ecological connectivity are species-dependent, even the most direct routes require multi-annual connectivity timescales.

Plain Language Summary

With a warming Arctic Ocean, it has been suggested that the ocean currents that connect the Pacific to the Atlantic may change. This could have potential biological consequences, including bringing Pacific species of plankton to the Atlantic. We investigate how the pathways bringing Pacific water to the Atlantic have changed, identify a pathway that takes less time that other routes to bring waters from Pacific to the Atlantic (but that is only occasionally available), and note that even the shortest timescales are over 2 years.

5.1. Introduction

5.1.1. Marine Ecological Connectivity

The term "marine ecological connectivity" is used to describe the exchange of individual organisms within and between distinct subpopulations within the ocean (Cowen et al., 2006; Cowen and Sponaugle, 2009).

Ecological connectivity aims to explain how different ecosystems are linked in time and space, describing which subpopulations are sources of biota for other regions, sinks for biota from elsewhere, or whether a two-way exchange takes place. This is an inherently interdisciplinary problem linking the biology and physics of the oceans, and is influenced by both the circulation of the ocean and the biological characteristics of the species themselves (Cowen and Sponaugle, 2009).

Marine ecological connectivity can be broadly split into (passive) circulation connectivity and active migratory connectivity (Popova et al., 2019). Circulation connectivity describes the advective pathways along which ocean currents transport waters from one region to another (van Gennip et al., 2017), whereas active migratory connectivity is driven directly by species themselves swimming between one region and another for breeding and feeding (Webster et al., 2002). The two are not fully independent of each other – even marine species which are capable of active migration as adults typically have a planktonic stage earlier in their lifecycles (Selkoe and Toonen, 2011). However, as a large number of marine species are not capable of active migration, and because of the additional complexity of active migration (drivers, locomotion), we focus on passive circulation connectivity in this study.

In addition to understanding how different regions are connected spatially, it is important to understand how they are connected in time; specifically, their connectivity timescales. From a purely oceanographic point of view, one part of the ocean may be connected to another by circulation pathways, but this does not automatically imply that ecological connectivity between the two places exists. When considering marine ecosystems, the timescales on which different regions are linked becomes important to describe whether or not different regions are ecologically connected by ocean currents (Jönsson and Watson, 2016).

The timescales required to allow for ecological connectivity vary depending on the context of the problem. For species with a planktonic stage early in their lifecycle, their pelagic larval duration (PLD) can be used as a proxy for the timescale required for a source location

to be ecologically connected to a sink location during that part of its lifecycle (Selkoe and Toonen, 2011; Shanks, 2009). PLD can be the key limiting factor in describing the ecological connectivity – for example in the case of corals, which are dispersed entirely during their pelagic larval stages but remain static throughout their adult lives (Mayorga-Adame et al., 2017). However, for fish and other species with an active migratory adult stage, passive circulation connectivity during the PLD provides only part of the story and is limited to describing their connectivity during that planktonic stage.

Pelagic larval duration varies highly between species (Bradford et al., 2015; van Herwerden et al., 2006), but it is not the only limiting factor when considering connectivity timescales. Other barriers to connectivity exist, including the survival of the larvae as it is transported from source to sink (Treml et al., 2012). For larvae and plankton, limiting factors can include temperature, the availability of food, and predation (Cowen and Sponaugle, 2009), as well as access to nutrients and sunlight in the case of phytoplankton (Arteaga et al., 2014). For a source to be ecologically connected to a sink, it is essential that the connectivity timescale and conditions encountered along the route allow for the species to reach the sink alive.

These biophysical limitations, which are species specific, as well as changes in strength and direction of purely oceanic connectivity pathways (van Gennip et al., 2017) provide the limits as to whether or not one region is ecologically connected to another. Here, we investigate the connectivity pathways and timescales linking the North Pacific (source) to the North Atlantic (sink) across the Arctic, and discuss the implications of potentially increased ecological connectivity between the two regions as the Arctic changes.

5.1.2. Motivation: Changing Trans-Arctic Connectivity

Sea ice cover in the Arctic Ocean has declined significantly over recent decades due to anthropogenic climate change (Overland and Wang, 2013). It has been hypothesized that this reduction in sea ice is causing an acceleration of Arctic surface currents e.g. (Armitage et al., 2017), which in turn is causing accelerated Pacific-Atlantic connectivity, with potential biological consequences such as non-native species colonizing the Atlantic Ocean (Reid et al., 2007).

Increased circulation connectivity (Popova et al., 2019) between the North Pacific and the North Atlantic could lead to the enhanced ecological connectivity between their ecosys-

tems in ways that previously have not been possible (Reid et al., 2007). This makes understanding the consequences of acceleration in Arctic currents for ecological connectivity important.

One of the striking examples of increased ecological connectivity between these basins is the recent Atlantic appearance of the Pacific diatom, *Neodenticula seminae* (Reid et al., 2007). This species was observed by a Continuous Plankton Recorder (CPR) survey in the Atlantic Ocean in 1999, seemingly its first occurrence in the Atlantic for millennia, and Reid et al. (2007) proposed accelerated connectivity due to reduced sea ice cover as an explanation. Subsequent analysis of sediment cores has suggested that, although not found in any CPR surveys prior to 1999, the species may in fact have been present in the Fram Strait as early as 1989 (Matul et al., 2018).

Since its initial recording in the Labrador Sea in 1999, *N. seminae* has established itself in the North Atlantic, blooming in several locations since (Miettinen et al., 2013; Reid et al., 2007), and it has been suggested that trans-Arctic connectivity responsible for *N. seminae's* arrival may either still be active or even accelerated in more recent years (Miettinen et al., 2013). This provides motivation for this research: if Pacific to Atlantic connectivity has changed, it is important to understand how, in order to better understand the potential for future trans-Arctic migrations of species previously endemic to the two basins.

N. seminae is not the only example of trans-Arctic migration of Pacific-native species to the North Atlantic. *Mytilus trossulus* is a species of mussel extant in the North Pacific, North Atlantic and Arctic Ocean with a planktonic period of 2 weeks to 3 months (Yaroslavtseva and Sergeeva, 2006). A population of the species around northern and northwestern Greenland was analyzed and found to be more genetically similar to populations in the Pacific than the rest of the Atlantic, leading the authors to suggest that Pacific to Atlantic transport of mussels is already sporadically taking place, given favorable climate and hydrodynamic events (Bach et al., 2019).

It has been predicted that an "opening up" of the Arctic gateway could result in at least 35% (77 of 219) of shallow water mollusk species native to the northern Bering Sea becoming established in the North Atlantic Ocean without direct human aid (Vermeij and Roopnarine, 2008). Other research suggests that Pacific to Atlantic "invasions" will include species at higher trophic levels, including fish (Wisz et al., 2015). Adult species are described by active ecological connectivity, but they have a pelagic larval stage earlier in their lifecycles where they are distributed by ocean currents. How long this stage lasts is

defined by their pelagic larval duration, which can be as short as 2-4 weeks for some species of mackerel (van Herwerden et al., 2006) or as long as 1.5 years for rock lobsters (Bradford et al., 2015).

Assessing the ecological impacts of non-native species establishing populations in the North Atlantic is a complex question to address. While extinctions of pre-existing species as a result of marine invasions are uncommon (Vermeij and Roopnarine, 2008), other possible consequences include hybridization of existing species and increased competition for resources with Pacific-native species (Vermeij and Roopnarine, 2008).

In order to understand the potential impacts of non-native species reaching the Atlantic Ocean, it is necessary to understand how they manage to traverse the Arctic Ocean. To address this, we focus on answering the question of how passive ecological connectivity between the Pacific and Atlantic oceans has changed in recent decades.

The large-scale advective pathways of the Arctic Ocean are well-described (Aksenov et al., 2011; Aksenov et al., 2016; Wassmann et al., 2015), and it is known that Pacific waters reach the Atlantic via the Arctic. Key pathways are highlighted here in Figure 5.1. Three main Pacific inflow pathways are shown, through Barrow Canyon, Herald Canyon, and a central channel between the two that flows via Herald and Hana shoals (Aksenov et al., 2016; Lin et al., 2016; Timmermans et al., 2014). The anti-cyclonic Beaufort Gyre is the dominant surface feature in the western Arctic (Proshutinsky et al., 2002), and the transpolar drift transports water from Siberia towards the Atlantic Ocean (Steele et al., 2004). Water exits the Arctic through one of two pathways: either via Fram Strait, where the East Greenland Current brings it to the Atlantic (Bacon et al., 2014), or it reaches the Atlantic via one of many possible routes through the Canadian Archipelago (Rudels, 2015).

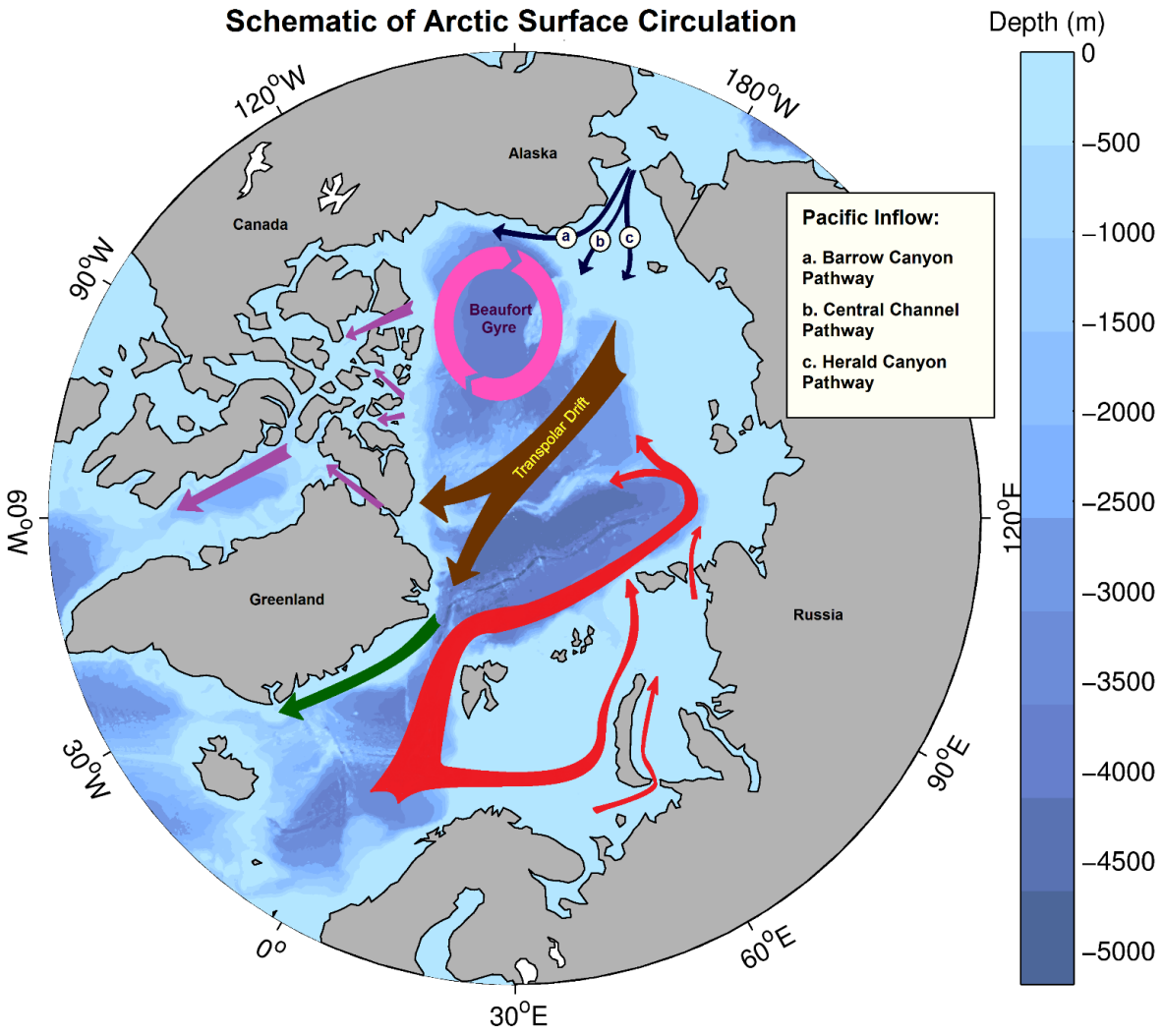

***Figure 5.1**: Schematic of large-scale Arctic Ocean circulation pathways. In dark blue, the three main Pacific inflow pathways are highlighted, via the Barrow Canyon, Central Channel and Herald Canyon. The anti-cyclonic Beaufort Gyre is highlighted in pink. The transpolar drift, which brings water from Siberia to the Atlantic is shown in brown. Water exits the Arctic via either the Fram Strait by following the East Greenland Current shown in green, or via the Canadian Arctic Archipelago. Pathways through the Archipelago are complex, and example pathways are highlighted with purple arrows. Finally, the red arrows show Atlantic water circulation pathways, entering via the eastern Fram Strait and Barents Sea opening, before following the Arctic Circumpolar Boundary Current cyclonically along the Eurasian shelf break.*

However, climate change is altering Arctic advection, and connectivity pathways, and this is believed to be the driver behind Pacific species reaching the Atlantic (Reid et al., 2007). There are several ways that trans-Arctic connectivity could change to make “invasions” of non-native species more likely. One such mechanism is an acceleration of currents across the Arctic (Armitage et al., 2017). As the Artic is a harsh environment for subpolar species minimizing transit times across it increases the likelihood of planktonic species surviving the journey.

We hypothesize that any increased circulation-based ecological connectivity is not as simple as accelerating Arctic currents in general, and that three possible changes (or their combinations) could be involved. In addition to an acceleration of Arctic currents, it is possible that connectivity timescales could be reduced by shifting advective pathways, or even opening up of new ones. Finally, it is also possible that the changed conditions in a

warmer, more ice-free Arctic could play a key role in making existing, but previously non-viable advective pathways survivable.

We suggest the following three hypotheses (or some combination of them) as explanations for how Pacific species could reach the Atlantic Ocean:

- Acceleration of surface currents
- Changing of dominant trans-arctic advective pathways and/or appearance of new / faster trans-Arctic routes
- Changes to ecologically-important properties along the routes (e.g. temperature, availability of light / nutrients)

Additionally, we note that non-oceanographic changes could be responsible for invasive species traversing the Arctic. Specifically, ballast water has been invoked as a potential explanation for successful long-range colonization events in the Arctic (Reid et al., 2007) and elsewhere (Smith et al., 2018). Reid et al. (2007) discuss this possibility as a potential explanation for the appearance of *N.* Seminae, but argue against it on the basis of the limited amount of trans-Arctic shipping that took place in the 1990s, coupled with the fact that any alternative shipping route would require the sub-polar diatoms to survive tropical conditions, which the authors concluded was highly unlikely. However, with trans-Arctic shipping likely to increase as a consequence of reduced sea ice in the region (Aksenov et al., 2017; Østreng et al., 2013), this must be noted as another indirect way in which a changing Arctic could facilitate an ecological regime shift in the North Atlantic in the future.

Here, we aim to address the first two of these hypothesises by analyzing output from a 1/12 degree NEMO ocean model (specifically, ORCA0083-N006) from a Lagrangian perspective. As we are motivated by understanding potential biological consequences of changing connectivity, we focus primarily on investigating the advective pathways with the shortest connectivity timescales.

5.2. Methods

5.2.1. NEMO model and Ariane particle-tracking

For the experiments in this paper, we used the NEMO model (NEMO stands for Nucleus for European Modelling of the Ocean framework) in conjunction with the Ariane Lagrangian analysis tool. We utilized pre-saved 5 day mean output from the 1/12° resolution

ORCA0083-N006 configuration of NEMO (Madec, 2014). This version of NEMO has approximately 3-5km horizontal resolution in the Arctic Ocean, and 75 vertical depth layers (31 levels between the surface and 200 m depth), and was run coupled to the Louvian-la-Neuve Ice Model (LIM2) (Fichefet and Maqueda, 1997; Goosse and Fichefet, 1999). At the time of writing, this was the highest resolution version of NEMO available, with horizontal resolution sufficient for it to be eddy-resolving throughout much of the Arctic Ocean, though only eddy-permitting on the shelves due to their small Rossby radii (Nurser and Bacon, 2014).

The configuration of NEMO used here was forced with version 5.2 of the DRAKKAR forcing set (DFS) (Brodeau et al., 2010). DFS 5.2 is based on ERA40 reanalysis data, comprising of 6-hourly means for wind, humidity and atmospheric temperature, daily means for radiative fluxes (both longwave and shortwave), and monthly means for precipitation. A monthly climatology is used for river runoff, taken from CORE2 reanalysis (Brodeau et al., 2010; Timmermann et al., 2005). The model hindcast used in this experiments was created using this forcing set for the period 1958-2015.

NEMO has been extensively validated throughout the Arctic. (Kelly et al., 2018) investigated how well NEMO reproduced sea ice coverage, and how the modelled SSH and barotropic streamfunction compared to satellite measurements (Armitage et al., 2016). This was expanded upon in (Kelly et al., 2019), where the modelled mixed layer was validated against observational data (Peralta-Ferriz and Woodgate, 2015) and good model skill was found. Similar configurations of NEMO have been further validated, with modelled water mass types and stratification found to be in agreement with observations (Aksenov et al., 2016; Janout et al., 2015; Luneva et al., 2015).

Here, we use the Ariane (Blanke and Raynaud, 1997) Lagrangian particle tracking tool to analyze output from the NEMO model. This software works by reading in the (pre-calculated) 5-day mean output from the NEMO model, and using it to advect virtual ‘particles’ around the ocean.

Ariane interpolates the NEMO output to solve for particle translation through model grid cells, and saving particle positions daily. The fact that Ariane (and other Lagrangian analysis packages) make use of pre-existing model output makes it a powerful tool to answer questions where an online model run with passive tracers would be prohibitively computationally expensive (van Sebille et al., 2018). However, small scale processes which are parameterized in the model, such as mixing and diffusion, cannot be directly assessed by Lagrangian analysis of advective pathways in a straightforward way (Wagner et al., 2019).

Lagrangian analysis has been widely used to investigate the Arctic Ocean in NEMO. Relevant to the research undertaken here, Pacific inflow pathways have been investigated using Ariane in conjunction with an Arctic regional configuration of NEMO (Hu and Myers, 2013), and online passive tracer multi-model inter-comparison experiments (Aksenov et al., 2016) have since supported these results. Outflow from the Arctic to the Atlantic Ocean (via Fram and Davis Straits) was investigated in a coarser ¼ resolution version of NEMO (Lique et al., 2010). Other questions, including the dynamics of the Beaufort Gyre (Kelly et al., 2019) and the fate of potential oil spills from Arctic shipping (Kelly et al., 2018) have used Ariane alongside the same configuration of NEMO employed in this paper.

5.2.2. Experiment Design

Firstly, the Eulerian changes in Arctic surface currents were investigated. We compared the mean current speeds for each decade (1970s – 2000s) to the overall mean for that period. The lack of coherence in the decadal anomalies, with some regions accelerating and others slowing down (see Figure 5.2a) motivated a Lagrangian experiment to investigate changing connectivity between the North Pacific and Atlantic Oceans.

For each Lagrangian experiment 1,000 particles were initialized, uniformly distributed across the Bering Strait. These particles were then tracked for 10 years, with positions recorded daily. 'Releases' of particles took place every month between 1970 and 2003, with the same initial 1,000 particle grid used for each experiment. The initial release of each year was performed on the 5th of January, with subsequent releases taking place at 30 day intervals beyond that. Particles were initialized in the surface layer of the ocean, and then advected via ocean currents (not sea ice velocities) in 3 dimensions. No diffusion was manually added to the advective signal read in from the NEMO, in order to maximize the generality of our experiments. For example, some species are able to control their buoyancy in order to remain in the upper mixed layer. In these cases, manually adding diffusion (e.g. via a random walk) would not be desirable given the biological context of these experiments, and so we only consider the impact of advection in order to keep the experiments as generic as possible.

After their release in the Bering Strait, the advective pathways followed by each of particles were characterized by using various 'traps' to define the route taken to reach the Atlantic Ocean. The definition of distinct pathways is discussed in more detail in Section 5.3.1. Each 'trap' is simply a region on the globe, and if a particle spends a timestep within

its defined latitude and longitude limits, it is recorded as having passed through said trap. By comparing which traps each particles does or does not pass through, it is possible to define distinct advective pathways. Grouping these pathways into meaningful routes allows us to compare how the connectivity between the Pacific and Atlantic has changed over the duration of the experiment, by considering how the number of particles following each defined route varies with year and season of release.

This trap-based approach has intrinsic limitations. As particle locations are recorded at discrete points rather than continuously, it is in principle possible for a particle to 'skip over' a trap that, physically, a water parcel would have passed through in reality. This can be accounted for by using large traps, at the cost of having rather broadly defined pathways. Where smaller traps are necessary to be physically meaningful (e.g. the Barrow Canyon trap in section 5.3.1.), the impact of overshooting can be mitigated by including an extra trap downstream to tag any particles that would otherwise have been missed.

As well as being interested in the routes taken to reach the Atlantic, we also need to consider the time taken. To do this, we define a single end trap, taken to be everything south of 60N in the Atlantic Ocean. Other definitions of when a particle has reached the Atlantic are possible (e.g. one could consider anything south of the Fram Strait), but this limit was chosen to approximately coincide with the region where *N. seminae* was first recorded in 1999 (Reid et al., 2007), thus making it a logical end goal when considering Atlantic to Pacific connectivity. When considering timescales, we make a point to consider the trajectories with the shortest connectivity timescales. The reason for this is that accelerated Pacific to Atlantic connectivity has been hypothesized to be a cause for Pacific species reaching the Arctic. If minimizing the total time spent in harsh (for sub-polar species) Arctic conditions is the limiting factor for a successful trans-Arctic crossing, focusing on the connectivity pathways with the shortest advective timescales makes sense.

5.3. Results

In order to address the first hypothesis identified in Section 5.1, we begin by comparing Eulerian output from the NEMO model as a first attempt to address whether the surface currents in the Arctic Ocean have accelerated. To do this, we took the annual mean modelled surface currents from the period studied in these experiments, and compared how each decade varied compared to the overall mean.

The 2000s anomaly is presented in Figure 5.2a as an illustrative example. It is apparent from this that there is no spatially coherent pattern to the changes in sea surface velocities: some regions accelerate, others decelerate and some currents shift their position. Similar lack of coherence was found for the 1970s, 80s and 90s (not shown). This, coupled with the multi-year timescales required for trans-Arctic crossings, makes addressing either Hypothesis 1 or Hypothesis 2 from an exclusively Eulerian viewpoint inconclusive.

This necessitates investigating the problem from a Lagrangian viewpoint. As described in Section 5.2, we do this by releasing virtual 'particles' into the NEMO model in the Bering Strait, and track their progress over ten years. 1000 particles were released every month between January 1970 and December 2002. As an illustrative example of the output produced by these experiments, all trajectories from the September 1980 release (arbitrary choice of experiment) are shown in Figure 5.2b.

The trajectories in Figure 5.2b are colored to highlight the advective pathways with the shortest connectivity timescales. This is useful for giving a first order estimate of the fastest advective timescales between the Bering Strait and the Atlantic Ocean (approximately 4 years), but at the price of masking much more of the detail. In order to extract more meaningful information from these trajectories, it is helpful to classify them based on shared characteristics. We do this by introducing 'traps' to identify which particles pass through given regions (and those which do not).

5.3.1. Characterizing different connectivity pathways

From what is already known about the Arctic Ocean circulation, as well as trajectory maps such as Figure 5.2b, the following traps were decided on to elucidate distinct pathways:

Trap 1: Barrow Canyon: South of 72N, between 155W and 157W,
Trap 2: Southern Beaufort Sea: South of 73N, between 135W and 145W,
Trap 3: East Siberian Sea: South of 73N, between 155E and 175E,
Trap 4: North Pole: North of 80N, between 120E and 150W,
Trap 5: Fram Strait: Between 75N and 80N, between 25W and 20E,
And finally an 'end' trap south of 60N in the Atlantic Ocean (between 70W and 20E).

These traps are shown geographically in Figure 5.2c. The logic behind this choice of traps is as follows:

Traps 1 and 2 were chosen to sample the Alaskan Coastal Current, which flows through the Barrow Canyon into the Beaufort Sea. Trap 1 records particles which spend at least one

timestep in this part of the Barrow Canyon, but, as it is a relatively small trap, it is possible for some trajectories to overshoot it. The larger Trap 2 is therefore included to catch the minority of particles which follow the same pathway but would otherwise have been missed. In both cases, a particle is only tagged by these traps if it passes through them within the first 2 years of its trajectory, in order to avoid false positives from particles re-circulated by the Beaufort Gyre.

Trap 3 was chosen because, as can be seen in Figure 5.2b, some trajectories begin by flowing from the Chukchi Sea into the East Siberian Sea. This trap quantifies those, although they are later grouped with other pathways (as suggested by Figure 5.2d). As with Traps 1 and 2, this trap is only triggered in the first 2 years of particles' trajectories.

Trap 4 was designed to sample the Transpolar Drift Stream. Necessarily a large trap, due to the shifting position of the Transpolar Drift due with the shift of the Beaufort Gyre, the vast majority of trajectories are tagged by this trap. Unlike the previous 3, this trap can be triggered at any time.

Trap 5 defines the route trajectories take out of the Arctic Ocean. Only two options are available: Fram Strait or Canadian Arctic Archipelago (hereafter CAA). Any trajectory that exits the Arctic without triggering the Fram Strait trap is assumed to have come through the CAA instead. (This assumption is valid, see Figure 5.3.) In principle, one could further investigate the myriad of possible pathways through the Archipelago, but we chose to simplify the problem by considering it a singular route.

The Atlantic Trap was chosen to be at 60N because this marks a consistent end point, regardless of which side of Greenland trajectories flow. It is also an interesting choice from a biological perspective, as it also corresponds approximately to the region where non-native phytoplankton were found to be blooming in (Reid et al., 2007).

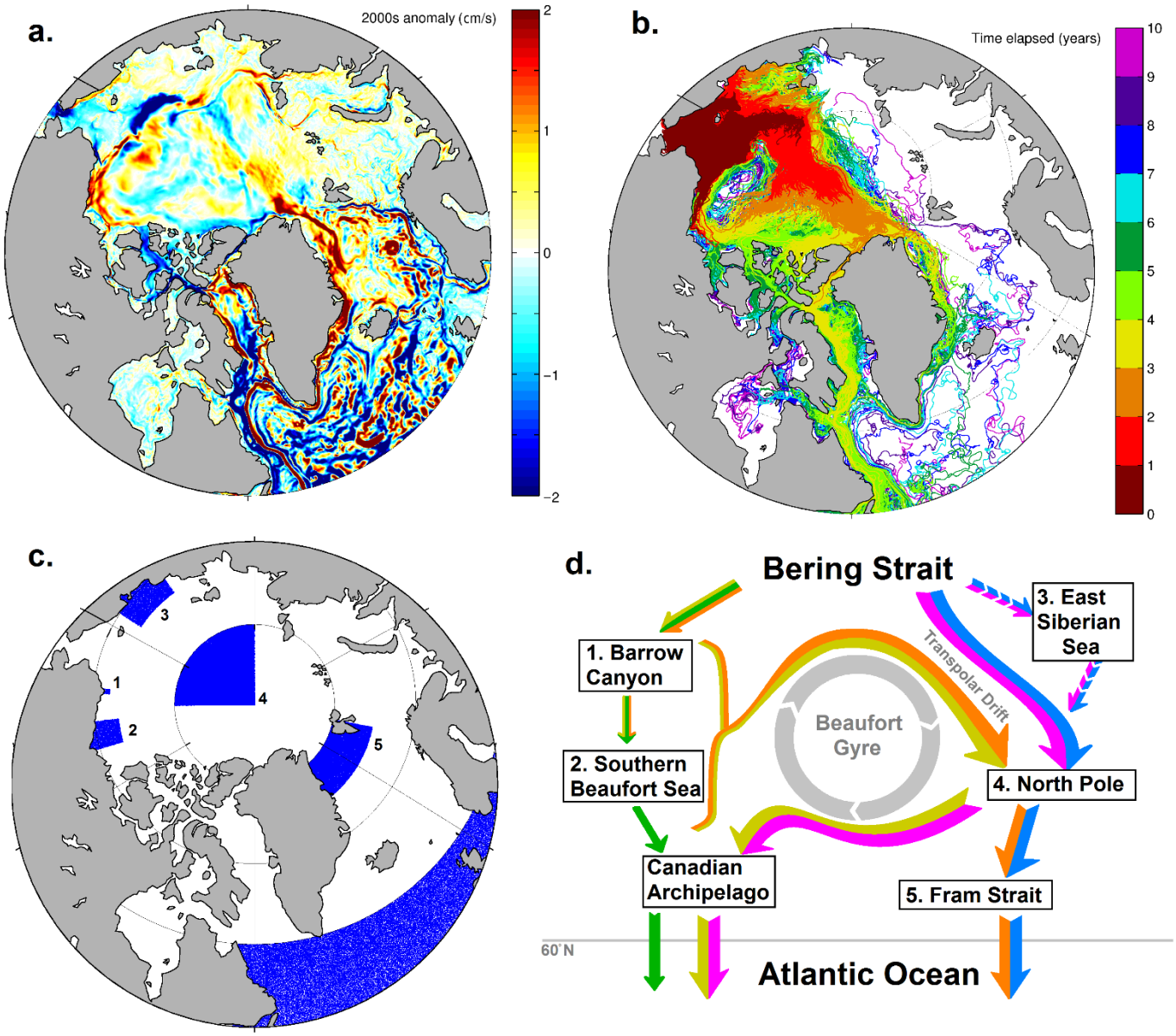

Figure 5.2: a) *The anomaly in NEMO modelled Eulerian surface currents between 2000-2009, relative to the 1970-2009 mean. No uniform pattern is apparent, with some regions accelerating and others decelerating, necessitating a Lagrangian approach to investigate changing Pacific to Atlantic connectivity* ***b)*** *Example of output from Lagrangian experiments, showing the trajectories of all 1000 particles released in September 1980. (Arbitrary choice of year / month). Color of trajectories denotes their age.* ***c)*** *Map showing the location of the 'traps' used to classify trajectories from the Lagrangian experiments. 1 = Barrow Canyon, 2 = Southern Beaufort Sea, 3 = East Siberian Sea, 4 = North Pole, 5 = Fram Strait. Also shown is the 60N trap in the Atlantic Ocean, considered the end of each trajectory. Traps 1-3 only recorded particles which passed through in the first 2 years of the experiment. Trajectories which reach the Atlantic Ocean trap without passing through the Fram Strait are assumed to have passed through the Canadian Arctic Archipelago instead.* ***d)*** *Simplified schematic showing the 5 main advective pathways identified using the traps in (c). See Table 5.1 for a more detailed explanation of how these pathways were defined.*

Using these traps, we were able to identify distinct advective pathways and group them into 5 main routes, as illustrated in Figure 5.2d. The grouping was done after identifying every possible combination of traps, and counting the fraction of trajectories which triggered each set. Each unique combination of traps was termed a 'pathway.' Pathways which were followed by at less than 0.1% of trajectories (i.e. an average of less than one trajectory per experiment) were considered negligible.

Of the non-negligible pathways, similar pathways were identified and grouped together into ‘routes’. (Pathways with < 0.1% of trajectories were also included in the groupings if sufficiently similar.) 5 main routes were identified, as shown by the simplified schematic in Figure 5.2d. These are as follows:

1. The ‘pink route’, which follows the transpolar drift and exits the Arctic Ocean via the Canadian Arctic Archipelago (CAA). Pathways 2 and 6.
2. The ‘blue route’, which follows the transpolar drift but leaves the Arctic via the Fram Strait. (With both this and the pink route, trajectories are considered part of the same route regardless of whether or not they enter the East Siberian Sea). Pathways 3 and 7.
3. The ‘yellow route’, which enters the Arctic via Barrow Canyon, changes direction and then joins the pink route to follow the Transpolar Drift and exit via the CAA. Pathways 10, 18 and 26.
4. The ‘orange route’, which begins like the yellow route (Barrow Canyon, then reversing to join the Transpolar Drift) but leaves through the Fram Strait as with the blue route. Pathways 11, 29 and 27.
5. The ‘green route’ – a markedly different pathway followed by a minority of particles. The green route enters the Beaufort Sea via Barrow canyon, then flows directly to the CAA. It is the only major pathway which doesn’t interact with the Transpolar Drift Stream. Pathways 8* and 24*. In addition to the traps described above, this group was further filtered to remove false-positive trajectories which trigger the trap after becoming entrained in the Beaufort Gyre. This is done by removing trajectories north of 75N in the Beaufort Gyre region.

Additionally, ‘other’ trajectories which don’t fit well into these definitions were identified. The majority of these are attributed to pathway 16, which appears to be something between the yellow route and the periphery of the Beaufort Gyre. (See Figure 5.3f). The full list of pathways, the total number of particles (that reach the Atlantic Ocean) following them, and their groupings is presented in Table 5.1:

Pathway Number	1. Barrow Canyon	2. Southern Beaufort Sea	3. East Siberian Sea	4. North Pole	5. Fram Strait	% of all trajectories
0						< 0.1
1					✓	0
2				✓		40.1
3				✓	✓	18.0
4			✓			0
5			✓		✓	0
6			✓	✓		4.3
7			✓	✓	✓	3.2
8*		✓				< 0.1
9		✓			✓	0
10		✓		✓		< 0.1
11		✓		✓	✓	< 0.1
12		✓	✓			0
13		✓	✓		✓	0
14		✓	✓	✓		0
15		✓	✓	✓	✓	0
16	✓					0.3
17	✓				✓	< 0.1
18	✓			✓		25.2
19	✓			✓	✓	4.8
20	✓		✓			0
21	✓		✓		✓	0

22	✓		✓	✓		< 0.1
23	✓		✓	✓	✓	< 0.1
24*	✓	✓				0.2
25	✓	✓			✓	0
26	✓	✓		✓		3.1
27	✓	✓		✓	✓	0.7
28	✓	✓	✓			< 0.1
29	✓	✓	✓		✓	0
30	✓	✓	✓	✓		< 0.1
31	✓	✓	✓	✓	✓	< 0.1

Table 5.1: *Classification of distinct pathways using the 'traps' identified in Figure 5.2c. Only trajectories which reached the final Atlantic Ocean (60N) trap are considered. The final column shows the percentage of trajectories which reached the Atlantic Ocean that followed a given pathway. Minor pathways followed by < 0.1% of trajectories were initially deemed to be negligible. Other pathways were grouped, along with similar pathways (including minor pathways), into five 'routes' (see Figure 5.2d and Figure 5.4) denoted by the color which their row is highlighted. Pathways 8* and 24* were further processed to exclude particles entrained into the Beaufort Gyre by removing trajectories which passed north of 75N in the Beaufort Gyre region. (In both cases, the trajectories removed accounted for < 0.1% of all trajectories which reached the Atlantic). Pathway 16 was non-negligible (0.3% of trajectories) but does not fit well into our classification system and is instead grouped with 'others.'*

Having grouped our trajectories into 5 main routes, it is now possible to compare how they differ spatially and vary temporally. Maps showing trajectory density for each of the five routes, as well as the 'other' group, are presented in Figure 5.3.

Figures 5.3a and 5.3b (pink and blue routes) show significant Pacific inflow through Herald Canyon (see north-south oriented white region on the American side of Wrangel Island) which is absent in Figures 5.3c – 5.3f, despite Herald Canyon not being explicitly defined with a trap.

Figures 5.3c – 5.3e all show a clear pattern of inflow dominated by Barrow Canyon, demonstrating that the 'trap' method used here works well. The return flow towards the Transpolar Drift is clearly present in Figures 5.3d and 5.3e, supporting the picture in the simplified schematic in Figure 5.2d.

Notably, the pathway through the Canadian Archipelago is visibly different in Figure 5.3e compared to the other main CAA pathways (Figures 5.3b and 5.3d.) Figure 5.4f demonstrates that the ‘other’ routes appear to be something between the green and yellow routes identified from our traps – it flows around the northern periphery of the Beaufort Gyre, but passes through the Canadian Archipelago via a path more similar to the green than yellow / pink routes.

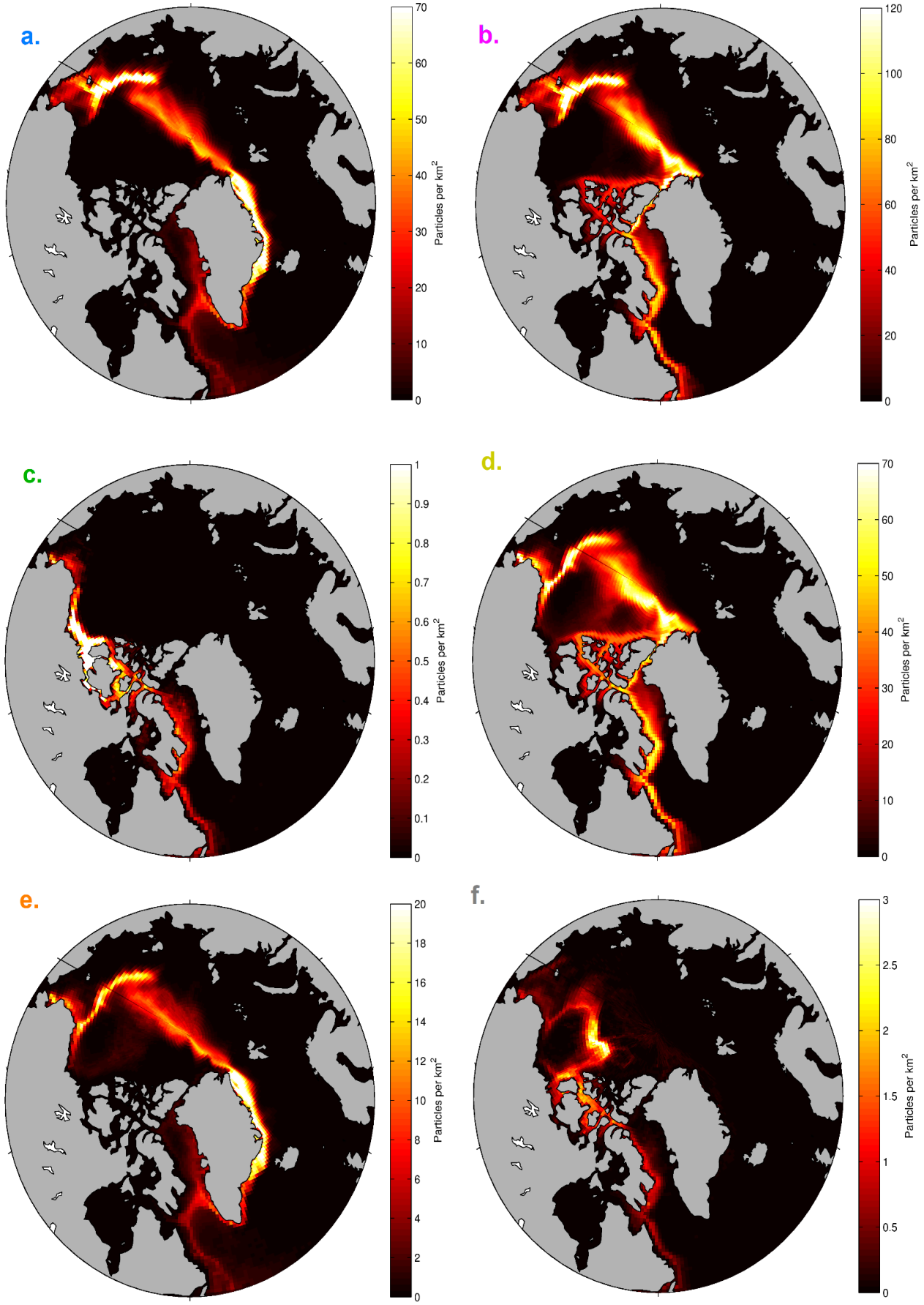

Figure 5.3: *A more detailed illustration of the advective pathways identified in Figure 5.2d. In each subplot, trajectory density (particles / km^2) is shown. Note the different scale in each panel. From each route, every particle's position at each time step was binned into a 0.5° (lat) x 1° (lon) grid, then weighted by cell area to produce these density maps.* ***a)*** *'Blue route' from Figure 5.2d, comprised of trajectories avoiding Barrow Canyon and joining the transpolar drift, be-*

fore exiting the Arctic via the Fram Strait. ***b)*** *'Pink route' from Figure 5.2d. Initially the same as the blue route, this pathway branches off to exit the Arctic via the Canadian Arctic Archipelago (CAA) instead of the Fram Strait.* ***c)*** *'Green route' from Figure 5.2d, comprised of trajectories which reach the Beaufort Sea via Barrow Canyon, and then flow directly through the CAA to the Atlantic.* ***d)*** *'Yellow route' from Figure 5.2d, flows through the Barrow Canyon as in the green route, before changing direction to join the transpolar drift and then leave the Arctic via the CAA.* ***e)*** *'Orange route' from Figure 5.2d. Initially the same as the yellow route, but branches off to exit the Arctic via the Fram Strait.* ***f)*** *Trajectories not assigned to any of the previous five advective pathways.*

5.3.2. Variability of Pacific – Atlantic Routes

Having identified the main advective pathways connecting the Bering Strait to the Atlantic Ocean and how they differ from each other, we now investigate how they vary with time. Initially, we simply consider how the number of particles successfully reaching the Atlantic Ocean changes. From Figures 5.4a and 5.4b (red and black lines), it is clear that the number of 'successful' trajectories is sensitive to time of release, but that the 10 year experiment duration is sufficient for approximately half (47.7%) of all trajectories to reach the Atlantic trap. The large number of particles remaining in the Arctic for the duration of the experiment should not be unexpected, in no small part due to those which become entrained into the Beaufort Gyre (e.g. Kelly et al (2019)). From Figure 5.4a, we can see that late summer releases typically had the greatest chance of reaching the Atlantic within 10 years. Figure 5.4b shows significant interannual variability in whether or not trajectories successfully reach the Atlantic Ocean.

Investigating the seasonal cycle (Figure 5.4a) further shows that there is a clear oscillation whereby the pink and yellow routes (both via Barrow Canyon) are favored in spring / summer whereas the blue and pink routes (both via Herald Canyon) are favored in autumn / winter. This is in line with well-established seasonality in the Pacific inflow to the Arctic Ocean (Aksenov et al., 2016). Three main Pacific inflow pathways are known to exist: the Alaskan Coastal Current / Beaufort shelf break jet through Barrow Canyon, a pathway through the Herald Canyon, and a central channel via the Herald and Hana Shoals (Timmermans et al., 2014). The Beaufort shelf break jet, corresponding to the yellow, green and orange pathways here, is known to peak in summer (Lin et al., 2016).

The sensitivity to time of release was similarly investigated by tracking the number of trajectories following each route based on when they released. This is shown in Figure 5.4b, where the time series has been smoothed by applying a 12-month running average to remove the seasonal cycle evident in Figure 5.4a. Given the sizable variation in the number of particles reaching the Atlantic by year, it makes more sense to consider the relative

number of trajectories following each route than the raw numbers shown in Figure 5.4b; the relative fraction of trajectories following each route is shown in Figure 5.4c.

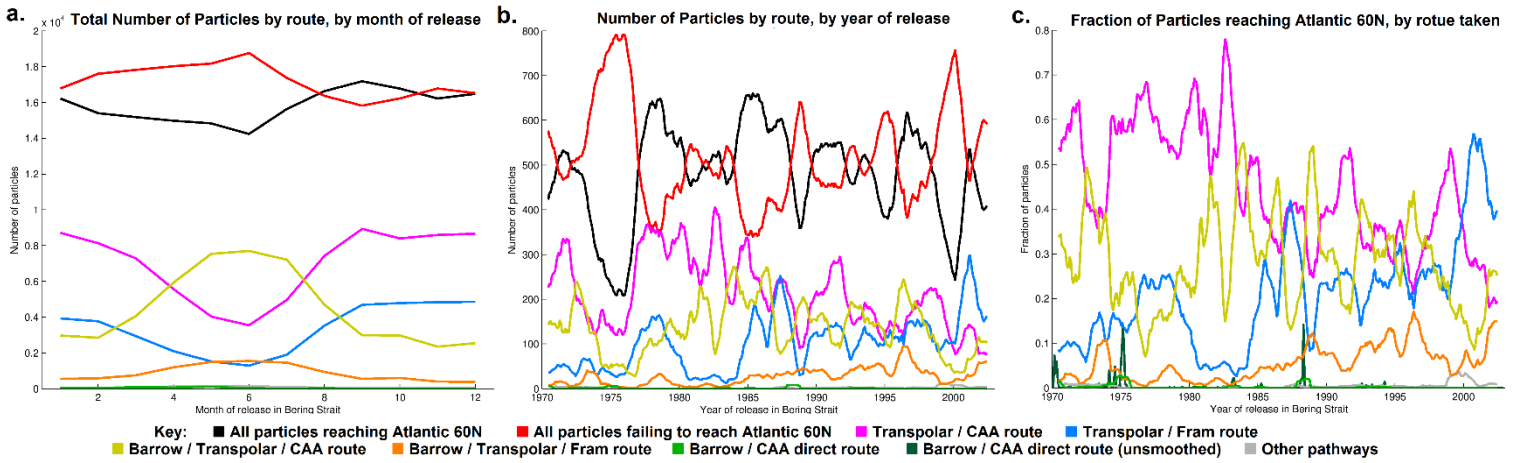

Figure 5.4: a) *Comparison of the number of trajectories reaching (black) or failing to reach (red) 60N in the Atlantic Ocean within 10 years of being released in the Bering Strait. Other colors show how the routes taken vary by season – see key for explanation of each color. Trajectories passing (not passing) through the Barrow Canyon are more (less) frequent in spring/summer releases than in autumn/winter.*
b) *Comparison of the number of trajectories reaching (black) or not reaching (red) 60N in the Atlantic Ocean, and following each route (all other colors) by time of release, in all cases with the seasonal cycle in (a) removed by taking a running 12-month average. The (non-Barrow Canyon) transpolar drift to Canadian Arctic Archipelago (pink) route is the dominant pathway for the majority of the experiment, before being usurped by the (non-Barrow Canyon) transpolar drift to Fram Strait route towards the end of the study period.*
c) *Comparison of the trajectories which reach 60N in the Atlantic Ocean, showing the fraction of 'successful' trajectories which take each path way. As in (b), a running 12-month average is used to remove the seasonal cycle, with the exception of the dark green line, to demonstrate that although typically either unavailable or negligible, the green pathway can represent a significant number of trajectories when available.*

Figure 5.4c yields several interesting results. The first thing that can be noted is that the pink (Herald Canyon – transpolar drift – CAA) route is the dominant advective pathway throughout the 1980s, before declining and eventually being replaced by the blue (Herald Canyon – transpolar drift – Fram Strait) route in the later years of the experiment. The yellow (Barrow Canyon – transpolar drift – CAA) route shows considerable interannual variability but no clear trend, and the orange (Barrow Canyon – transpolar drift – Fram Strait) route shows a small positive trend. In all cases, the trends have considerably more noise than the more significant trend evident in Figure 5.4a, and the statistical significance of these trends is impacted by the interannual variability in number of successful trajectories. Some real variability due to the Arctic Oscillation may be expected (Morison et al., 2012; Steele et al., 2004), but artifacts of model spin up is another possible explanation discussed in Section 5.4.

The green (Barrow Canyon – Beaufort Sea – CAA) route and 'other' routes are largely negligible when considering the 12 monthly rolling average. However, using a rolling average masks the true importance of the intermittent green route. In Figure 5.4c, the un-averaged time series for the green route is shown in darker green. While still usually negligible, there are two major peaks – 1975 and 1988 – where the green route represents > 10% of successful trajectories. Thus, we identify this as an intermittent, yet significant advective

pathway for Pacific to Atlantic connectivity. The importance of this route becomes apparent when considering advective timescales, and is discussed more thoroughly in Section 5.4.1.

5.3.3. Advective Timescales

We now move on to considering the differences in connectivity timescales between the Pacific – Atlantic connectivity pathways. As we are interested in ecological connectivity, for example non-native planktonic species being brought from the Pacific to the Atlantic, it is sensible to consider the fastest cross-Arctic transits. This is for two reasons: each particle represents a large volume of water, potentially containing a large volume of biomass, so even one particle in our Lagrangian experiments could be sufficient to explain a phytoplankton bloom. Secondly, the Arctic is a harsh environment, so it stands to reason that minimizing the time spent in the Arctic corresponds to maximizing the survival chances of sub-polar Pacific species.

In Figure 5.5a, we present the shortest advective timescale along each route from each release. This produces a noisy time series (which is smoothed in Figure 5.5b), but unlike in Figure 5.4, this cannot be attributed to a seasonal cycle: as Figure 5.5c shows, aside from a small trend whereby summer releases take less time for the yellow and orange routes (both via Barrow Canyon), there is no seasonal trend for the also noisy blue and pink routes.

Nevertheless, the same 12-monthly running average was applied to smooth the data and attempt to elucidate a trend. No clear long-term trend showing a shortening / lengthening on the typical advective timescales was found in this experiment, however it can be noted that both Fram Strait routes (blue and orange) took up to 2 years longer than was typical for the other routes during the first half of the 1980s, during which time the number of particles following the blue route also dropped (Figure 5.4b and c). Aside from this, the advective timescales associated with four most important (by number of trajectories) pathways largely varied in phase with each other. We can also note that the ‘other’ group of pathways consistently has a much longer associated timescale than the other routes, justifying our decision to neglect them from the main routes.

Taking a running average of the green route makes little sense given the intermittency of this route (see faint green line in Figure 5.5b). For this reason, the connectivity timescales associated with this route are plotted as individual dots as and when the route exists. It is interesting to note that, in the releases identified in Figure 5.4c as having an anomalously large fraction of particles following this pathway, the green route takes approximately one

year less to reach the Atlantic than any of the other routes. As well as the 1975 and 1988 peaks identified in Figure 5.4, this pathway provides anomalously rapid transport to the Atlantic for other releases in the early 1980s and early 1990s. We identify this as not just a markedly different advective pathway from the more common transpolar routes, but also as a potential shortcut.

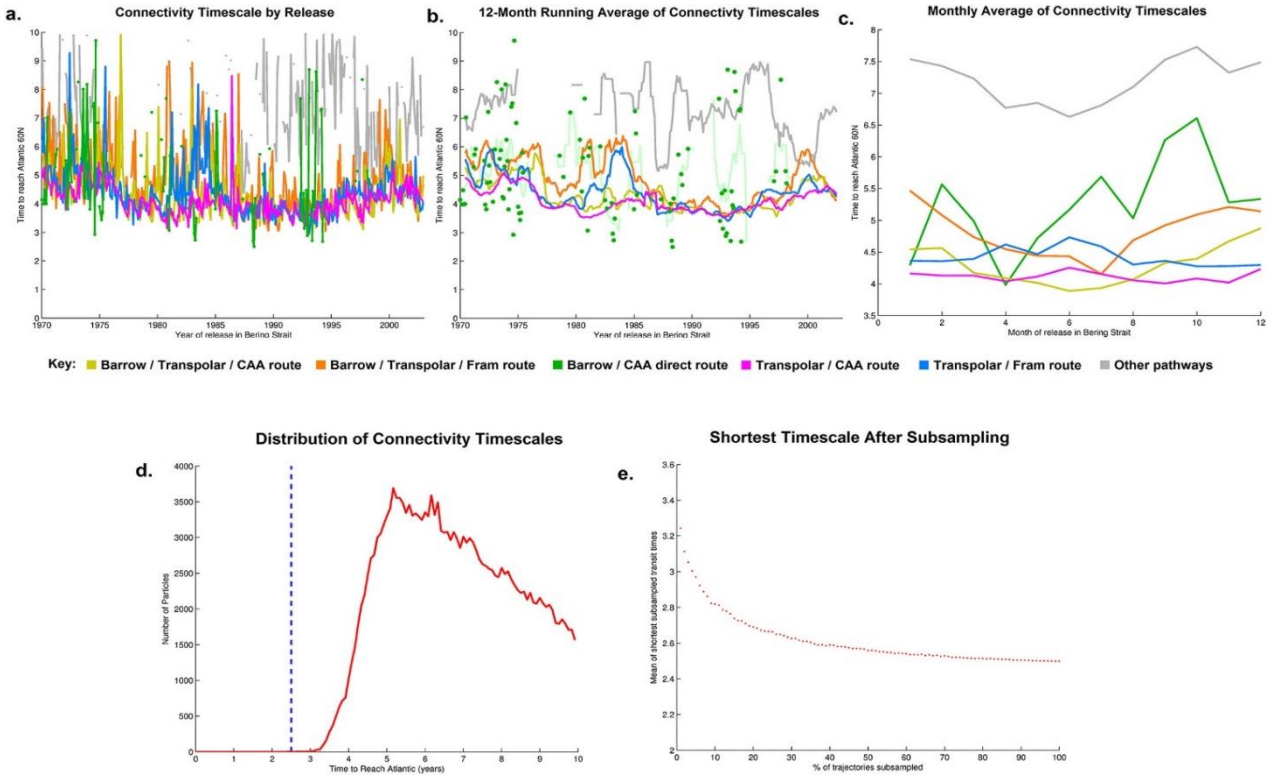

Figure 5.5 a. *Comparison of how connectivity timescale, defined to be the time taken by the first trajectory to reach 60°N in the Atlantic Ocean, varies with time of release for each of the routes identified in Figure 5.2d. No clear trend is evident, and variability between releases is considerable in all routes.* ***b.*** *Comparison of connectivity timescales, this time smoothed with 12-montly rolling averages. Years on which no trajectories followed a route are ignored. Due to the green route only being occasionally available, the timescale for each release is plotted as a dot rather than the running average.* ***c.*** *Monthly averages of connectivity timescales for each route. No trend is apparent for the pink, blue, or green routes; however, the orange and yellow routes have shorter connectivity timescales in summer than in winter.* ***d.*** *Distribution of all connectivity timescales, binned at 1/12 yearly intervals. Dashed blue line shows the absolute shortest timescale (2.50 years) recorded.* ***e.*** *Mean of absolute shortest remaining connectivity timescale, after random subsampling (without replacement) at the rate shown by the x-axis 1000 times.*

The distribution of connectivity timescales (binned at 1/12 yearly frequency) is presented in Figure 5.5d. This shows skewed distribution, with a relatively sharp cutoff on the short timescale side and a much longer tail for long connectivity timescales. In order to test how well our 1,000 particles-per-release experiments capture extreme values at the short-timescale end of the distribution, we performed a subsampling experiment. This was done by randomly sampling (without replacement) 1%, 2%, … , 98%, 99% of connectivity timescales and comparing the minimum remaining timescale in each case. This subsampling was repeated 1,000 times, with the mean shortest remaining connectivity timescale rec-

orded for each subsampling rate. The result of this is shown in Figure 5.5e. The trend becomes asymptotic as the subsampling rate tends to 100%, and even reducing the number of particles by a factor of 10 only increases the minimum timescale by ~3 months. This suggests that the shortest connectivity timescales recorded in our experiments are a good approximation of the true minima that would be recorded with an arbitrarily large number of trajectories.

5.4. Discussion

5.4.1. Variability and trends in advective pathways

The four main advective pathways (blue, pink, yellow and orange) described in Section 5.3.1 show significant temporal variability, both seasonally and interannually. The seasonal variability, seen in Figure 5.4a, shows a clear split between Pacific inflow to the Arctic via Barrow Canyon (yellow and orange) and other pathways (blue and pink), with the Barrow Canyon pathways favored by particles released in the Bering Strait during spring / summer, and the other pathways favored by autumn / winter releases.

This is in agreement with previous research into Pacific Water pathways in the Arctic Ocean (Aksenov et al., 2016; Timmermans et al., 2014) which note three main Pacific Water pathways across the Chukchi Sea: a branch through Barrow Canyon (corresponding to the orange, yellow and green routes in our experiment), a branch through Herald Canyon, and flow between the two over the central shelf. We group the latter two pathways together, both of which contribute to our blue and pink routes here.

The yellow, orange and green routes which flow through Barrow Canyon are attributed to the Beaufort Sea shelf break jet (Appen and Pickart, 2012). The relative increase / decrease in number of trajectories following these pathways is in agreement with the seasonal cycle of cyclonic (winter) and anti-cyclonic (summer) atmospheric wind forcing (Proshutinsky et al., 2009), which we would expect to drive an Ekman transport conveying trajectories either towards (summer) or away from (winter) the shelf break jet.

Van Appen and Pickart (2012) note that the winter configuration of the shelf break jet can extend over a sufficient distance that it should be able to reach the Canadian Archipelago. This is in agreement with the pathway followed by the green route in our Lagrangian experiments. However, the majority of Pacific Water transported to the Atlantic is known to follow the transpolar drift (Nguyen et al., 2011). Our results also support this, with the

'green route' identified here being dwarfed by the four other routes (all of which are characterized by following the transpolar drift).

The interannual variability of advective pathways was also investigated. Significant interannual variability, but no clear trend, was found between the relative importance of the Barrow Canyon (orange, yellow, green) and non-Barrow Canyon routes. A trend was apparent in the exit points to the Atlantic Ocean, however. For particles released in the Bering Strait between 1980 and 2003 there was a relative increase in pathways exiting via the Fram Strait. Observations show that the Pacific connectivity to the Canadian Archipelago and/or Fram Strait is linked to the Arctic Oscillation regime (Morison et al., 2012; Steele et al., 2004), however, due to the start of the experiment being relatively close to the beginning of the model run, the effect of model drift due to the spin up period cannot be discounted as another possible influence on these trends. Barotropic circulation spin-up typically takes few months and baroclinic circulation trend is 2% per year after ~20 years (Aksenov et al., 2016; Wang et al., 2016), however this is difficult to disentangle with varying forcing.

5.4.2. Causes of Intermittent 'Green Route'

As identified in Section 5.3.3, the 'green route' can have an anomalously rapid connectivity timescale, in some cases over a year shorter than all other pathways. However, as previously noted in Section 5.3.2, the availability of this pathway is intermittent. From Figure 5.4c, the two clearest examples of this route existing as a major pathway occur in 1975 and 1988.

In order to investigate potential causes for the pulse-like nature of this pathway, we compare two indices that describe the large-scale behavior of the Arctic Ocean: the Arctic Oscillation (AO) and the Arctic Ocean Oscillation (AOO). Both of these metrics describe the cyclonicity (or anti-cyclonicity) of the Arctic: in the case of the AO, the index describes the relative strength of the anti-cyclonicity of the large-scale atmospheric forcing driving the ocean (Thompson and Wallace, 1998), with negative indices corresponding to stronger anti-cyclonic winds. The AOO is an index derived from a 2-level model to describe the barotropic component of the ocean's response to atmospheric forcing: the sign and magnitude of the AOO are calculated as the gradient of sea surface height between the center and periphery of closed circulation in the Arctic (Proshutinsky and Johnson, 1997).

The signs of the two indices are essentially flipped, with positive AOO corresponding to an anti-cyclonic response from the Arctic Ocean, and negative indices associated with more a more cyclonic ocean (Proshutinsky et al., 2015; Proshutinsky and Johnson, 1997). These indices are presented in Figure 5.6a.

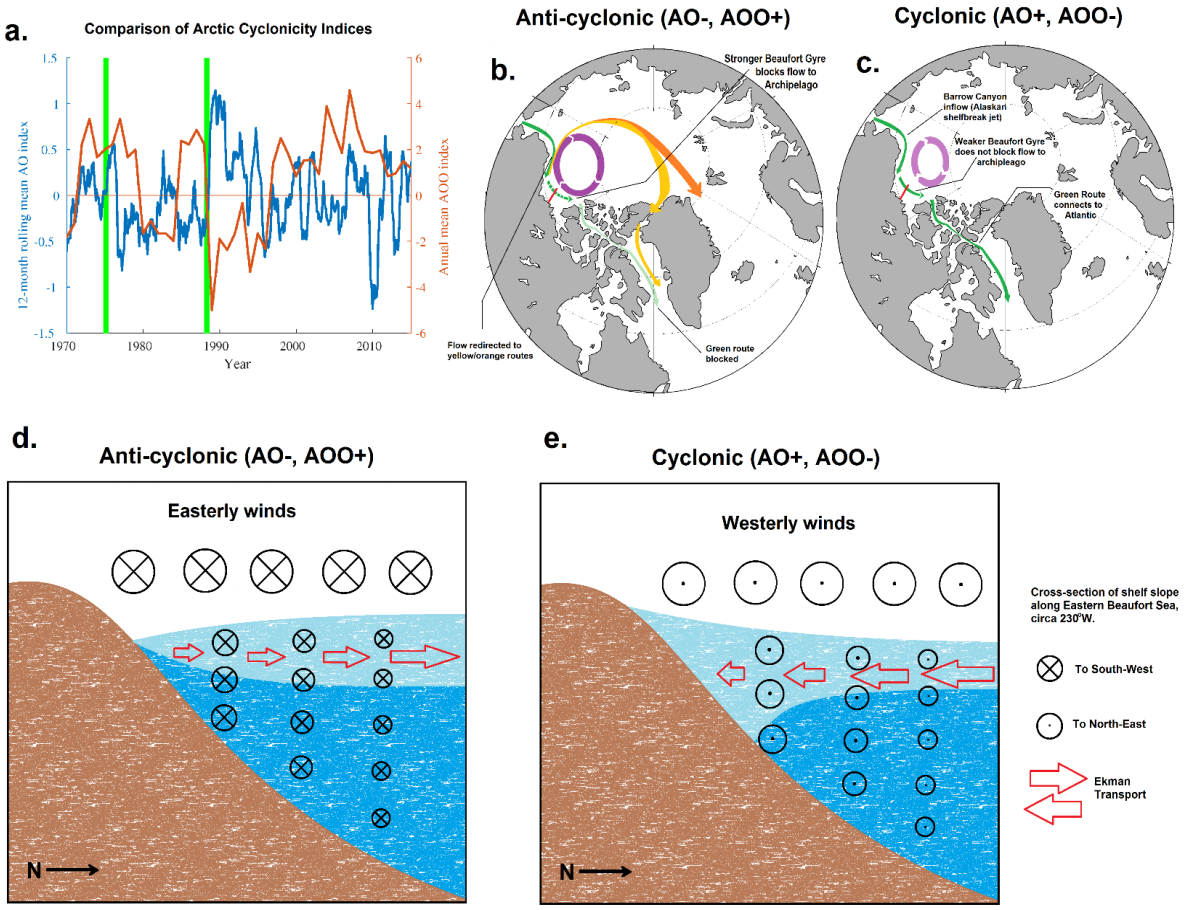

Figure 5.6: a) *Comparison of the 12-monthly rolling mean Arctic Oscillation (AO, blue) index taken from the NOAA, and the annual Arctic Ocean Oscillation (AOO, orange) index over the period 1970-2015. Vertical green lines show the two release times that were associated with the largest fraction of trajectories following the 'green route' (see Figure 5.4c).* ***b)*** *Simplified circulation schematic showing the anti-cyclonic regime in which the green route is blocked and diverted to yellow/orange routes.* ***c)*** *Simplified circulation schematic showing the more cyclonic regime in which the green route is permitted.* ***d)*** *Idealized cross section along red line in figures 5.6b and 5.6c, under the anti-cyclonic regime. Easterly winds are favored, driving an Ekman transport away from the shore. By continuity, this induces a sea surface slope downwards towards the coast, which supports a barotropic geostrophic flow towards the west (stronger closer to the coast), which blocks the green route as in Figure 5.6b.* ***e)*** *Idealized cross section along the same line, but in the cyclonic case that favors the green route in Figure 5.6c. Cyclonic regime favors westerly winds, which drives Ekman transport to the coast. By continuity, this induces a sea surface gradient up towards the shore, which in turn supports a geostrophic barotropic flow towards the Canadian Archipelago.*

Figure 5.6a shows that describing the large scale cyclonicity/anti-cyclonicity of the Arctic is not trivial, and the two indices do not always have opposite signs to each other. However, 1989 - an anomalously cyclonic year – is clearly picked out by both measures. As well as showing the AO and AOO indices, Figure 5.6a highlights the two releases (March 1975 and May 1988) which had the greatest fraction of trajectories following the 'green route' pathway that avoids the transpolar drift (see Figure 5.3c). Note that it is the initial

time of release highlighted by the vertical lines in Figure 5.6a – even the trajectories with the shortest connectivity timescales take at least 2-3 years to reach the Atlantic, so trajectories are affected by forcing (at least) 2-3 years after the green lines indicates.

A comparison of the circulation with the green route open/closed is presented in Figures 5.6b and 5.6c. The May 1988 release stands out as special because it has the single largest number of particles following the green route from any release in these experiments. The 1975 peak in Figure 5.4c is in part due to the relatively small number of particles reaching the Atlantic at all from that release, whereas the 1989 peak comes from a year with a greater fraction of 'successful' trajectories.

It is also interesting to note that, shortly after these particles were released, the Arctic Ocean switched from anti-cyclonic to anomalously cyclonic –as highlighted in both the maxima in AO and minima in AOO indices in 1989. This also occurs in the AO index (though not the AOO) with the 1975 release.

We suggest that this increased cyclonicity is a driver for the 'green route' Pacific to Atlantic connectivity pathway. The mechanism behind this is as follows: cyclonic atmospheric forcing drives stronger westerly winds along the Beaufort Sea shelf break, which causes an Ekman transport towards the coastline, causing downwelling at the coast. By continuity, this induces a slope in sea surface height, with a downward gradient away from the shore. This sea surface gradient in turn drives a barotropic current towards the Canadian Archipelago, consistent with the 'green route' identified in Figure 5.3c. A simplified 2-layer schematic of this is presented in Figure 5.6e.

Conversely, in the anti-cyclonic case, upwelling-favorable easterly winds (Brugler et al., 2014; Pickart et al., 2009) drive a barotropic current away from the Canadian Archipelago that serves to block the green route. The mechanism for this is the opposite of that in Figure 5.6e, as this time easterly winds create a downward sea surface gradient towards the coast, which induces the blocking current and prevents the green route from connecting to the Canadian Archipelago. This is presented schematically in Figure 5.6d.

Observational data, based on mooring arrays in the Beaufort Sea, support this idea. In January 2005, pulse-like enhancements of the Beaufort Sea shelf break current were recorded at a mooring in the south-east of the Beaufort Sea (Barber et al., 2015). This mooring (CA13) is located downstream of where trajectories following the "orange" and "yellow" routes diverge from the "green route" in Figure 5.3. Dmitrenko et al. (2016) investigated these pulse like enhancements and found that they were associated with cyclones to the north of the shelf slope causing an Ekman transport towards the coast, creating a cross-

slope pressure gradient in turn driving the eastward geostrophic current. Two modes of the shelf break current were identified, with downwelling-favorable winds driving a current along the Beaufort shelf towards the Canadian Archipelago, whereas upwelling-favorable winds drive an oppositely directed current to the west (Dmitrenko, 2018), which is in agreement with the mechanism described here. In a modelling study, Hu and Myers (2013) compared two routes ("Alaskan" and "Transpolar") linking the Pacific Ocean to the Canadian Archipelago, and found connectivity timescales comparable to those presented here. They also noted wind-driven freshwater storage in the Beaufort Gyre as a driving mechanism of increased geostrophic transport along the Alaskan route during the model spin up period (Hu and Myers, 2013).

We propose that cyclonic wind-driven current events are responsible for providing the link between the well-established Alaskan shelf break current and the Canadian Arctic Archipelago. The intermittent, pulse-like nature of the geostrophic current observed by moorings (Barber et al., 2015; Dmitrenko et al., 2016) supports the pulse-like nature of the "green" Pacific to Atlantic connectivity pathway highlighted here.

5.4.3. Ecological Context

The most rapid advective pathways found in these experiments suggest that at least 2 years is required for a successful transit from Pacific to Atlantic via the Arctic Ocean, and that the advective pathway permitting this was only sporadically open. Of the more typical advective pathways, the shortest possible connectivity timescales were 3-4 years, with a slight decrease in timescales occurring between 1970 and the mid-1990s.

As discussed in Section 5.1.1, the key limiting factor between circulation connectivity is not just whether or not species from the Pacific could potentially reach the Atlantic, but whether or not they could make it there alive. For species with a pelagic larval stage, the pelagic larval duration (PLD) is another limiting factor that dictates whether passive circulation connectivity is sufficient fast to permit ecological connectivity between two regions (Cowen et al., 2006; Selkoe and Toonen, 2011).

As these limiting timescales vary significantly between species (Bradford et al., 2015; van Herwerden et al., 2006), it is beyond the scope of this research to address whether or not the connectivity changes described in Section 5.3 would constitute a tipping point for any specific species. However, with even the shortest Pacific to Atlantic connectivity timescales being greater than 2 years, our results suggest that the tipping point for any species

requiring a single-summer transit to avoid Arctic winters is highly improbable. The >2 year connectivity timescales found here are beyond the PLD of even rock lobsters at 18 months (Bradford et al., 2015), but does not necessarily preclude a stepping-stone style transit with species reproducing along the journey (Selkoe and Toonen, 2011). Planktonic species, such as the *Neodenticula seminae* diatoms found in the North Atlantic and discussed by Reid et al. (2007), are not limited by PLD and so >2 year transits cannot automatically be ruled out. However, assessing whether or not a tipping point has been reached for any individual species requires knowledge of the species lifecycle, what conditions it requires to survive, and whether or not it could reproduce in transit. It might be expected that shorter connectivity timescales, such as those in the green route highlighted here, could be more favorable as they minimize time spent in harsh Arctic conditions, but analysis of individual species is required to fully answer these questions.

5.4.4. Limitations and Future Work

The research presented here used a 1/12 degree resolution ocean model. This was the highest resolution model available to us, and it is important to note that connectivity pathways described here – including the anomalously short-timescale route through the Canadian Archipelago pass through narrow passageways that may not be sufficiently well resolved in coarser models. How trans-Arctic connectivity could change in future decades remains an open question, but future-projection ocean models are typically only available at lower spatial resolution than used here (Yool et al., 2015). High resolution models are required to accurately assess Pacific to Atlantic connectivity.

Offline Lagrangian modelling has the advantage that, by utilizing existing model output, it allows experiments that would otherwise be prohibitively computationally expensive to run. The Lagrangian particles in these experiments were driven by pre-saved output from the NEMO ocean model, and this was saved as 5-day means. However, this coarse time resolution loses the variability and structure in advection in the sub-hourly timesteps that the model was run with online. This averaging could potentially remove anomalously fast and anomalously slow, but short-lived currents.

In the context of these experiments, where we are primarily interested in the most rapid connectivity pathways, this implies another limitation of our experiments: there is a chance that the averaging of NEMO output used to drive our Lagrangian experiments could lengthen the shortest connectivity timescales reported here, potentially causing a system-

atic underestimate of connectivity timescales. Further, more computationally intensive, experiments run either with Lagrangian particles or online tracers would be necessary to fully answer this question.

We are further limited by the use of only one ocean model run with only one forcing set. Although NEMO has been extensively validated (Aksenov et al., 2016; Janout et al., 2015; Kelly et al., 2019; Luneva et al., 2015), an intercomparison project using an ensemble of models would increase the validity of this work.

5.5. Summary and Conclusions

Three hypothesises that could potentially explain increased ecological connectivity between the North Pacific and North Atlantic Oceans were identified. These were: 1) Acceleration of advective timescales connecting the Pacific and Atlantic; 2) A change in relative importance of existing advective pathways and/or appearance of new, more rapid pathways; 3) Changing conditions along the route.

The third hypothesis is beyond the scope of this paper, and remains an interesting open question for future research to address. The first and second hypothesises were investigated using a Lagrangian particle tracking experiment.

Five main advective pathways, including one pathway which was only sporadically available were defined. All four of the main advective pathways showed significant interannual variability in advective timescales, with an overall decrease from 5-6 to 4 years between 1970 and 1995, and a slight increase in advective timescales in the period 1995 to 2003. Even the absolute shortest advective timescales were still multi-year, implying that any species making trans-Arctic migrations would necessarily have to be capable of surviving Arctic winters in order to colonize the North Atlantic.

Two main trends in the relative importance of these advective pathways were found. A seasonal trend, with pathways favoring the Barrow Canyon in summer and other inflow pathways in the winter was found, in line with previous research onto Pacific water pathways in the Arctic Ocean (Aksenov et al., 2016). Moreover, an interannual trend was found, showing the Fram Strait increasing in importance as an outflow pathway for Pacific to Atlantic connectivity since 1980, especially post 1989, replacing the Canadian Archipelago as the dominant outlet at the end of the experiment. The influence of the Arctic Oscil-

lation on Pacific connectivity to the Fram Strait and/or Canadian Archipelago has been discussed by Steele et al. (2004) is one potential explanation for this, but model spin-up effects may also be a contributing factor.

In addition to the four main advective pathways, a fifth, sporadically available and markedly different connectivity pathway between the Pacific and Atlantic Oceans was identified. This pathway (referred to as the 'green' route here) follows the Barrow Canyon inflow after entering the Arctic Ocean, but, unlike the main pathways, avoids the transpolar drift. Instead, this route sticks to the North American coastline, before exiting the Arctic via Parry Channel in the Canadian Archipelago.

This route is special from an ecological context because it is anomalously rapid compared to the main Pacific to Atlantic pathways. It has connectivity timescales in some cases over 1 year more rapid than other routes starting in the Bering Strait at the same time, and is the only route which allows for below 3 year connectivity timescales between the Pacific and North Atlantic. From a biological perspective, this is potentially important because ecological connectivity requires connectivity pathways with a short enough timescale for Pacific species to reach the Atlantic alive. A sporadically available advective pathway with a shorter than usual connectivity timescale provides such a potential ecological connectivity pathway. However, the timescale required for a successful transit is dependent on both the species in question and the conditions it experience along route. Further research is required to establish whether or not this pathway has played a role in previous ecological transits or if it could play a role in future transits.

Chapter 6: Discussion, Summary and Outlook

The purpose of this section is to summarise and put into context the results of the preceding research papers, to elaborate on my contribution to other work completed during my PhD but separate from the main results chapters, and to discuss potential avenues for future research.

6.1. Synthesis, Lessons Learned and Future Outlook

Throughout the research chapters of this thesis, a common theme has emerged: The Arctic Ocean is strongly interconnected, and Lagrangian particle tracking is a powerful tool for investigating connectivity. Many lessons were learned along the way, and areas in which this work could be improved upon were identified. This section aims to address these lessons, highlight the linkages between all three papers, and set out suggestions for what could have been done differently.

In Chapter 4, the second research chapter presented here but the first to be written and published as S. Kelly et al. (2018), we began by looking at the impact of connectivity pathways on potential oil spills originating from the Northern Sea Route. Particle release experiments were preformed and repeated at 15 different locations, sampling different parts of the shipping pathway. Metrics to quantify the impact of advection on a spill at each of these sites were defined, including how far it would likely travel within a year and the size of area potentially at risk – the circulation footprint. Another metric was defined to quantify how these footprints varied between experiments, in order to give a measure of the uncertainty in the potential fate of oil spills from a given location. The risk of dissolved pollutants being subducted into deeper water was assessed, and this was found to be most likely in the Barents Sea. These advective pathways identified were then discussed in the context of their importance for pollutants, particularly oil spills in the Arctic.

A key element of this research was the definition of initial conditions, which were later replicated when modelling of the Sanchi oil spill. A 10km x 10km ‘release box’ was chosen, over which particles were initially distributed. The sensitivity of results to the size of release box was investigated, and it was found that either increasing or decreasing the initial release area by a factor of four typically made little difference to the advective footprint metrics. However, this is not the only thing that could be varied – a square oil spill is clearly unphysical, so a next logical step could be to explore how the choice of initial release shape, as well as area, affects the experimental results. One other improvement would be that, as with any Lagrangian experiment, more trajectories would make for more accurate characterisation of advective pathways. Another potential avenue for future research would be a statistical investigation of the minimum number of particles required for meaningful metrics to be defined.

Because S. Kelly et al. (2018) was a very applied paper, I chose to investigate a physical problem for the next chapter of my thesis (but owing to its purer physical nature, it is presented before the applied

chapters in this thesis). The objective of this project was originally to understand changes in the freshwater sources to the Beaufort Gyre, and then expanded to explore potentially related changes in mixed layer depth. The physical mechanisms driving changing advective pathways, with a particular emphasis on Pacific water pathways, were also investigated here. This research comprises Chapter 3 of this thesis and is published as Kelly et al. (2019).

As with Chapter 4, there are alternative approaches that could have been used here. For instance, the choice of initial positions for Lagrangian experiments, defined here based on the boundaries of the Beaufort Gyre region used in Proshutinsky et al. (2009) was not the only possible method. This approach had the advantage of being consistent between all experimental releases, but alternative methods of defining the Beaufort Gyre's boundaries exists – for instance, the work could be repeated redefining the Beaufort Gyre's boundaries based on either sea surface height or barotropic stream-function. However, this would come at the expense of consistency between particle releases, and would require each release to be individually redesigned.

Another potentially interesting avenue to build on this research would be to investigate not just the sources of Beaufort Gyre water, but also the export from the Gyre. This could be done by replicating the backwards-tracking experiments described in Chapter 3, but running forward-integrated experiments from the same initial positions. By comparing the retention of particles in the Beaufort Gyre region in both forward and backtracked experiments, it would be possible to quantify accumulation / release of water in the Beaufort Gyre region. Fresh water accumulation/release in the Beaufort Gyre has been linked to the Arctic Ocean Oscillation (Proshutinsky and Johnson, 1997), and this would give an opportunity to explore how that is reproduced in the NEMO model.

Finally, in Chapter 5, we return to a more applied ecological question: how has trans-Arctic connectivity between the Pacific and Atlantic Oceans changed over recent decades? At the time of submission, the work presented in this chapter was under review at the AGU journal *Earth's Future*, and is now published as Kelly et al. (2020). Exploring connectivity pathways from the Pacific Ocean is a natural follow on from the Pacific focused work presented in Chapter 3. Motivated in part by the discovery of a Pacific diatom in the North Atlantic Ocean (Reid et al., 2007), this paper aimed to investigate which advective pathways were potentially important for invasive species.

Building on lessons learned in previous papers, experiments were designed such that that number of particles per experiment were maximised. 1,000 particles were seeded in the Bering Strait every month between 1970 and 2003, and the progress of each particle tracked for 10 years. Using a 'trap' method, described in Chapter 5, five distinct connectivity routes were identified, and the number of particles following each pathway was recorded. How these pathways varied between seasons and years was then investigated. Regular seasonal variability was identified and explained by established seasonality in the Pacific inflow to the Arctic, and interannual changes in the relative importance of different routes were identified.

The variability of pathways provided multiple potential avenues for extended research, and of particular interest was one unusual, but anomalously rapid pathway via the North American coastline and Canadian Archipelago. This pathway was only sporadically available, and a large-scale wind-driven mechanism is proposed for its intermittency. While this was the story focussed on in this paper, other perspectives on these experiments could have instead focussed on the relative changes in importance of other routes, and understanding the physical mechanisms driving the long-terms shifts identified there.

Another alternate approach would have been to focus specifically on the species of diatom discussed by Reid et al. (2007). This would be an interesting question to explore, but would require a more interdisciplinary approach – looking at a specific species (in this case *Neodenticula Seminae*) would require knowledge of the species lifecycle and the limiting environmental factors that would preclude a successful transit for that particular diatom. That pushes it outside of the scope of this more general outlook, but remains an interesting question for future research to explore.

For a future project, it would be of great interest to return to the problem discussed in Chapter 5 but specifically including biota behaviour to more fully answer the question of whether changing Arctic connectivity pathways could allow for Pacific to Atlantic migration. In Chapter 5, particles were treated as passive. In principle, it would be possible to modify the methodology to add criteria for which trajectories "die", whether due to lack of nutrients, crossing a temperature threshold, or due to lack of sunlight. Determining what these thresholds should be is itself a non-trivial question, and would need to be tailored to a specific species to be meaningful. If considering the behaviour of a particular species rather than passive connectivity in general, it would also be necessary to revisit assumptions about their movement through the water column. For species which are able to control their buoyancy, it would be possible to reflect this by resetting Lagrangian particles vertical positions appropriately. While an approach focusing on biota behaviour would lack the generality of the research presented in Chapter 5 by virtue of only being applicable for specific organisms, it would potentially shed significant light on what the key limiting factors to trans-Arctic ecological connectivity are.

Additionally, given the possibility of climate change leading to increased Pacific to Atlantic connectivity, it would be particularly interesting to repeat the research in Chapter 5 using output from a forward projection ocean model. A Lagrangian approach has been used to explore projected changes in connectivity globally (van Gennip et al., 2017), but given the importance of pathways through the Canadian Archipelago identified in Chapter 5, the 1/4° resolution model available to perform such an experiment may be too coarse to properly resolve such pathways. In general, investigating projected changes in trans-Arctic connectivity will be an important question to address when higher resolution future projections become available.

6.2. Other Research

In addition to the research papers presented in chapters 3-5, various other work was undertaken during my time as a PhD student at the Graduate School of the National Oceanography Centre, Southampton. The two main examples of this are my contribution to Popova et al., (2019), and my modelling of connectivity pathways from the site of the Sanchi oil spill.

6.2.1. Areas Beyond National Jurisdiction (ABNJ) Project

Firstly, my contribution to (Popova et al., 2019). The aim of this project was to demonstrate the connectivity between areas beyond national jurisdiction (ABNJs) and the coastal zones of developing countries. ABNJs are defined to be the regions of the global ocean beyond the exclusive economic zones (EEZs) of sovereign states (Matz-Lück and Fuchs, 2014). Using a Lagrangian particle tracking method, we aimed to demonstrate the timescales upon which the ABNJ is connected to least developed countries, both passively via circulation connectivity and actively via marine species migratory connectivity.

My role in this project was to perform the Lagrangian particle tracking experiments to demonstrate passive connectivity, and to design the metrics to quantify this. I produced all figures bar Figure 1 for this paper, though my role in Figure 2 (showing the distributions of various marine species) was purely artistic – I simply plotted regions that other co-authors had defined.

For the Lagrangian experiments themselves, a backtracking approach was used to investigate connectivity to least developed countries' coastlines. Particles were uniformly initialised along the coastal zone of each least developed country, based on the 2014-2017 DAC list of ODA recipients. The 'coastal zone' was defined to be the strip of ocean within 15km of the shore, and particles were distributed at a density of 9 particles per 1/12° model grid cell, all at the ocean surface. To capture the seasonal and interannual variability of connectivity pathways, a total of 40 releases were preformed, with releases taking place quarterly between 2005 and 2014 in the model. In each case, particles were tracked backwards for one year in order to ascertain their upstream sources. Examples of output from 2 of these experiments (Somalia and Senegal) are presented in Figure 3 of (Popova et al., 2019), alongside Eulerian fields with major currents annotated.

The next task was to define country-by-country metrics to quantify the strength of connectivity between the ABNJ and each coastline. For each individual particle, the time taken to be backtracked out of the EEZ was calculated. The strength of connectivity between the ABNJ and any given country could then be calculated by either considering the fraction of particles which had been backtracked to the ABNJ after some fixed time, or a connectivity timescale could be defined by considering the amount of time required for some threshold number of particles to be connected. In Figure 4 of (Popova et al., 2019), country-by-country metrics are presented showing the "connectivity index" – i.e. the fraction of particles which had been tracked back to the ABNJ after 6 months of backtracking,

and a “connectivity timescale” based on the time required for the ABNJ to be connected to 25% of particles from a countries coastal zone.

The choice of appropriate thresholds to define connectivity indices or timescales is a non-trivial problem, and some countries are more sensitive than others to choice of threshold for each metric. In order to answer more specific questions, different thresholds timescales or connectivity fractions may be required. Future research could build upon the framework presented in this paper, quantifying how sensitive each country is to the thresholds used to define connectivity. Extending this research to include more countries, as well as investigating downstream connectivity would be an interesting niche for future research to explore.

While this research did not contribute directly to this thesis, and hence is not included the research chapters, the lessons learned throughout the project were invaluable. Collaborating with scientists who specialise in other fields, and contributing a well-defined piece of a wider picture was beneficial for my development as a scientist, while experience in designing experiments and metrics that could be efficiently replicated around different coastlines was a technical challenge that helped ensure that future experiments for my PhD were more robust. Finally, the opportunity to study regions away from the Arctic, where different physical features (e.g. monsoonal variability) play an important role, gave me a broader perspective as an oceanographer than would have been possible from the three research chapters alone.

6.2.2. The Sanchi Oil Spill

In January 2018, the Sanchi Oil tanker – carrying 136,000 tons of natural gas condensate, as well as its own bunker oil – exploded in the East China Sea (Carswell, 2018). Given the expertise in ocean modelling at the NOC, and the fact that Chapter 4 of this thesis, (S. Kelly et al., 2018) was going through review at the time, the decision was made to model the advective pathways relevant to a potential spill. This work was operational in nature, performed as an immediate response to breaking news with experiments performed as and when new information about the status if Sanchi became available. This resulted in the publication of three press releases (NOC, 2018a; NOC, 2018b; NOC, 2018c) featuring figures based on those in S. Kelly et al. (2018) to illustrate the potential advective pathways that pollutants entrained into the water column could follow. Our results were immediately put into the public domain with the intention of informing any clean up or preparedness action.

The experiments were performed were all based on the methodology described in Chapter 4. At the location of the potential spill, 100 particles were uniformly distributed over a 10km x 10km grid at the ocean surface, then tracked for 100 days. In each case, releases were performed every 5 days throughout Januaries 2006-2015 in the model hindcast, giving a total of 6,000 particles per experiment. These were used to produce probabilistic footprints highlighting regions potentially at risk of

being reached by contaminated waters. Three experiments were performed – one based on the original explosion site, another based on the location at which the Sanchi sank, and a final experiment based upon an island where oil believed to be from the Sanchi was reported to have washed up.

After each experiment, press releases were assembled, with the 'spaghetti' figures showing connectivity timescales used as illustrative examples of which regions may be at risk within a given timeframe, which attracted considerable media attention. (e.g. Reuters: http://fingfx.thomsonreuters.com/gfx/rngs/CHINA-SHIPPING-SPILL/010060NC166/index.html and The Guardian: https://www.theguardian.com/world/2018/jan/18/oil-from-sunken-iranian-tanker-spreads-over-100-sq-km-of-east-china-sea). It is noteworthy that, reports of oil washing up on the beaches of Amami Ōshima at approximately the timescale suggested by the Lagrangian experiments.

Deeper scientific analysis of the spill was later undertaken by (Chen et al., 2019). This served as useful validation of the method used throughout this work, with visually similar circulation footprints obtained. They noted that, although natural gas condensates are significantly more volatile than the heavier hydrocarbons more commonly associated with oil spills, and hence surface slicks evaporate over a timescale of hours to days (Reddy et al., 2012), these lighter hydrocarbons are more susceptible to becoming dissolved into the water column. Chen et al. (2019) surmised that dissolved pollutants are the main environmental risk posed by condensate spills, and the limiting timescale over which they remain an active pollutant is governed primarily by rates biodegradation. As dissolved pollutants follow the advective pathways taken by the water masses in which they are suspended, the Lagrangian technique described in S. Kelly et al. (2018) and employed for these experiments is of particular value when assessing the ecological impact of lighter hydrocarbon releases. Further exploring the fate of such a spill, and updating the methodology to account for rates of biodegradation would be an exciting avenue for future research.

6.3. Concluding remarks

This thesis has focused on exploring marine connectivity pathways and timescales in the Arctic Ocean, primarily from a Lagrangian particle-tracking perspective. Three case studies: one concerning marine pollution, another concerning the physical properties of the Arctic, and another focused on an ecological question have been used to explore the wider topic of Arctic connectivity. The power of a computationally inexpensive Lagrangian approach has been demonstrated, and the applications of such an outlook have shown to be diverse and valuable.

References :

Aagaard, K. & Carmack, E. C. 1989. The role of sea ice and other fresh water in the Arctic circulation. *Journal of Geophysical Research: Oceans,* 94**,** 14485-14498.

Aagaard, K., Coachman, L. K. & Carmack, E. 1981. On the halocline of the Arctic Ocean. *Deep Sea Research Part A. Oceanographic Research Papers,* 28**,** 529-545.

Afenyo, M., Veitch, B. & Khan, F. 2015. A state-of-the-art review of fate and transport of oil spills in open and ice-covered water. *Ocean Engineering,* 119, 233-248.

Aksenov, Y., Bacon, S., Coward, A. C. & Nurser, A. J. G. 2010. The North Atlantic inflow to the Arctic Ocean: High-resolution model study. *Journal of Marine Systems,* 79**,** 1-22.

Aksenov, Y., Ivanov, V. V., Nurser, A. J. G., Bacon, S., Polyakov, I. V., Coward, A. C., Naveira-Garabato, A. C. & Beszczynska-Moeller, A. 2011. The Arctic Circumpolar Boundary Current. *Journal of Geophysical Research: Oceans,* 116**,** C09017.

Aksenov, Y., Karcher, M., Proshutinsky, A., Gerdes, R., De Cuevas, B., Golubeva, E., Kauker, F., Nguyen, A. T., Platov, G. A., Wadley, M., Watanabe, E., Coward, A. C. & Nurser, A. J. G. 2016. Arctic pathways of Pacific Water: Arctic Ocean Model Intercomparison experiments. *Journal of Geophysical Research: Oceans,* 121**,** 27-59.

Aksenov, Y., Popova, E. E., Yool, A., Nurser, A. J. G., Williams, T. D., Bertino, L. & Bergh, J. 2017. On the future navigability of Arctic sea routes: High-resolution projections of the Arctic Ocean and sea ice. *Marine Policy,* 75**,** 300-317.

Alkire, M. B., Morison, J., Schweiger, A., Zhang, J., Steele, M., Peralta-Ferriz, C. & Dickinson, S. 2017. A Meteoric Water Budget for the Arctic Ocean. *Journal of Geophysical Research: Oceans,* 122**,** 10020-10041.

Amante, C. and Eakins, B. (2009). Etopo1 1 arc-minute global relief model: Procedures, data sources and analysis. Report.

Amap 2015. Summary for Policy-makers: Arctic Pollution Issues 2015. Oslo, Norway: Arctic Monitoring and Assessment Programme (AMAP).

Appen, W.-J. V. & Pickart, R. S. 2012. Two Configurations of the Western Arctic Shelfbreak Current in Summer. *Journal of Physical Oceanography,* 42**,** 329-351.

Arakawa, A. & Lamb, V. R. 1977. Computational Design of the Basic Dynamical Processes of the UCLA General Circulation Model. *In:* CHANG, J. (ed.) *Methods in Computational Physics: Advances in Research and Applications.* Elsevier.

Armitage, T. W. K., Bacon, S., Ridout, A. L., Petty, A. A., Wolbach, S. & Tsamados, M. 2017. Arctic Ocean surface geostrophic circulation 2003–2014. *The Cryosphere,* 11**,** 1767-1780.

Armitage, T. W. K., Bacon, S., Ridout, A. L., Thomas, S. F., Aksenov, Y. & Wingham, D. J. 2016. Arctic sea surface height variability and change from satellite radar altimetry and GRACE, 2003–2014. *Journal of Geophysical Research: Oceans,* 121**,** 4303-4322.

Arteaga, L., Pahlow, M. & Oschlies, A. 2014. Global patterns of phytoplankton nutrient and light colimitation inferred from an optimality-based model. *Global Biogeochemical Cycles,* 28**,** 648-661.

Bach, L., Zbawicka, M., Strand, J. & Wenne, R. 2019. Mytilus trossulus in NW Greenland is genetically more similar to North Pacific than NW Atlantic populations of the species. *Marine Biodiversity,* 49**,** 1053-1059.

Bacon, S., Marshall, A., Holliday, N. P., Aksenov, Y. & Dye, S. R. 2014. Seasonal variability of the East Greenland Coastal Current. *Journal of Geophysical Research: Oceans,* 119**,** 3967-3987.

Barber, D. G., Hop, H., Mundy, C. J., Else, B., Dmitrenko, I. A., Tremblay, J.-E., Ehn, J. K., Assmy, P., Daase, M., Candlish, L. M. & Rysgaard, S. 2015. Selected physical, biological and biogeochemical implications of a rapidly changing Arctic Marginal Ice Zone. *Progress in Oceanography,* 139**,** 122-150.

Bauch, D., Dmitrenko, I. A., Wegner, C., Hölemann, J., Kirillov, S. A., Timokhov, L. A. & Kassens, H. 2009. Exchange of Laptev Sea and Arctic Ocean halocline waters in response to atmospheric forcing. *Journal of Geophysical Research: Oceans,* 114, C05008

Beszczynska-Möller, A., Fahrbach, E., Schauer, U. & Hansen, E. 2012. Variability in Atlantic water temperature and transport at the entrance to the Arctic Ocean, 1997–2010. *ICES Journal of Marine Science,* 69**,** 852-863.

Bi, H., Liang, Y., Wang, Y. et al. Arctic multiyear sea ice variability observed from satellites: a review. *J. Ocean. Limnol*. 38, 962–984 (2020)

Björk, G., Jakobsson, M., Rudels, B., Swift, J. H., Anderson, L., Darby, D. A., Backman, J., Coakley, B., Winsor, P., Polyak, L. & Edwards, M. 2007. Bathymetry and deep-water exchange across the central Lomonosov Ridge at 88–89°N. *Deep Sea Research Part I: Oceanographic Research Papers,* 54**,** 1197-1208.

Blanke, B. & Delecluse, P. 1993. Variability of the Tropical Atlantic Ocean Simulated by a General Circulation Model with Two Different Mixed-Layer Physics. *Journal of Physical Oceanography,* 23**,** 1363-1388.

Blanke, B. & Raynaud, S. 1997. Kinematics of the Pacific Equatorial Undercurrent: An Eulerian and Lagrangian Approach from GCM Results. *Journal of Physical Oceanography,* 27**,** 1038-1053.

Bluhm, B. A., Kosobokova, K. N. & Carmack, E. C. 2015. A tale of two basins: An integrated physical and biological perspective of the deep Arctic Ocean. *Progress in Oceanography,* 139**,** 89-121.

Boe, J., Hall, A. & Qu, X. 2009. September sea-ice cover in the Arctic Ocean projected to vanish by 2100. *Nature Geosci,* 2**,** 341-343.

Bouillon, S., Morales Maqueda, M. Á., Legat, V. & Fichefet, T. 2009. An elastic–viscous–plastic sea ice model formulated on Arakawa B and C grids, *Ocean Modeling*, 27, 174-184.

Bourdalle Badie, R., Treguier, A., Molines, J., Coward, A., Scheinert, M., Lu, Y., Lecointre, A., and Tranchant, B. (2012). The orca12 bathymetry v3.2. technical report. Report.

Boxall, S. 2009. From rubber ducks to ocean gyres. *Nature,* 459**,** 1058-1059.

Bradford, R. W., Griffin, D. & Bruce, B. D. 2015. Estimating the duration of the pelagic phyllosoma phase of the southern rock lobster, *Jasus edwardsii* (Hutton). *Marine and Freshwater Research,* 66**,** 213-219.

Brodeau, L., Barnier, B., Treguier, A.-M., Penduff, T. & Gulev, S. 2010. An ERA40-based atmospheric forcing for global ocean circulation models. *Ocean Modelling,* 31**,** 88-104.

Brugler, E. T., Pickart, R. S., Moore, G. W. K., Roberts, S., Weingartner, T. J. & Statscewich, H. 2014. Seasonal to interannual variability of the Pacific water boundary current in the Beaufort Sea. *Progress in Oceanography,* 127**,** 1-20.

Cao, Y., Liang, S., Chen, X., He, T., Wang, D. & Cheng, X. 2017. Enhanced wintertime greenhouse effect reinforcing Arctic amplification and initial sea-ice melting. *Scientific Reports,* 7**,** 8462.

Carlsson, P., Breivik, K., Brorström-Lundén, E., Cousins, I., Christensen, J., Grimalt, J. O., Halsall, C., Kallenborn, R., Abass, K., Lammel, G., Munthe, J., Macleod, M., Odland, J. Ø., Pawlak, J., Rautio, A., Reiersen, L.-O., Schlabach, M., Stemmler, I., Wilson, S. & Wöhrnschimmel, H. 2018. Polychlorinated biphenyls (PCBs) as sentinels for the elucidation of Arctic environmental change processes: a comprehensive review combined with ArcRisk project results. *Environmental Science and Pollution Research,* 25**,** 22499-22528.

Carmack, E. & Wassmann, P. 2006. Food webs and physical–biological coupling on pan-Arctic shelves: Unifying concepts and comprehensive perspectives. *Progress in Oceanography,* 71**,** 446-477.

Carmack, E. C., Yamamoto-Kawai, M., Haine, T. W. N., Bacon, S., Bluhm, B. A., Lique, C., Melling, H., Polyakov, I. V., Straneo, F., Timmermans, M.-L. & Williams, W. J. 2016. Freshwater and its role in the Arctic Marine System: Sources, disposition, storage, export, and physical and biogeochemical consequences in the Arctic and global oceans. *Journal of Geophysical Research: Biogeosciences,* 121**,** 675-717.

Carson, R. T., Mitchell, R. C., Hanemann, M., Kopp, R. J., Presser, S. & Ruud, P. A. 2003. Contingent Valuation and Lost Passive Use: Damages from the Exxon Valdez Oil Spill. *Environmental and Resource Economics,* 25**,** 257-286.

Carswell, C. 2018. Unique oil spill in East China Sea frustrates scientists. *Nature News*. (https://www.nature.com/articles/d41586-018-00976-9)

Cavalieri, C. L. P., P. Gloersen, and H. J. Zwally 1996. Sea Ice Concentrations from Nimbus-7 SMMR and DMSP SSM/I-SSMIS Passive Microwave Data, Version 1. *In:* CAVALIERI, C. L. P., P. GLOERSEN, AND H. J. ZWALLY (ed.). Boulder, Colorado USA. NASA National Snow and Ice Data Center Distributed Active Archive Center.

Chen, L., Yang, J. & Wu, L. 2019. Modeling the Dispersion of Dissolved Natural Gas Condensates From the Sanchi Incident. *Journal of Geophysical Research: Oceans,* 124, 8439– 8454.

Cohen, J., Screen, J. A., Furtado, J. C., Barlow, M., Whittleston, D., Coumou, D., Francis, J., Dethloff, K., Entekhabi, D., Overland, J. & Jones, J. 2014. Recent Arctic amplification and extreme mid-latitude weather. *Nature Geoscience,* 7**,** 627.

Condie, S. A., Waring, J., Mansbridge, J. V. & Cahill, M. L. 2005. Marine connectivity patterns around the Australian continent. *Environmental Modelling & Software,* 20**,** 1149-1157.

Cowen, R. K., Paris, C. B. & Srinivasan, A. 2006. Scaling of Connectivity in Marine Populations. *Science,* 311**,** 522-527.

Cowen, R. K. & Sponaugle, S. 2009. Larval Dispersal and Marine Population Connectivity. *Annual Review of Marine Science,* 1**,** 443-466.

Davis, P. E. D., Lique, C., Johnson, H. L. & Guthrie, J. D. 2016. Competing Effects of Elevated Vertical Mixing and Increased Freshwater Input on the Stratification and Sea Ice Cover in a Changing Arctic Ocean. *Journal of Physical Oceanography,* 46**,** 1531-1553.

De Boisséson, E., Thierry, V., Mercier, H. & Caniaux, G. 2010. Mixed layer heat budget in the Iceland Basin from Argo. *Journal of Geophysical Research: Oceans,* 115, C10055.

De Boyer Montégut, C., Madec, G., Fischer, A. S., Lazar, A. & Iudicone, D. 2004. Mixed layer depth over the global ocean: An examination of profile data and a profile-based climatology. *Journal of Geophysical Research: Oceans,* 109, C12003.

De Wit, C. A., Herzke, D. & Vorkamp, K. 2010. Brominated flame retardants in the Arctic environment — trends and new candidates. *Science of The Total Environment,* 408**,** 2885-2918.

Dmitrenko, I. A., Kirillov, S. A., Forest, A., Gratton, Y., Volkov, D. L., Williams, W. J., Lukovich, J. V., Belanger, C. & Barber, D. G. 2016. Shelfbreak current over the Canadian Beaufort Sea continental slope: Wind-driven events in January 2005. *Journal of Geophysical Research: Oceans,* 121**,** 2447-2468.

Dmitrenko, I. A., Rudels, B., Kirillov, S. A., Aksenov, Y. O., Lien, V. S., Ivanov, V. V., Schauer, U., Polyakov, I. V., Coward, A. & Barber, D. G. 2015. Atlantic water flow into the Arctic Ocean through the St. Anna Trough in the northern Kara Sea. *Journal of Geophysical Research: Oceans,* 120**,** 5158-5178.

Dmitrenko, I. A., Tyshko, K. N., Kirillov, S. A., Eicken, H., Hölemann, J. A. & Kassens, H. 2005. Impact of flaw polynyas on the hydrography of the Laptev Sea. *Global and Planetary Change,* 48**,** 9-27.

Döös, K., Jönsson, B. & Kjellsson, J. 2017. Evaluation of oceanic and atmospheric trajectory schemes in the TRACMASS trajectory model v6.0. *Geosci. Model Dev.,* 10**,** 1733-1749.

Duchez, A., Hirschi, J. J.-M., Cunningham, S. A., Blaker, A. T., Bryden, H. L., Cuevas, B. D., Atkinson, C. P., Mccarthy, G. D., Frajka-Williams, E., Rayner, D., Smeed, D. & Mizielinski, M. S. 2014. A New Index for the Atlantic Meridional Overturning Circulation at 26°N. *Journal of Climate,* 27**,** 6439-6455.

Dukhovskoy, D. S., Myers, P. G., Platov, G., Timmermans, M.-L., Curry, B., Proshutinsky, A., Bamber, J. L., Chassignet, E., Hu, X., Lee, C. M. & Somavilla, R. 2016. Greenland freshwater pathways in the sub-Arctic Seas from model experiments with passive tracers. *Journal of Geophysical Research: Oceans,* 121**,** 877-907.

Fichefet, T. & Maqueda, M. a. M. 1997. Sensitivity of a global sea ice model to the treatment of ice thermodynamics and dynamics. *Journal of Geophysical Research: Oceans,* 102**,** 12609-12646.

Fingas, M. F. & Hollebone, B. P. 2003. Review of behaviour of oil in freezing environments. *Marine Pollution Bulletin,* 47**,** 333-340.

Fisher, J. A., Jacob, D. J., Soerensen, A. L., Amos, H. M., Steffen, A. & Sunderland, E. M. 2012. Riverine source of Arctic Ocean mercury inferred from atmospheric observations. *Nature Geosci,* 5**,** 499-504.

Fisher, N. S., Fowler, S. W., Boisson, F., Carroll, J., Rissanen, K., Salbu, B., Sazykina, T. G. & Sjoeblom, K.-L. 1999. Radionuclide Bioconcentration Factors and Sediment Partition Coefficients in Arctic Seas Subject to Contamination from Dumped Nuclear Wastes. *Environmental Science & Technology,* 33**,** 1979-1982.

Giles, K. A., Laxon, S. W., Ridout, A. L., Wingham, D. J. & Bacon, S. 2012. Western Arctic Ocean freshwater storage increased by wind-driven spin-up of the Beaufort Gyre. *Nature Geoscience,* 5**,** 194.

Goosse, H. & Fichefet, T. 1999. Importance of ice-ocean interactions for the global ocean circulation: A model study. *Journal of Geophysical Research: Oceans,* 104**,** 23337-23355.

Graham, R. M., Itkin, P., Meyer, A., Sundfjord, A., Spreen, G., Smedsrud, L. H., Liston, G. E., Cheng, B., Cohen, L., Divine, D., Fer, I., Fransson, A., Gerland, S., Haapala, J., Hudson, S. R., Johansson, A. M., King, J., Merkouriadi, I., Peterson, A. K., Provost, C., Randelhoff, A., Rinke, A., Rösel, A., Sennéchael, N., Walden, V. P., Duarte, P., Assmy, P., Steen, H. & Granskog, M. A. 2019. Winter storms accelerate the demise of sea ice in the Atlantic sector of the Arctic Ocean. *Scientific Reports,* 9**,** 9222.

Graversen, R. G., Mauritsen, T., Tjernström, M., Källén, E. & Svensson, G. 2008. Vertical structure of recent Arctic warming. *Nature,* 451**,** 53.

Hadfield, R. E., Wells, N. C., Josey, S. A. & Hirschi, J. J.-M. 2007. On the accuracy of North Atlantic temperature and heat storage fields from Argo. *Journal of Geophysical Research: Oceans,* 112.

Halsall, C. J. 2004. Investigating the occurrence of persistent organic pollutants (POPs) in the arctic: their atmospheric behaviour and interaction with the seasonal snow pack. *Environmental Pollution,* 128**,** 163-175.

Ho, J. 2010. The implications of Arctic sea ice decline on shipping. *Marine Policy,* 34**,** 713-715.

Hop, H. & Gjøsæter, H. 2013. Polar cod (Boreogadus saida) and capelin (Mallotus villosus) as key species in marine food webs of the Arctic and the Barents Sea. *Marine Biology Research,* 9**,** 878-894.

Hu, X. & Myers, P. G. 2013. A Lagrangian view of Pacific water inflow pathways in the Arctic Ocean during model spin-up. *Ocean Modelling,* 71**,** 66-80.

Hunke, E. C. & Dukowicz, J. K. 1997. An Elastic–Viscous–Plastic Model for Sea Ice Dynamics. *Journal of Physical Oceanography,* 27**,** 1849-1867.

International Hydrographic Organization, I. 2002. *Limits of Ocean and Seas, rep. S-23, draft, 4th ed.* Monaco: INTERNATIONAL HYDROGRAPHIC BUREAU.

Ivanov, V., Maslov, P., Aksenov, Y. & Coward, A. 2015. Shelf-basin exchange in the Laptev Sea in the warming climate: a model study. *Geophysical & Astrophysical Fluid Dynamics,* 109**,** 254-280.

Ivanov, V. V. & Golovin, P. N. 2007. Observations and modeling of dense water cascading from the northwestern Laptev Sea shelf. *Journal of Geophysical Research: Oceans,* 112**,** C09003.

Izumiyama, K., Uto, S. & Sakai, S. 2004. Prediction of Oil-ice Sandwich Formation, International Journal of Offshore and Polar Engineering, 14(3), 169–175..

Jackett, D. R. & Mcdougall, T. J. 1995. Minimal Adjustment of Hydrographic Profiles to Achieve Static Stability. *Journal of Atmospheric and Oceanic Technology,* 12**,** 381-389.

Jahn, A., Kay, J. E., Holland, M. M. & Hall, D. M. 2016. How predictable is the timing of a summer ice-free Arctic? *Geophysical Research Letters,* 43**,** 9113-9120.

Janout, M. A., Aksenov, Y., Hölemann, J. A., Rabe, B., Schauer, U., Polyakov, I. V., Bacon, S., Coward, A. C., Karcher, M., Lenn, Y.-D., Kassens, H. & Timokhov, L. 2015. Kara Sea freshwater transport through Vilkitsky Strait: Variability, forcing, and further pathways toward the western Arctic Ocean from a model and observations. *Journal of Geophysical Research: Oceans,* 120**,** 4925-4944.

Johnson, M., Proshutinsky, A., Aksenov, Y., Nguyen, A. T., Lindsay, R., Haas, C., Zhang, J., Diansky, N., Kwok, R., Maslowski, W., Häkkinen, S., Ashik, I. & De Cuevas, B. 2012. Evaluation of Arctic sea ice thickness simulated by Arctic Ocean Model Intercomparison Project models. *Journal of Geophysical Research: Oceans,* 117**,** C00D13.

Jönsson, B. F. & Watson, J. R. 2016. The timescales of global surface-ocean connectivity. *Nature Communications,* 7**,** 11239.

Kallenborn, R., Halsall, C., Dellong, M. & Carlsson, P. 2012. The influence of climate change on the global distribution and fate processes of anthropogenic persistent organic pollutants. *Journal of Environmental Monitoring,* 14**,** 2854-2869.

Karcher, M., Smith, J. N., Kauker, F., Gerdes, R. & Smethie Jr., W. M. 2012. Recent changes in Arctic Ocean circulation revealed by iodine-129 observations and modeling. *Journal of Geophysical Research: Oceans,* 117, C08007.

Kelly, C. W., Chipperfield, M. P., Plane, J. M. C., Feng, W., Sheese, P. E., Walker, K. A. & Boone, C. D. 2018. An Explanation for the Nitrous Oxide Layer Observed in the Mesopause Region. *Geophysical Research Letters,* 45**,** 7818-7827.

Kelly, S., Popova, E., Aksenov, Y., Marsh, R. & Yool, A. 2018. Lagrangian Modeling of Arctic Ocean Circulation Pathways: Impact of Advection on Spread of Pollutants. *Journal of Geophysical Research: Oceans,* 123**,** 2882-2902.

Kelly, S. J., Proshutinsky, A., Popova, E. K., Aksenov, Y. K. & Yool, A. 2019. On the Origin of Water Masses in the Beaufort Gyre. *Journal of Geophysical Research: Oceans,* 124**,** 4696-4709.

Kelly, S. J., Popova, E., Aksenov, Y., Marsh, R., & Yool, A. 2020. They came from the Pacific: How changing Arctic currents could contribute to an ecological regime shift in the Atlantic Ocean. *Earth's Future*, 8, e2019EF001394.

Kipp, L. E., Kadko, D. C., Pickart, R. S., Henderson, P. B., Moore, W. S. & Charette, M. A. 2019. Shelf-Basin Interactions and Water Mass Residence Times in the Western Arctic Ocean: Insights Provided by Radium Isotopes. *Journal of Geophysical Research: Oceans,* 124**,** 3279-3297.

Kjellsson, J. & Döös, K. 2012. Lagrangian decomposition of the Hadley and Ferrel cells. *Geophysical Research Letters,* 39, L15807.

Krembs, C., Eicken, H. & Deming, J. W. Exopolymer alteration of physical properties of sea ice and implications for ice habitability and biogeochemistry in a warmer Arctic. *PNAS*, 2011, 108 (9) 3653-3658

Krishfield, R. A., Proshutinsky, A., Tateyama, K., Williams, W. J., Carmack, E. C., Mclaughlin, F. A. & Timmermans, M.-L. 2014. Deterioration of perennial sea ice in the Beaufort Gyre from 2003 to 2012 and its impact on the oceanic freshwater cycle. *Journal of Geophysical Research: Oceans,* 119**,** 1271-1305.

Kwok, R., Arctic sea ice thickness, volume, and multiyear ice coverage: losses and coupled variability (1958–2018), *Environmental Research Letters,* 13(10).

Lange, M. & Van Sebille, E. 2017. Parcels v0.9: prototyping a Lagrangian ocean analysis framework for the petascale age. *Geosci. Model Dev.,* 10**,** 4175-4186.

Laxon, S. W., Giles, K. A., Ridout, A. L., Wingham, D. J., Willatt, R., Cullen, R., Kwok, R., Schweiger, A., Zhang, J., Haas, C., Hendricks, S., Krishfield, R., Kurtz, N., Farrell, S. and Davidson, M. (2013), CryoSat‐2 estimates of Arctic sea ice thickness and volume, Geophys. Res. Lett., 40, 732– 737

Lee, T. & Kim, H. J. 2015. Barriers of voyaging on the Northern Sea Route: A perspective from shipping Companies. *Marine Policy,* 62**,** 264-270.

Lin, P., Pickart, R. S., Stafford, K. M., Moore, G. W. K., Torres, D. J., Bahr, F. & Hu, J. 2016. Seasonal variation of the Beaufort shelfbreak jet and its relationship to Arctic cetacean occurrence. *Journal of Geophysical Research: Oceans,* 121**,** 8434-8454.

Lincoln, B. J., Rippeth, T. P., Lenn, Y.-D., Timmermans, M. L., Williams, W. J. & Bacon, S. 2016. Wind-driven mixing at intermediate depths in an ice-free Arctic Ocean. *Geophysical Research Letters,* 43**,** 9749-9756.

Lique, C., Guthrie, J. D., Steele, M., Proshutinsky, A., Morison, J. H. & Krishfield, R. 2014. Diffusive vertical heat flux in the Canada Basin of the Arctic Ocean inferred from moored instruments. *Journal of Geophysical Research: Oceans,* 119**,** 496-508.

Lique, C., Johnson, H. L. & Davis, P. E. D. 2015. On the Interplay between the Circulation in the Surface and the Intermediate Layers of the Arctic Ocean. *Journal of Physical Oceanography,* 45**,** 1393-1409.

Lique, C., Treguier, A. M., Blanke, B. & Grima, N. 2010. On the origins of water masses exported along both sides of Greenland: A Lagrangian model analysis. *Journal of Geophysical Research: Oceans,* 115**,** C05019.

Liu, M. & Kronbak, J. 2010. The potential economic viability of using the Northern Sea Route (NSR) as an alternative route between Asia and Europe. *Journal of Transport Geography,* 18**,** 434-444.

Liu, Y., Wilson, C., Green, M. A. & Hughes, C. W. 2018. Gulf Stream Transport and Mixing Processes via Coherent Structure Dynamics. *Journal of Geophysical Research: Oceans,* 123**,** 3014-3037.

Luneva, M. V., Aksenov, Y., Harle, J. D. & Holt, J. T. 2015. The effects of tides on the water mass mixing and sea ice in the Arctic Ocean. *Journal of Geophysical Research: Oceans,* 120**,** 6669-6699.

Ma, Y., Xie, Z., Halsall, C., Möller, A., Yang, H., Zhong, G., Cai, M. & Ebinghaus, R. 2015. The spatial distribution of organochlorine pesticides and halogenated flame retardants in the surface sediments of an Arctic fjord: The influence of ocean currents vs. glacial runoff. *Chemosphere,* 119**,** 953-960.

Macfadyen, A., Watabayashi, G. Y., Barker, C. H. & Beegle-Krause, C. J. 2013. Tactical Modeling of Surface Oil Transport During the Deepwater Horizon Spill Response. *Monitoring and Modeling the Deepwater Horizon Oil Spill: A Record-Breaking Enterprise.* American Geophysical Union.

Madec, G. 2014. "NEMO Ocean Engine" (Draft Edition r5171) "NEMO ocean engine" (Draft edition r5171). Note du Pôle de modélisation, Institut Pierre-Simon Laplace (IPSL), France, No 27 ISSN No 1288-1619.

Madec, G. & Imbard, M. 1996. A global ocean mesh to overcome the North Pole singularity. *Climate Dynamics,* 12**,** 381-388.

Main, C. E., Yool, A., Holliday, N. P., Popova, E. E., Jones, D. O. B. & Ruhl, H. A. 2016. Simulating pathways of subsurface oil in the Faroe–Shetland Channel using an ocean general circulation model. *Marine Pollution Bulletin,* 114, 315-326

Manucharyan, G. E. & Spall, M. A. 2016. Wind-driven freshwater buildup and release in the Beaufort Gyre constrained by mesoscale eddies. *Geophysical Research Letters,* 43**,** 273-282.

Mariano, A. J., Kourafalou, V. H., Srinivasan, A., Kang, H., Halliwell, G. R., Ryan, E. H. & Roffer, M. 2011. On the modeling of the 2010 Gulf of Mexico Oil Spill. *Dynamics of Atmospheres and Oceans,* 52**,** 322-340.

Marzocchi, A., Hirschi, J. J. M., Holliday, N. P., Cunningham, S. A., Blaker, A. T. & Coward, A. C. 2015. The North Atlantic subpolar circulation in an eddy-resolving global ocean model. *Journal of Marine Systems,* 142**,** 126-143.

Matul, A., Spielhagen, R. F., Kazarina, G., Kruglikova, S., Dmitrenko, O. & Mohan, R. 2018. Warm-water events in the eastern Fram Strait during the last 2000 years as revealed by different microfossil groups. *Polar Research,* 37**,** 1540243.

Matz-Lück, N. & Fuchs, J. 2014. The impact of OSPAR on protected area management beyond national jurisdiction: Effective regional cooperation or a network of paper parks? *Marine Policy,* 49**,** 155-166.

Mayorga-Adame, C. G., Batchelder, H. P. & Spitz, Y. H. 2017. Modeling Larval Connectivity of Coral Reef Organisms in the Kenya-Tanzania Region. *Frontiers in Marine Science,* 4:92.

Mclaughlin, F., Carmack, E., Macdonald, R., Weaver, A. J. & Smith, J. 2002. The Canada Basin, 1989–1995: Upstream events and far-field effects of the Barents Sea. *Journal of Geophysical Research: Oceans,* 107**,** 19-1-19-20.

Mclaughlin, F. A., Carmack, E. C., Macdonald, R. W. & Bishop, J. K. B. 1996. Physical and geochemical properties across the Atlantic/Pacific water mass front in the southern Canadian Basin. *Journal of Geophysical Research: Oceans,* 101**,** 1183-1197.

Mcphee, M. G., Proshutinsky, A., Morison, J. H., Steele, M. & Alkire, M. B. 2009. Rapid change in freshwater content of the Arctic Ocean. *Geophysical Research Letters,* 36, L10602.

Meier, W. N., Hovelsrud, G. K., Van Oort, B. E. H., Key, J. R., Kovacs, K. M., Michel, C., Haas, C., Granskog, M. A., Gerland, S., Perovich, D. K., Makshtas, A. & Reist, J. D. 2014. Arctic sea ice in transformation: A review of recent observed changes and impacts on biology and human activity. *Reviews of Geophysics,* 52**,** 185-217.

Meneghello, G., Marshall, J., Campin, J.-M., Doddridge, E. & Timmermans, M.-L. 2018. The Ice-Ocean Governor: Ice-Ocean Stress Feedback Limits Beaufort Gyre Spin-Up. *Geophysical Research Letters,* 45**,** 11,293-11,299.

Meneghello, G., Marshall, J., Cole, S. T. & Timmermans, M.-L. 2017. Observational Inferences of Lateral Eddy Diffusivity in the Halocline of the Beaufort Gyre. *Geophysical Research Letters,* 44**,** 12,331-12,338.

Miettinen, A., Koç, N. & Husum, K. 2013. Appearance of the Pacific diatom Neodenticula seminae in the northern Nordic Seas — An indication of changes in Arctic sea ice and ocean circulation. *Marine Micropaleontology,* 99**,** 2-7.

Moore, C., Obrist, D., Steffen, A. et al. Convective forcing of mercury and ozone in the Arctic boundary layer induced by leads in sea ice. Nature 506, 81–84 (2014)

Mouchet, A., Cornaton, F., Deleersnijder, É. & M. Delhez, É. J. 2016. Partial ages: diagnosing transport processes by means of multiple clocks. *Ocean Dynamics,* 66**,** 367-386.

Mueller, B. L., Gillett, N. P., Monahan, A. H. & Zwiers, F. W. 2018. Attribution of Arctic Sea Ice Decline from 1953 to 2012 to Influences from Natural, Greenhouse Gas, and Anthropogenic Aerosol Forcing. *Journal of Climate,* 31**,** 7771-7787.

Nevalainen, M., Helle, I. & Vanhatalo, J. 2017. Preparing for the unprecedented — Towards quantitative oil risk assessment in the Arctic marine areas. *Marine Pollution Bulletin,* 114**,** 90-101.

Newton, R., Schlosser, P., Martinson, D. G. & Maslowski, W. 2008. Freshwater distribution in the Arctic Ocean: Simulation with a high-resolution model and model-data comparison. *Journal of Geophysical Research: Oceans,* 113**,** C05024.

Newton, S., Bidleman, T., Bergknut, M., Racine, J., Laudon, H., Giesler, R. & Wiberg, K. 2014. Atmospheric deposition of persistent organic pollutants and chemicals of emerging concern at two sites in northern Sweden. *Environmental Science: Processes & Impacts,* 16**,** 298-305.

Nguyen, A. T., Menemenlis, D. & Kwok, R. 2011. Arctic ice-ocean simulation with optimized model parameters: Approach and assessment. *Journal of Geophysical Research: Oceans,* 116, C04025.

Nikolopoulos, A., Pickart, R. S., Fratantoni, P. S., Shimada, K., Torres, D. J. & Jones, E. P. 2009. The western Arctic boundary current at 152°W: Structure, variability, and transport. *Deep Sea Research Part II: Topical Studies in Oceanography,* 56**,** 1164-1181.

NOC 2018a. Coral reefs may be at risk from Sanchi oil tanker contamination. (https://noc.ac.uk/news/coral-reefs-may-be-risk-sanchi-oil-tanker-contamination)

NOC 2018b. Sanchi oil spill contamination could reach Japan within a month (update). (https://noc.ac.uk/news/sanchi-oil-spill-contamination-could-reach-japan-within-month-update)

NOC 2018c. Sanchi oil spill contamination could take three months to reach mainland. (https://noc.ac.uk/news/sanchi-oil-spill-contamination-could-take-three-months-reach-mainland)

North, E. W. E. W., Adams, E. E. E. E., Schlag, Z. Z., Sherwood, C. R. C. R., He, R. R., Hyun, K. H. K. H. & Socolofsky, S. a. S. A. 2013. Simulating Oil Droplet Dispersal From the Deepwater Horizon Spill With a Lagrangian Approach. *Monitoring and Modeling the Deepwater Horizon Oil Spill: A Record-Breaking Enterprise.* American Geophysical Union.

Notz, D. & Stroeve, J. 2016. Observed Arctic sea-ice loss directly follows anthropogenic CO2 emission. *Science,* 354**,** 747-750.

Nurser, A. J. G. & Bacon, S. 2014. The Rossby radius in the Arctic Ocean. *Ocean Sci.,* 10**,** 967-975.

Østreng, W., Eger, K. M., Fløistad, B., Jøgensen-Dahl, A., Lothe, L., Mejlnder-Larsen, M. & Wergeland, T. 2013. Shipping in arctic waters: A comparison of the northeast, northwest and trans polar passages, 10.1007/978-3-642-16790-4.

Overland, J. E. 2009. Meteorology of the Beaufort Sea. *Journal of Geophysical Research: Oceans,* 114, C00A07,.

Overland, J. E. & Wang, M. 2013. When will the summer Arctic be nearly sea ice free? *Geophysical Research Letters,* 40**,** 2097-2101.

Pacyna, J. M., Cousins, I. T., Halsall, C., Rautio, A., Pawlak, J., Pacyna, E. G., Sundseth, K., Wilson, S. & Munthe, J. 2015. Impacts on human health in the Arctic owing to climate-induced changes in contaminant cycling – The EU ArcRisk project policy outcome. *Environmental Science & Policy,* 50**,** 200-213.

Padman, L. & Erofeeva, S. 2004. A barotropic inverse tidal model for the Arctic Ocean. *Geophysical Research Letters,* 31**,** L02303.

Palumbi, S. R., Mcleod, K. L. & Grünbaum, D. 2008. Ecosystems in Action: Lessons from Marine Ecology about Recovery, Resistance, and Reversibility. *BioScience,* 58**,** 33-42.

Parkinson, C. L. & Comiso, J. C. 2013. On the 2012 record low Arctic sea ice cover: Combined impact of preconditioning and an August storm. *Geophysical Research Letters,* 40**,** 1356-1361.

Peralta-Ferriz, C. & Woodgate, R. A. 2015. Seasonal and interannual variability of pan-Arctic surface mixed layer properties from 1979 to 2012 from hydrographic data, and the dominance of stratification for multiyear mixed layer depth shoaling. *Progress in Oceanography,* 134**,** 19-53.

Perovich, D. K., Light, B., Eicken, H., Jones, K. F., Runciman, K. & Nghiem, S. V. 2007. Increasing solar heating of the Arctic Ocean and adjacent seas, 1979–2005: Attribution and role in the ice-albedo feedback. *Geophysical Research Letters,* 34, L19505.

Peterson, C. H., Rice, S. D., Short, J. W., Esler, D., Bodkin, J. L., Ballachey, B. E. & Irons, D. B. 2003. Long-Term Ecosystem Response to the Exxon Valdez Oil Spill. *Science,* 302**,** 2082-2086.

Pfirman, S. L., Kögeler, J. W. & Rigor, I. 1997. Potential for rapid transport of contaminants from the Kara Sea. *Science of The Total Environment,* 202**,** 111-122.

Pickart, R. S., Moore, G. W. K., Torres, D. J., Fratantoni, P. S., Goldsmith, R. A. & Yang, J. 2009. Upwelling on the continental slope of the Alaskan Beaufort Sea: Storms, ice, and oceanographic response. *Journal of Geophysical Research: Oceans,* 114, C00A13.

Pnyushkov, A. V., Polyakov, I. V., Ivanov, V. V., Aksenov, Y., Coward, A. C., Janout, M. & Rabe, B. 2015. Structure and variability of the boundary current in the Eurasian Basin of the Arctic Ocean. *Deep Sea Research Part I: Oceanographic Research Papers,* 101**,** 80-97.

Pnyushkov, A. V., Polyakov, I. V., Ivanov, V. V. & Kikuchi, T. 2013. Structure of the Fram Strait branch of the boundary current in the Eurasian Basin of the Arctic Ocean. *Polar Science,* 7**,** 53-71.

Polyakov, I. V., Alexeev, V. A., Ashik, I. M., Bacon, S., Beszczynska-Möller, A., Carmack, E. C., Dmitrenko, I. A., Fortier, L., Gascard, J.-C., Hansen, E., Hölemann, J., Ivanov, V. V., Kikuchi, T., Kirillov, S., Lenn, Y.-D., Mclaughlin, F. A., Piechura, J., Repina, I., Timokhov, L. A., Walczowski, W. & Woodgate, R. 2011. Fate of Early 2000s Arctic Warm Water Pulse. *Bulletin of the American Meteorological Society,* 92**,** 561-566.

Polyakov, I. V., Leonid A. Timokhov, Vladimir A. Alexeev, Sheldon Bacon, Igor A. Dmitrenko, Louis Fortier, Ivan E. Frolov, Jean-Claude Gascard, Edmond Hansen, Vladimir V. Ivanov, Seymour Laxon, Cecilie Mauritzen, Don Perovich, Koji Shimada, Harper L. Simmons, Vladimir T. Sokolov, Michael Steele & Toole, J. 2010. Arctic Ocean Warming Contributes to Reduced Polar Ice Cap. *Journal of Physical Oceanography,* 40**,** 2743-2756.

Polyakov, I. V., Pnyushkov, A. V., Alkire, M. B., Ashik, I. M., Baumann, T. M., Carmack, E. C., Goszczko, I., Guthrie, J., Ivanov, V. V., Kanzow, T., Krishfield, R., Kwok, R., Sundfjord, A., Morison, J., Rember, R. & Yulin, A. 2017. Greater role for Atlantic inflows on sea-ice loss in the Eurasian Basin of the Arctic Ocean. *Science*, 356, 6335, 285-291

Polyakov, I.V., Pnyushkov, A.V., Rember, R., Padman, L., Carmack, E.C., Jackson, J.M. 2013. Winter convection transports Atlantic water heat to the surface layer in the Eastern Arctic Ocean. *Journal of Physical Oceanography*, 43 (10), pp. 2142-2155,

Polyakov, I. V., Proshutinsky, A. Y. & Johnson, M. A. 1999. Seasonal cycles in two regimes of Arctic climate. *Journal of Geophysical Research: Oceans,* 104**,** 25761-25788.

Popova, E., Vousden, D., Sauer, W. H. H., Mohammed, E. Y., Allain, V., Downey-Breedt, N., Fletcher, R., Gjerde, K. M., Halpin, P. N., Kelly, S., Obura, D., Pecl, G., Roberts, M., Raitsos, D. E., Rogers, A., Samoilys, M., Sumaila, U. R., Tracey, S. & Yool, A. 2019. Ecological connectivity between the areas beyond national jurisdiction and coastal waters: Safeguarding interests of coastal communities in developing countries. *Marine Policy,* 104**,** 90-102.

Popova, E. E., Yool, A., Aksenov, Y. & Coward, A. C. 2013. Role of advection in Arctic Ocean lower trophic dynamics: A modeling perspective. *Journal of Geophysical Research: Oceans,* 118**,** 1571-1586.

Proshutinsky, A., Bourke, R. H. & Mclaughlin, F. A. 2002. The role of the Beaufort Gyre in Arctic climate variability: Seasonal to decadal climate scales. *Geophysical Research Letters,* 29**,** 15-1-15-4.

Proshutinsky, A., Dukhovskoy, D., Timmermans, M.-L., Krishfield, R. & Bamber, J. L. 2015. Arctic circulation regimes. *Philosophical Transactions of the Royal Society A: Mathematical, Physical and Engineering Sciences,* 373(2052): 20140160.

Proshutinsky, A., Krishfield, R., Timmermans, M.-L., Toole, J., Carmack, E., Mclaughlin, F., Williams, W. J., Zimmermann, S., Itoh, M. & Shimada, K. 2009. Beaufort Gyre freshwater reservoir: State and variability from observations. *Journal of Geophysical Research: Oceans,* 114, C00A10.

Proshutinsky, A. Y. & Johnson, M. A. 1997. Two circulation regimes of the wind-driven Arctic Ocean. *Journal of Geophysical Research: Oceans,* 102**,** 12493-12514.

Proshutinsky, A. Y., Polyakov, I. V. & Johnson, M. A. 1999. Climate states and variability of Arctic ice and water dynamics during 1946–1997. *Polar Research,* 18**,** 135-142.

Rabe, B., Karcher, M., Kauker, F., Schauer, U., Toole, J. M., Krishfield, R. A., Pisarev, S., Kikuchi, T. & Su, J. 2014. Arctic Ocean basin liquid freshwater storage trend 1992–2012. *Geophysical Research Letters,* 41**,** 961-968.

Raitsos, D. E., Brewin, R. J. W., Zhan, P., Dreano, D., Pradhan, Y., Nanninga, G. B. & Hoteit, I. 2017. Sensing coral reef connectivity pathways from space. *Scientific Reports,* 7**,** 9338.

Reddy, C. M., Arey, J. S., Seewald, J. S., Sylva, S. P., Lemkau, K. L., Nelson, R. K., Carmichael, C. A., Mcintyre, C. P., Fenwick, J., Ventura, G. T., Van Mooy, B. a. S. & Camilli, R. 2012. Composition and fate of gas and oil released to the water column during the Deepwater Horizon oil spill. *Proceedings of the National Academy of Sciences,* 109**,** 20229-20234.

Regan, H. C., Lique, C. & Armitage, T. W. K. 2019. The Beaufort Gyre Extent, Shape, and Location Between 2003 and 2014 From Satellite Observations. *Journal of Geophysical Research: Oceans,* 124**,** 844-862.

Reid, P. C., Johns, D. G., Edwards, M., Starr, M., Poulin, M. & Snoeijs, P. 2007. A biological consequence of reducing Arctic ice cover: arrival of the Pacific diatom Neodenticula seminae in the North Atlantic for the first time in 800000 years. *Global Change Biology,* 13**,** 1910-1921.

Riddell-Dixon, E. 2008. Canada and Arctic Politics: The Continental Shelf Extension. *Ocean Development & International Law,* 39**,** 343-359.

Rippeth, T. P., Lincoln, B. J., Lenn, Y.-D., Green, J. a. M., Sundfjord, A. & Bacon, S. 2015. Tide-mediated warming of Arctic halocline by Atlantic heat fluxes over rough topography. *Nature Geoscience,* 8**,** 191.

Robinson, J., New, A. L., Popova, E. E., Srokosz, M. A. & Yool, A. 2017. Far-field connectivity of the UK's four largest marine protected areas: Four of a kind? *Earth's Future,* 5**,** 475-494.

Robinson, J., Popova, E. E., Srokosz, M. A. & Yool, A. 2016. A tale of three islands: Downstream natural iron fertilization in the Southern Ocean. *Journal of Geophysical Research: Oceans,* 121**,** 3350-3371.

Robinson, J., Popova, E. E., Yool, A., Srokosz, M., Lampitt, R. S. & Blundell, J. R. 2014. How deep is deep enough? Ocean iron fertilization and carbon sequestration in the Southern Ocean. *Geophysical Research Letters,* 41**,** 2489-2495.

Rudels, B. 2015. Arctic Ocean circulation, processes and water masses: A description of observations and ideas with focus on the period prior to the International Polar Year 2007–2009. *Progress in Oceanography,* 132**,** 22-67.

Rudels, B., Anderson, L. G. & Jones, E. P. 1996. Formation and evolution of the surface mixed layer and halocline of the Arctic Ocean. *Journal of Geophysical Research: Oceans,* 101**,** 8807-8821.

Rudels, B., Jones, E. P., Schauer, U. & Eriksson, P. 2004. Atlantic sources of the Arctic Ocean surface and halocline waters. *Polar Research,* 23**,** 181-208.

Rudels, B., Korhonen, M., Schauer, U., Pisarev, S., Rabe, B. & Wisotzki, A. 2015. Circulation and transformation of Atlantic water in the Eurasian Basin and the contribution of the Fram Strait inflow branch to the Arctic Ocean heat budget. *Progress in Oceanography,* 132**,** 128-152.

Schøyen, H. & Bråthen, S. 2011. The Northern Sea Route versus the Suez Canal: cases from bulk shipping. *Journal of Transport Geography,* 19**,** 977-983.

Selkoe, K. A. & Toonen, R. J. 2011. Marine connectivity: a new look at pelagic larval duration and genetic metrics of dispersal. *Marine Ecology Progress Series,* 436**,** 291-305.

Shanks, A. L. 2009. Pelagic Larval Duration and Dispersal Distance Revisited. *The Biological Bulletin,* 216**,** 373-385.

Shapiro, G. I., Huthnance, J. M. & Ivanov, V. V. 2003. Dense water cascading off the continental shelf. *Journal of Geophysical Research: Oceans,* 108**,** 3390.

Sirevaag, A., De la Rosa, S., Fer, I., Nicolaus, M., Tjernström, M., McPhee, M.G.. 2011. Mixing, heat fluxes and heat content evolution of the Arctic Ocean mixed layer, *Ocean Science*, 7, pp. 335-349

Skagseth, Ø., Drinkwater, K. F. & Terrile, E. 2011. Wind- and buoyancy-induced transport of the Norwegian Coastal Current in the Barents Sea. *Journal of Geophysical Research: Oceans,* 116, C08007.

Skagseth, Ø., Furevik, T., Ingvaldsen, R., Loeng, H., Mork, K. A., Orvik, K. A. & Ozhigin, V. 2008. Volume and Heat Transports to the Arctic Ocean Via the Norwegian and Barents Seas. *In:* DICKSON, R. R., MEINCKE, J. & RHINES, P. (eds.) *Arctic–Subarctic Ocean Fluxes: Defining the Role of the Northern Seas in Climate.* Dordrecht: Springer Netherlands.

Smedsrud, L. H., Halvorsen, M. H., Stroeve, J. C., Zhang, R. & Kloster, K. 2017. Fram Strait sea ice export variability and September Arctic sea ice extent over the last 80 years. *The Cryosphere,* 11**,** 65-79.

Spall, M. A. 2013. On the Circulation of Atlantic Water in the Arctic Ocean. *Journal of Physical Oceanography,* 43**,** 2352-2371.

Spall, M. A., Pickart, R. S., Fratantoni, P. S. & Plueddemann, A. J. 2008. Western Arctic Shelfbreak Eddies: Formation and Transport. *Journal of Physical Oceanography,* 38**,** 1644-1668.

Spall, M. A., Pickart, R. S., Li, M., Itoh, M., Lin, P., Kikuchi, T. & Qi, Y. 2018. Transport of Pacific Water Into the Canada Basin and the Formation of the Chukchi Slope Current. *Journal of Geophysical Research: Oceans,* 123**,** 7453-7471.

Srokosz, M. A., Robinson, J., Mcgrain, H., Popova, E. E. & Yool, A. 2015. Could the Madagascar bloom be fertilized by Madagascan iron? *Journal of Geophysical Research: Oceans,* 120**,** 5790-5803.

Steele, M., Morison, J., Ermold, W., Rigor, I., Ortmeyer, M. & Shimada, K. 2004. Circulation of summer Pacific halocline water in the Arctic Ocean. *Journal of Geophysical Research: Oceans,* 109**,** C02027.

Stroeve, J., Holland, M. M., Meier, W., Scambos, T. & Serreze, M. 2007. Arctic sea ice decline: Faster than forecast. *Geophysical Research Letters,* 34, L09501.

Stroeve, J. C., Schroder, D., Tsamados, M. & Feltham, D. 2018. Warm winter, thin ice? *The Cryosphere,* 12**,** 1791-1809.

Thompson, D. W. J. & Wallace, J. M. 1998. The Arctic oscillation signature in the wintertime geopotential height and temperature fields. *Geophysical Research Letters,* 25**,** 1297-1300.

Timmermann, R., Goosse, H., Madec, G., Fichefet, T., Ethe, C. & Dulière, V. 2005. On the representation of high latitude processes in the ORCA-LIM global coupled sea ice–ocean model. *Ocean Modelling,* 8**,** 175-201.

Timmermans, M.-L., Marshall, J., Proshutinsky, A. & Scott, J. 2017. Seasonally derived components of the Canada Basin halocline. *Geophysical Research Letters,* 44**,** 5008-5015.

Timmermans, M. L., Proshutinsky, A., Golubeva, E., Jackson, J. M., Krishfield, R., Mccall, M., Platov, G., Toole, J., Williams, W., Kikuchi, T. & Nishino, S. 2014. Mechanisms of Pacific Summer Water variability in the Arctic's Central Canada Basin. *Journal of Geophysical Research: Oceans,* 119**,** 7523-7548.

Treml, E. A., Roberts, J. J., Chao, Y., Halpin, P. N., Possingham, H. P. & Riginos, C. 2012. Reproductive Output and Duration of the Pelagic Larval Stage Determine Seascape-Wide Connectivity of Marine Populations. *Integrative and Comparative Biology,* 52**,** 525-537.

Tschudi, W. N. M., J. S. Stewart, C. Fowler, and J. Maslanik 2019. Polar Pathfinder Daily 25 km EASE-Grid Sea Ice Motion Vectors, Version 4. Boulder, Colorado USA. NASA National Snow and Ice Data Center Distributed Active Archive Center.

Valentine, D. L., Fisher, G. B., Bagby, S. C., Nelson, R. K., Reddy, C. M., Sylva, S. P. & Woo, M. A. 2014. Fallout plume of submerged oil from Deepwater Horizon. *Proceedings of the National Academy of Sciences,* 111**,** 15906-15911.

Van Gennip, S. J., Popova, E. E., Yool, A., Pecl, G. T., Hobday, A. J. & Sorte, C. J. B. 2017. Going with the flow: the role of ocean circulation in global marine ecosystems under a changing climate. *Global Change Biology,* 23**,** 2602-2617.

Van Herwerden, L., Mcilwain, J., Al-Oufi, H., Al-Amry, W. & Reyes, A. 2006. Development and application of microsatellite markers for Scomberomorus commerson (Perciformes; Teleostei) to a population genetic study of Arabian Peninsula stocks. *Fisheries Research,* 79**,** 258-266.

Van Sebille, E., Griffies, S. M., Abernathey, R., Adams, T. P., Berloff, P., Biastoch, A., Blanke, B., Chassignet, E. P., Cheng, Y., Cotter, C. J., Deleersnijder, E., Döös, K., Drake, H. F., Drijfhout, S., Gary, S. F., Heemink, A. W., Kjellsson, J., Koszalka, I. M., Lange, M., Lique, C., Macgilchrist, G. A., Marsh, R., Mayorga Adame, C. G., Mcadam, R., Nencioli, F., Paris, C. B., Piggott, M. D., Polton, J. A., Rühs, S., Shah, S. H. a. M., Thomas, M. D., Wang, J., Wolfram, P. J., Zanna, L. & Zika, J. D. 2018. Lagrangian ocean analysis: Fundamentals and practices. *Ocean Modelling,* 121**,** 49-75.

Vermeij, G. J. & Roopnarine, P. D. 2008. The Coming Arctic Invasion. *Science,* 321**,** 780-781.

Wagner, P., Rühs, S., Schwarzkopf, F. U., Koszalka, I. M. & Biastoch, A. 2019. Can Lagrangian Tracking Simulate Tracer Spreading in a High-Resolution Ocean General Circulation Model? *Journal of Physical Oceanography,* 49**,** 1141-1157.

Wang, M. & Overland, J. E. 2012. A sea ice free summer Arctic within 30 years: An update from CMIP5 models. *Geophysical Research Letters,* 39**,** L18501.

Wang, Q., Ilicak, M., Gerdes, R., Drange, H., Aksenov, Y., Bailey, D. A., Bentsen, M., Biastoch, A., Bozec, A., Böning, C., Cassou, C., Chassignet, E., Coward, A. C., Curry, B., Danabasoglu, G., Danilov, S., Fernandez, E., Fogli, P. G., Fujii, Y., Griffies, S. M., Iovino, D., Jahn, A., Jung, T., Large, W. G., Lee, C., Lique, C., Lu, J., Masina, S., Nurser, A. J. G., Rabe, B., Roth, C., Salas Y Mélia, D., Samuels, B. L., Spence, P., Tsujino, H., Valcke, S., Voldoire, A., Wang, X. & Yeager, S. G. 2016. An assessment of the Arctic Ocean in a suite of interannual CORE-II simulations. Part I: Sea ice and solid freshwater. *Ocean Modelling,* 99**,** 110-132.

Wang, Q., Wekerle, C., Danilov, S., Sidorenko, D., Koldunov, N., Sein, D., Rabe, B. & Jung, T. 2019. Recent Sea Ice Decline Did Not Significantly Increase the Total Liquid Freshwater Content of the Arctic Ocean. *Journal of Climate,* 32**,** 15-32.

Wassmann, P., Kosobokova, K. N., Slagstad, D., Drinkwater, K. F., Hopcroft, R. R., Moore, S. E., Ellingsen, I., Nelson, R. J., Carmack, E., Popova, E. & Berge, J. 2015. The contiguous domains of Arctic Ocean advection: Trails of life and death. *Progress in Oceanography,* 139**,** 42-65.

Webster, M. S., Marra, P. P., Haig, S. M., Bensch, S. & Holmes, R. T. 2002. Links between worlds: unraveling migratory connectivity. *Trends in Ecology & Evolution,* 17**,** 76-83.

Weingartner, T., Aagaard, K., Woodgate, R., Danielson, S., Sasaki, Y. & Cavalieri, D. 2005. Circulation on the north central Chukchi Sea shelf. *Deep Sea Research Part II: Topical Studies in Oceanography,* 52**,** 3150-3174.

Weingartner, T. J., Danielson, S. L. & Royer, T. C. 2005. Freshwater variability and predictability in the Alaska Coastal Current. *Deep Sea Research Part II: Topical Studies in Oceanography,* 52**,** 169-191.

Weisberg, R. H., Lianyuan, Z. & Liu, Y. 2017. On the movement of Deepwater Horizon Oil to northern Gulf beaches. *Ocean Modelling,* 111**,** 81-97.

Whitmore, L. M., Morton, P. L., Twining, B. S. & Shiller, A. M. 2019. Vanadium cycling in the Western Arctic Ocean is influenced by shelf-basin connectivity. *Marine Chemistry,* 216**,** 103701.

Williams, W. J. & Carmack, E. C. 2015. The 'interior' shelves of the Arctic Ocean: Physical oceanographic setting, climatology and effects of sea-ice retreat on cross-shelf exchange. *Progress in Oceanography,* 139**,** 24-41.

Wisz, M. S., Broennimann, O., Grønkjær, P., Møller, P. R., Olsen, S. M., Swingedouw, D., Hedeholm, R. B., Nielsen, E. E., Guisan, A. & Pellissier, L. 2015. Arctic warming will promote Atlantic–Pacific fish interchange. *Nature Climate Change,* 5**,** 261.

Woodgate, R. A. 2018. Increases in the Pacific inflow to the Arctic from 1990 to 2015, and insights into seasonal trends and driving mechanisms from year-round Bering Strait mooring data. *Progress in Oceanography,* 160**,** 124-154.

Woodgate, R. A., Aagaard, K., Muench, R. D., Gunn, J., Björk, G., Rudels, B., Roach, A. T. & Schauer, U. 2001. The Arctic Ocean Boundary Current along the Eurasian slope and the adjacent Lomonosov Ridge: Water mass properties, transports and transformations from moored instruments. *Deep Sea Research Part I: Oceanographic Research Papers,* 48**,** 1757-1792.

Woodgate, R. A., Weingartner, T. J. & Lindsay, R. 2012. Observed increases in Bering Strait oceanic fluxes from the Pacific to the Arctic from 2001 to 2011 and their impacts on the Arctic Ocean water column. *Geophysical Research Letters,* 39, L24603.

Xie, H., Yapa, P. D. & Nakata, K. 2007. Modeling emulsification after an oil spill in the sea. *Journal of Marine Systems,* 68**,** 489-506.

Yaroslavtseva, L. M. & Sergeeva, E. P. 2006. Adaptivity of the bivalve Mytilus trossulus larvae to short-and long-term changes in water temperature and salinity. *Russian Journal of Marine Biology,* 32**,** 82-87.

Yool, A., Popova, E. E. & Coward, A. C. 2015. Future change in ocean productivity: Is the Arctic the new Atlantic? *Journal of Geophysical Research: Oceans,* 120**,** 7771-7790.

Zhao, M., Timmermans, M.-L., Cole, S., Krishfield, R. & Toole, J. 2016. Evolution of the eddy field in the Arctic Ocean's Canada Basin, 2005–2015. *Geophysical Research Letters,* 43**,** 8106-8114.